INAUGURAL - DISSERTATION

zur Erlangung der Doktorwürde der
Gesamtfakultät für Mathematik, Ingenieur-
und Naturwissenschaften der
Ruprecht-Karls-Universität Heidelberg

vorgelegt von
Marco Bauer
Tag der mündlichen Prüfung: 17.04.2024

Development, Extension and Application of Electronic Structure Methods for Ground and Excited States

Marco Bauer

March 3, 2024

Gutachter: Prof. Dr. Andreas Dreuw

Prof. Dr. Oriol Vendrell

Abstract

Nowadays research in various fields of natural science and engineering requires insight, which can only be provided by computational simulations, due to the complexity of the systems under consideration. Predicting energies and properties of molecular systems is especially hard, due to the many body problem and the fact, that the mean-field only yields insufficient accuracy in most applications. For this purpose many different methods have been developed over the past century, which all offer a tradeoff between accuracy and computational effort.

Contributing to this field of research, in this thesis major breakthroughs in the development of a novel fragmentation scheme, named Excitonic Renormalization, XR, are presented along with the extension of established methods based on perturbation theory, to consistently describe the influence of polariton formation on the electronic structure of molecules as well as the application of electronic structure methods to investigate a novel crystallization-induced ring opening reaction observed in a derivative of a compound used in organic semiconductors.

The first major achievement in the development of the XR method is the reformulation of the overlap matrix into a series of orbital rotations, which is shown to converge quickly, lifting the necessity of numerically orthogonalizing the full sets of orbitals between fragments, which is a big advantage of XR over related fragmentation methods. Moreover, fast convergence is observed for approximate densities with increasing order of perturbation theory, indicating that densities obtained from established post-Hartree-Fock methods yield sufficient accuracy for the XR method. Method independent approximations to higher particle densities are presented as well, with little success though. It is further pointed out, how to increase the performance of the XR method and its approximations.

The perturbation theoretical methods, extended to describe polaritons consistently, are based on two different partitionings of the Hamiltonian, yielding polaritonic ground and excited state methods corresponding to the Møller-Plesset Perturbation Theory and the Algebraic Diagrammatic Construction Theory, respectively. The methods were shown to yield similar results for intermediate coupling strengths, up to second order of perturbation theory. Later the necessity of consistently treating the vacuum field contribution in the strong coupling regime is shown for the photodissociation dynamics of Pyrrole, which is only provided by one of the two partitionings of the Hamiltonian. For the excited state method based on this partitioning of the Hamiltonian a "quasi-diabatic" representation is given as well, which can be utilized to simulate wavepacket dynamics between polaritonically coupled surfaces using standard quantum dynamical methods

without further adjustments. This method requires negligible additional computational effort for small state spaces compared to the approach widely applied in literature, which also yields a "quasi-diabatic" representation, but is shown to yield qualitatively wrong dissociation dynamics for Pyrrole for very strong coupling strengths.

In the investigation of the crystallization-induced reversible ring opening of Tetraazahexacene derivatives to Pyrazinopyrazine derivatives the experimental spectra are reproduced first. Further, assuming the Carbon-Carbon distance of the reversibly dissociating bond as the active reaction mode, the energy profile along this reaction path is computed with and without the explicit crystal environment, revealing double wells for all compounds and environments. Within reasonable accuracy the experimental findings of open and closed derivatives could then be mapped onto kinetical as well as thermodynamical stability and the reaction is shown to follow a concerted electrocyclic mechanism. Finally the dominant force, leading to ring opening in Tetraazahexacene derivatives, is found to be the force, that asymmetrically twists the aromatic core.

Zusammenfassung

Heutzutage erfordert die Forschung in verschiedensten Bereichen der Natur- und Ingenieurswissenschaften Erkenntnisse, die aufgrund der Komplexität der betrachteten Systeme nur durch computerbasierte Simulationen gewonnen werden können. Die Vorhersage von Energien und Eigenschaften molekularer Systeme ist aufgrund des Vielteilchenproblems und der Tatsache, dass das gemittelte Feld in den meisten Anwendungen nur eine unzureichende Genauigkeit liefert, besonders schwierig. Im vergangenen Jahrhundert wurden dafür viele verschiedene Methoden entwickelt, die alle einen Kompromiss zwischen Genauigkeit und Rechenaufwand bieten.

Als Beitrag zu diesem Forschungsgebiet werden in dieser Arbeit wichtige Durchbrüche bei der Entwicklung einer neuartigen Fragmentierungsmethode, der so genannten Exzitonischen Renormalization, XR, vorgestellt, ebenso wie die Erweiterung etablierter, auf Störungstheorie basierender Methoden zur konsistenten Beschreibung des Einflusses der Bildung von Polaritonen auf die elektronische Struktur von Molekülen sowie die Anwendung von Elektronenstruktur Methoden zur Untersuchung einer neuartigen kristallisationsinduzierten Ringöffnungsreaktion, die in einem Derivat einer Verbindung beobachtet wurde, die häufige Anwendung in organischen Halbleitern findet.

Die erste große Errungenschaft bei der Entwicklung der XR Methode ist die Umformulierung der Überlappmatrix in eine Reihe von Orbitalrotationen, von der gezeigt wird, dass sie schnell konvergiert, wodurch die Notwendigkeit der numerischen Orthogonalisierung der vollständigen Orbitalsätze zwischen den Fragmenten aufgehoben wird, was ein großer Vorteil von XR gegenüber verwandten Fragmentierungsmethoden ist. Darüber hinaus wird eine schnelle Konvergenz für approximative Dichten mit zunehmender Ordnung der Störungstheorie beobachtet, was darauf hindeutet, dass Dichten, die aus etablierten post-Hartree-Fock Methoden gewonnen werden, eine ausreichende Genauigkeit für die XR Methode liefern. Es werden auch methodenunabhängige Näherungen für höhere Teilchendichten vorgestellt, welche allerdings nur mäßigen Erfolg zeigen. Es wird außerdem aufgezeigt, wie der computerbasierte Aufwand der XR Methode und ihrer Näherungen verringert werden kann.

Die störungstheoretischen Methoden, die erweitert wurden, um Polaritonen konsistent zu beschreiben, basieren auf zwei verschiedenen Partitionierungen des Hamilton Operators, die zu polaritonischen Grund- und angeregten Zustandsmethoden führen, die der Møller-Plesset-Störungstheorie beziehungsweise der Algebraischen Diagrammatischen Konstruktionstheorie entsprechen. Es wird gezeigt, dass diese Methoden für mittlere Kopplungsstärken bis zur zweiten

störungstheoretischen Ordnung ähnliche Ergebnisse liefern. Später wird für die Photodissoziationsdynamik von Pyrrol gezeigt, dass der Beitrag des Vakuumfeldes bei starker Kopplung konsistent behandelt werden muss, was aber nur von einer der beiden Partitionierungen des Hamilton Operators geliefert wird. Für die Methode der angeregten Zustände, die auf dieser Partitionierung des Hamilton Operators beruht, wird auch eine "quasi-diabatische" Darstellung angegeben, die ohne weitere Anpassungen zur Simulation der Wellenpaketdynamiken zwischen polaritonisch gekoppelten Potentialhyperflächen mit Hilfe von quantendynamischen Standardmethoden verwendet werden kann. Diese Methode erfordert für kleine Zustandsräume einen vernachlässigbaren zusätzlichen Rechenaufwand im Vergleich zu dem in der Literatur weit verbreiteten Ansatz, der ebenfalls eine "quasi-diabatische" Darstellung liefert, aber wie gezeigt wird, eine qualitativ falsche Dissoziationsdynamik für Pyrrol bei sehr starken Kopplungsstärken ergibt.

Bei der Untersuchung der kristallisationsinduzierten reversiblen Ringöffnung von Tetraazahexacen-Derivaten zu Pyrazinopyrazin-Derivaten werden zunächst die experimentellen Spektren reproduziert. Unter der Annahme, dass der Kohlenstoff-Kohlenstoff-Abstand der reversibel dissozierenden Bindung der aktiven Reaktionsmode entspricht, wird dann das Energieprofil entlang dieses Reaktionsweges mit und ohne die explizite Kristallumgebung berechnet, wobei sich für alle Verbindungen und Umgebungen zweifache Potentialtöpfe ergeben. Mit angemessener Genauigkeit konnten die experimentellen Befunde offener und geschlossener Derivate dann auf die kinetische und thermodynamische Stabilität abgebildet werden, und es wurde gezeigt, dass die Reaktion einem konzertierten elektrozyklischen Mechanismus folgt. Schließlich wurde festgestellt, dass die dominante Kraft, die zur Ringöffnung in Tetraazahexacen-Derivaten führt, die Kraft ist, die den aromatischen Kern asymmetrisch verdreht.

List of Figures

Contents

1. Introduction

The main task in quantum chemistry is the calculation of energy levels and their stationary as well as dynamical properties. Gaining theoretical insight and being able to predict experimental outcomes on such systems is vital for many fields of science. Well-known examples from biology are photosynthesis[1], photoisomerization of retinal[2] as well as analyzing active sites of proteins e.g. for SARS-COVID-19[3]. Prominent examples from physics include Lasers[4] and other systems, able to emit coherent light with a very small width in energy like Masers[5], as well as photovoltaic systems, converting photon energy into an electric voltage, and the inverse effect, utilized e.g. in light emitting diodes[6–8]. Medical applications are for instance markers, which either increase detectability, like Gadolinium(III)-based markers, which enhance relaxation of the surrounding nuclear spins of protons for magnetic resonance imaging due to the large magnetic moment of Gadolinium[9], or enable detection at all, as used for instance in fluorescence imaging, which allows for resolution beyond the diffraction barrier of standard optical microscopy[10]. Furthermore, lanthanide-doped nanoparticles, functionalized to bind e.g. tumor cells, can either enhance detectability or kill surrounding tissue by photon-upconversion of otherwise harmless irradiation, without any chemical interaction of the nanoparticles in the body at all[11, 12]. An other application which gained increasing interest over the past decade are quantum computers, offering access to much larger state spaces, due to the superposition of qubits, as well as their entanglement. Algorithms, which utilize these properties, can then provide much lower scalings in the number of qubits[13], as e.g. the Fourier transformation and its inverse, used for phase estimation[14], or the variational quantum eigensolver[15], where an expectation value is solved for on quantum hardware. Understanding and therefore being able to efficiently optimize the given examples and related applications is almost impossible without theoretical modelling and simulation of such system, due to their high complexity.

How to calculate these energies and properties is known for almost 100 years, due to Schroedinger [16] and later Dirac[17]. However, due to the many body problem fully expanding the configuration space is only computationally feasible for systems with a few electrons, because of the exponential scaling of the computational effort with the system size. Hence, practically relevant calculations can never be performed without approximations, when running computations on classical hardware.

This can in principle be circumvented using quantum hardware[13], but development of the hardware is rather slow, especially because of the highly demanding engineering challenges. Hence, the most research intensive field of quantum chemistry remains the challenge of computing accurate energies and properties of large systems. Over the past century many methods have been proposed, which all offer a trade-off between computational effort and accuracy. The most common methods are either based on the variational principle, like Hartree-Fock, HF, configuration interaction, CI and coupled cluster, CC, or perturbation theory, like Møller-Plesset, MP, and the algebraic diagrammatic construction, ADC, theory[18–20]. Note, that all of these methods are based on an mean-field ansatz, which is usually some variant of Hartree-Fock. Also very common are semi-empirical methods, like density functional theory[18], DFT, and extended tight binding methods[21], XTB, which yield reliable results for standard organic systems, because they only require small variations of the empirical parameters. However, they can break down even for such systems, e.g. when describing charge transfer states[22]. An other class of quantum chemical methods, which gained increasing interest over the past decade, are fragmentation methods, where large systems of molecules are divided into smaller systems, which are calculated independent of each other, while their interaction is approximated. Most methods provide large scalings, at least to fourth order, with the overall size of the system, which results in very large but sparse tensors, requiring very tedious optimization of the algorithm and the corresponding implementation, in order to achieve reasonable computational effort for practically relevant systems, as for example done for coupled cluster in form of its domain-based local pair natural orbital implementation[23]. Fragmentation approaches on the other hand exploit these sparse tensors, by separating them into subsystems, which are expected to be dense sections of the large tensors, and then trying to recover the couplings between these separated sections without ever expanding to the full state space. Hence, they expose the sparse nature of the tensors spanned by the full state space without having to build the full tensors and then apply numerical techniques to lower the computational requirements.

Many different flavors of fragmentation approaches have been developed for the application of quantum chemistry. Probably the most well known of these methods are symmetry-adapted perturbation-theory[24], SAPT, block correlated[25], BC, and active space decomposition[26], ASD, methods, as well as the very successful density-matrix renormalization-group, DMRG[27]. Besides the fact, that all quantum chemical methods lack either in their performance for some properties of molecular systems, or are so expensive, that they are impractical, most fragmentation approaches provide severe drawbacks. BC and ASD methods require explicit orthogonalization for all fragments, which explicitly spans the full Fock space again, like in all methods based on HF, while SAPT requires tedious derivation for global anti-symmetry and lacks cooperative effects at low orders of perturbation theory, which is why SAPT was successfully applied to only two fragment systems.

Semiempirical fragmentation approaches exist as well, but like most semiempirical methods, they are not generalizable at the very least. The nowadays most successful fragmentation approach is DMRG, which lacks in its description of dynamical correlation, which makes it only applicable as a FCI extension and therefore also to describe active spaces. It further lacks from its description of interactions between orbitals, since the orbitals are in principle ordered as a one dimensional array, where interactions between them are only included one by one, with the density being truncated in each step. The excited renormalization method, XR, provides none of the drawbacks listed above, making it a promising method to investigate[28, 29]. However, since XR is rather new, the method still struggles from computational bottlenecks, hindering its applicability to practically relevant system. In this thesis crucial steps toward achieving this goal are presented, which have been developed in collaboration with Prof. Dr. Anthony Dutoi.

In addition to describing quantized matter and its interaction with classical fields, as required to calculate e.g. absorption spectra, the ability to accurately model the interaction of quantized matter with quantized fields gained increasing interest over the past decade, due to great success from experimental research. Examples for such achievements are superfluidity, i.e. Bose-Einstein condensate effects, at roomtemperature by coupling photons to excitons[30]. Similarly electron-phonon coupling, which is required for superconductivity, can be massively enhanced[31]. Coupling photons to vibronic excitations is useful to alter chemical reactions, e.g. by lowering yields of side-products, increasing overall reaction speeds or inducing enantioselectivity[32, 33]. Sufficiently large couplings to alter chemical reactions this way are already achieved by reaction chambers, which easily allow for yields on the scale of milligrams. Similarly, electronic excitations can also be coupled to photons, altering their energies and properties, which however requires more sophisticated experimental setups though. Nevertheless, using plasmonic cavities, which are closely related in their physical description to photonic cavities, the strong coupling limit has been surpassed even for single molecules[34]. Such coupled fermion-boson systems are called polaritons. Note, that these polaritons of vibronic or electronic excitations with photons or other bosonic fields, like plasmons, do not require chemical alteration of the reactants. Hence, e.g. in the case of vibronic polaritons, this could substitute or enhance the effect obtained from catalysts. However, only few methods exist, able to model polaritonic effects properly. The most widely applied approach is to use only few states, which are completely decoupled from the quantized bosonic system, and then using them to build the polaritonic Hamiltonian matrix, which is shown to be correct through first order of perturbation theory later[35–37]. The strength of this approach is, that it is easily implemented and is already in a "quasi-diabatic" representation, with the polaritonic couplings on the off-diagonals of the matrix. At resonance these polaritonic couplings dominate the coupling of the diabatic states, which does not require any reformulation before being used in dynamics

simulations. On the other hand this approach is not very accurate and therefore breaks down for strong couplings. Besides semi-empirical methods mainly based on DFT for ground[38–40] and excited states[41–44], introducing more unknown functionals, two polaritonic variants of coupled cluster, applicable to ground and excited states, have been developed, which are the only two *ab initio* post-HF methods currently available[45, 46]. However, they inherit the high computational scaling from the corresponding non-polaritonic methods, which is why in this thesis new *ab initio* post-HF methods based on perturbation theory are presented, which inherit the lower scaling with the system size of the corresponding non-polaritonic methods, MP and ADC, compared to coupled cluster. Furthermore, the polaritonic ADC method can also be unitarily transformed into a form, which can be truncated in good approximation and yields a "quasi-diabatic" representation as well. This approach has been devoloped up to second order of perturbation theory and therefore also the truncated approach is correct through second order of perturbation theory. Hence, it converges to the full state space limit much faster, than the widely applied approach described above, which is only correct through first order of perturbation theory.

Finally a project is presented, which has been investigated in collaboration with an experimental group, where a novel isomerization upon crystallization has been observed for a derivative of tetraazahexacene, which is commonly used in organic semiconductors[47]. Organic semiconductors are widely used nowadays and are intended to replace inorganic semiconductors whenever possible, since they are easier to process, less dangerous and much cheaper to produce. Their performance is highly dependent on the crystal structure, since it determines the conductivity along a crystal axis, governed by the transfer integral[48]. These are large, when e.g. the overlap of large delocalized aromatic systems is large. Usually this is solely determined by the spatial orientation of the molecules in the crystal, but in this collaborative work it was found for the first time, that crystallization can also lead to a ring-opening in the aromatic system, yielding small transfer integrals, even if the original aromatic systems would provide large overlaps. Hence, understanding why and how the system isomerizes is important for designing future tetraazahexacene derivatives with application in organic semiconductors.

2. Theory

The reader is expected to be familiar with the basic concepts of quantum mechanics, such as the Born-Oppenheimer approximation, the Rayleigh-Ritz variational principle, the methodology of second quantization and how to evaluate their expectation values of operator strings using Wicks theorem[18]. Also note, that the orbitals are expected to be real throughout the whole thesis.

2.1. Hartree-Fock

As is well known, the Schroedinger equation can not be solved for efficiently, due to the many body problem. However, its mean-field can be computed efficiently. Furthermore, it is used as a starting point for most of the methods presented in this thesis, which aim to efficiently recover the difference between the full electronic Schroedinger solution and the mean-field solution, which we refer to as correlation.

This mean-field solution to the electronic Schroedinger equation within the non-relativistic regime and under the Born-Oppenheimer approximation is better known as Hartree-Fock[18, 20], HF. The working equations can be obtained from

$$\left\langle \Phi_0 \right| \hat{H} \left| \Phi_0 \right\rangle = \left\langle \Phi_0 \right| \sum_{pq,\sigma} h_{pq} a^\dagger_{p\sigma} a_{q\sigma} + \frac{1}{2} \sum_{pqrs,\sigma\tau} V_{pqrs} a^\dagger_{p\sigma} a^\dagger_{q\tau} a_{s\tau} a_{r\sigma} \left| \Phi_0 \right\rangle + V_{NN}, \tag{2.1}$$

where $|\Phi_0\rangle$ denotes the ground state determinant, which is build from an orthonormal set of single particle wavefunctions, H the non-relativistic Hamiltonian within the Born-Oppenheimer approximation and a and $a^\dagger$ fermionic annihilation and creation operators, respectively. Moreover, the one- and two-electron operator integrals are defined as $h_{pq} = \left\langle \phi_p \right| h \left| \phi_q \right\rangle$ and $V_{pqrs} = \left\langle \phi_p \phi_q \right| V \left| \phi_r \phi_s \right\rangle$, where $|\phi\rangle$ refers to a single-particle wavefunction, better known as orbitals. V_{NN} denotes the nuclear-nuclear repulsion and is trivially evaluated, so we only focus on evaluating the expectation value on the right hand side. Using Wicks theorem we can easily evaluate the expectation value, as

$$\sum_{pq} h_{pq} \left\langle \Phi_0 \right| a^\dagger_p a_q \left| \Phi_0 \right\rangle = \sum_i h_{ii} \tag{2.2}$$

and

$$\frac{1}{2}\sum_{pqrs} V_{pqrs} \left\langle \Phi_0 \right| a_p^\dagger a_q^\dagger a_s a_r \left| \Phi_0 \right\rangle = \frac{1}{2}\sum_{ij}(V_{ijij} - V_{ijji}) = \frac{1}{2}\sum_{ij} \langle ij|\,|ij\rangle\,. \tag{2.3}$$

Note, that due to simplicity we omitted the spin contribution here, while denoting occupied-, virtual- and arbitrary orbitals with indices $\{i, j, ...\}$, $\{a, b, ...\}$ and $\{p, q, ...\}$, respectively. Furthermore, the common notation of the antisymmetrized two-electron integrals has been introduced, along with omitting the ϕ in the bras and kets, leaving only the orbital index. Hence, we obtain the HF energy, E_{HF}, as a functional of the set of orbitals

$$E_{HF}[\{\phi\}] = \sum_i h_{ii} + \frac{1}{2}\sum_{ij} \langle ij|\,|ij\rangle + V_{NN}. \tag{2.4}$$

In the next step we minimize the HF energy with respect to the orbitals, which either requires functional variation and the introduction of Lagrange multipliers, or we introduce rotation matrices and solve them via the Baker-Campbell-Hausdorff, BCH, expansion. The latter approach does not require constraints and is therefore the algebraically more convenient one, however, we will refer to the Fock matrix later many times and therefore need to introduce it here. Hence, the first approach will be described in more detail in the following.

Under variation of the orbitals their orthonormality is not ensured, so a Lagrange multiplier is introduced for this condition.

$$\delta E_{HF} = E_{HF}[\delta\{\phi\}] = \sum_i \delta h_{ii} + \frac{1}{2}\sum_{ij} \delta \langle ij|\,|ij\rangle + \delta V_{NN} - \sum_{ij} \delta\epsilon_{ij} \langle i\,|j\rangle = 0. \tag{2.5}$$

Taking the variation into the integrals yields a sum of all the possible variations. However, since all integrals as well as the Lagrange multiplier are hermitian and the electrons are indistinguishable, the result can be written as

$$\sum_i \delta \langle i| \left[\left(\hat{h} + \sum_j \left(\langle j|\, V\, |j\rangle - \left\langle j\right|\, VP_{ij}\, \left|j\right\rangle \right) \right) |i\rangle - \sum_j \epsilon_{ij}\, |j\rangle \right] = 0, \tag{2.6}$$

where P_{ij} denotes the permutation operator, swapping indices i and j in the ket. Since the orbitals are orthonormal, they are also linearly independent, so we obtain

$$\left(\hat{h} + \sum_j \left(\langle j|\, V\, |j\rangle - \left\langle j\right|\, VP_{ij}\, \left|j\right\rangle \right) \right) |i\rangle - \sum_j \epsilon_{ij}\, |j\rangle = 0. \tag{2.7}$$

Note, that one of the indices in the Lagrange multiplier is redundant now, so we can sum over the right hand term. This yields the final expression

$$\left(\hat{h} + \sum_j \left(\langle j| \; V \; |j\rangle - \left\langle j\right| \; VP_{ij} \; \left|j\right\rangle\right)\right)|i\rangle - \epsilon_i |i\rangle = F|i\rangle - \epsilon_i |i\rangle = 0, \tag{2.8}$$

where F denotes the Fock operator. The last equality is the key equation here, because it shows, that the Lagrange multipliers are the spectrum of the one particle operator, so they can be intepreted as energies of the converged orbitals, which is a key quantity in quantum chemistry. Hence, the final HF energy can also be given as

$$E_{HF}[\{\phi\}] = \sum_i h_{ii} + \frac{1}{2}\sum_{ij} \langle ij||ij\rangle + V_{NN} = \sum_i \epsilon_i - \frac{1}{2}\langle ij||ij\rangle + V_{NN}. \tag{2.9}$$

In order to yield a computable result it is also required to expand the orbitals in a set of initial orbitals. However, in this thesis the main focus is laid on the derivation and the final numerical results of novel methods instead of their implementation, so we will not go into further detail on how HF solution are actually computed.

2.2. Rayleigh-Schroedinger Perturbation Theory

Almost all *ab-initio* quantum chemistry methods, which aim to recover most of the correlation, are based on some variant of Hartree-Fock as a reference. Most of these so-called post-Hartree-Fock methods are either based on utilizing the variational principle, such as Configuration Interaction and Coupled Cluster, which will be discussed in sections 2.6 and 2.7 respectively, or they are based on perturbation theory of some sort. Mixtures are also common, as will be shown in section 2.8. However, most of the theoretical development of this thesis is based on Rayleigh-Schroedinger perturbation theory[18–20], which is the most common perturbation theory. In this approach the Hamiltonian is separated into a part, for which the eigenvalue problem can be solved for and the remainder, which we will refer to as the unperturbed system, H_0 and the perturbation, H_1, respectively. Furthermore, a series expansion around an auxiliary parameter λ is postulated for the exact eigenenergies and -vectors, such that

$$(H_0 + \lambda H_1)\sum_{n=0}^{\infty}\lambda^n \left|\psi_I^{(n)}\right\rangle = \left(\sum_{n=0}^{\infty}\lambda^n E_I^{(n)}\right)\sum_{n=0}^{\infty}\lambda^n \left|\psi_I^{(n)}\right\rangle, \quad H_0 + H_1 = \hat{H}. \tag{2.10}$$

Now one can group the terms on the left and right hand side according to their order in λ and then take the limit for λ against zero. Equations for the energies and wavefunctions of a certain order of

perturbation theory can then be obtained by projection onto the same state and the resolution of identity excluding the same state, respectively. There is, however, one additional degree of freedom, which is set such, that a state of the unperturbed system is orthonormal to that exact state of an higher order. The eigenenergies are then obtained as

$$E_I^{(0)} = \left\langle \psi_I^{(0)} \right| H_0 \left| \psi_I^{(0)} \right\rangle, \qquad E_I^{(n)} = \left\langle \psi_I^{(0)} \right| H_1 \left| \psi_I^{(n-1)} \right\rangle, \tag{2.11}$$

while the eigenstates are obtained as

$$\left|\psi_I^{(1)}\right\rangle = \sum_{J \neq I} \left|\psi_J^{(0)}\right\rangle \frac{\left\langle \psi_J^{(0)} \right| H_1 \left| \psi_I^{(0)} \right\rangle}{E_I^{(0)} - E_J^{(0)}}, \quad \left|\psi_I^{(2)}\right\rangle = \sum_{J \neq I} \left|\psi_J^{(0)}\right\rangle \frac{\left\langle \psi_J^{(0)} \right| H_1 - E_I^{(1)} \left| \psi_I^{(1)} \right\rangle}{E_I^{(0)} - E_J^{(0)}}, \quad \ldots \tag{2.12}$$

Note, that with this expansion all n-th order quantities can be build from the quantities up to $n-1$-th order.

2.3. Møller-Plesset Perturbation Theory

The most common variant of applied Rayleigh-Schroedinger perturbation theory nowadays is Møller-Plesset perturbation theory[18–20], MP, which sets H_0 to F, denoting the full Fock-operator, as introduced in section 2.1. The partitioning of the Hamiltonian then results in

$$H_0 = F = \sum_{pq} f_{pq} a_p^\dagger a_q \stackrel{!}{=} \sum_p \epsilon_p a_p^\dagger a_p \tag{2.13}$$

and

$$H_1 = H - H_0 = \frac{1}{4} \sum_{pqrs} \langle pq || rs \rangle a_p^\dagger a_q^\dagger a_s a_r - \sum_{pqk} \langle pk || qk \rangle a_p^\dagger a_q. \tag{2.14}$$

Note, that we are operating in the converged orbital basis, so the Fock operator is diagonal. Plugging that into Eq. (2.11) and evaluating up to first order yields

$$E_0^{(0)} + E_0^{(1)} = \sum_i \epsilon_i - \frac{1}{2} \sum_{ij} \langle ij || ij \rangle = E_{HF}. \tag{2.15}$$

This is an important feature of MP, since it recovers the mean-field of the two particle interaction of the Hamiltonian, which corrects the one-particle solutions to the HF result. This needs to be true, since no higher order contributions were included into the wavefunction yet, yielding corrections

outside of the single determinant regime. Plugging the MP partitioning into Eq. (2.12) shows, that one obtains contributions from wavefunctions up to the double excitation manifold, where two electrons from the occupied orbitals of the reference determinant now occupy virtual orbitals. The single and double excitation manifolds can be evaluated using Wicks theorem, while the first one yields zero and the latter results in

$$\left|\psi_0^{(1)}\right\rangle = -\frac{1}{4}\sum_{ijab}\left|\Phi_{ij}^{ab}\right\rangle \frac{\left\langle\Phi_{ij}^{ab}\right| H_1 \left|\Phi_0\right\rangle}{\epsilon_a + \epsilon_b - \epsilon_i - \epsilon_j} = -\frac{1}{4}\sum_{ijab}\left|\Phi_{ij}^{ab}\right\rangle \frac{\langle ab||ij\rangle}{\epsilon_a + \epsilon_b - \epsilon_i - \epsilon_j} = -\frac{1}{4}\sum_{ijab} t_{ijab}\left|\Phi_{ij}^{ab}\right\rangle . \quad (2.16)$$

With this result obtains the second order energy correction as

$$E_0^{(2)} = -\frac{1}{4}\sum_{ijab} t_{ijab}\,\langle ij|\,|ab\rangle . \quad (2.17)$$

Starting from the second order energy correction, the total energy result then goes beyond the mean-field approximation and more of the correlation is recovered in every further energy correction. However, this is only true from an algebraic point of view, since MP is known to numerically diverge, starting even from around fifth order for some molecules.

2.4. Algebraic Diagrammatic Construction Theory

In order to also access excited states using perturbation theory, most approaches utilize Greens-function theory and evaluate the expressions using diagrammatic approaches. In this chapter the Algebraic Diagrammatic Construction Theory[19, 49, 50], ADC, is presented, which also has its historic origin in the procedure described above. To be more precise, one starts from the propagator describing the process of interest. Here the polarization propagator is used, which will end up in the Polarization-Propagator ADC scheme, which is the standard ADC method, so it is referred to as just ADC, yielding neutrally charged excited states. Using the electron propagator one can either obtain Ionization-Potential ADC, IP-ADC, or Electron-Attachment ADC, EA-ADC, by only using the corresponding term of the electron propagator. The Greens-function based approach will be outlined briefly in the following, since it applies all concepts of ADC theory in a straightforward fashion. Starting from the polarization propagator in its common *Lehmann* representation

$$\Pi_{pq,rs}(\omega) = \lim_{\eta\to 0}\sum_{n\neq 0}\left(\frac{\langle\Psi_0|a_q^\dagger a_p|\Psi_n\rangle\langle\Psi_n|a_r^\dagger a_s|\Psi_0\rangle}{\omega - (E_n - E_0) + i\eta} - \frac{\langle\Psi_0|a_r^\dagger a_s|\Psi_n\rangle\langle\Psi_n|a_q^\dagger a_p|\Psi_0\rangle}{\omega + (E_n - E_0) + i\eta}\right), \quad (2.18)$$

where ω denotes the energy of the perturbing electromagnetic field and η describes an infinitesimal real number, ensuring adiabaticity during a previous integration. Setting η to zero one obtains the excitation energies by determining the poles of either term. However, in this representation one needs to solve the full Hamiltonian, in order to obtain the excitation energies. This can be circumvented by using the projected representation of the polarization propagator

$$\Pi_{pq,rs}(\omega) = \sum_{n\neq 0} x_{pq}^{0n} \left(\langle \Psi_n | \ \omega - H \ | \Psi_n \rangle\right)^{-1} x_{sr}^{n0}, \tag{2.19}$$

where $x_{pq}^{0n} = \langle \Psi_0 | a_q^\dagger a_p | \Psi_n \rangle$ defines the transition amplitudes. This is in fact the basis to not only ADC, but also to other excited state methods, e.g. time-dependent density functional theory, TDDFT. Note, that the Hamiltonian and the transition amplitudes are resolved in the exact state basis and are therefore diagonal. ADC now postulates a non-diagonal representation of each of these two quantities. Therefore, the transition amplitudes are modified by a vector y_n, as

$$f_{pq}^{0n} = y_n x_{pq}^{0n}. \tag{2.20}$$

From this relation follows, that

$$MY = YH, \tag{2.21}$$

where Y is build from all y_n and M denoting the non-diagonal matrix. Note, that we still operate in the exact state basis, so the Hamiltonian is diagonal, resulting in an eigenvalue problem. ADC further postulates, that M and f can be expanded in a perturbation series, such that

$$M = M^{(0)} + M^{(1)} + M^{(2)} + M^{(3)} + ... \tag{2.22}$$

$$f = f^{(0)} + f^{(1)} + f^{(2)} + f^{(3)} + ... \tag{2.23}$$

These expressions can now be evaluated using diagrammatic techniques, since this way no explicit basis needs to be defined, in which the theory is extended. However, the lack of the basis, in which the Hamiltonian is expanded, inherits the problem, that the converged eigenvectors cannot be mapped onto the exact states, and therefore no densities can be build, denying the access to properties. This basis has been found though and is required to obtain transition densities, required for the Excitonic Renormalization method 2.12. On the other hand it can be extended to the polaritonic theory, which will be presented later, as straightforwardly as the diagrammatic approach. Hence, M is presented in the so-called Intermediate-State Representation, ISR, in the

following. ADC uses MP as its reference ground state, so the ISR is based on the span of the MP vectors. In order to obtain a basis, in which excited states can be represented, the MP ground state of a specific order is excited using fermionic field operators acting on the Fock space. However, this span is not orthonormal and therefore not a basis. Hence, in a first step the span of a specific perturbation order and excitation manifold is orthogonalized with respect to all lower excitation manifolds of the same perturbation order, yielding the so-called precursor states

$$|\Psi_I^{\#(n)}\rangle = |\Psi_I^{(n)}\rangle - \left(|\Psi_J\rangle\langle\Psi_J|\Psi_I\rangle\right)^{(n)}, \quad I > J, \tag{2.24}$$

where (n) denotes the order of perturbation theory, while I and J denote the excitation manifold. For instance doubly excited MP wavefunctions need to be orthogonalized to singly excited MP wavefunctions and the MP ground state. In order to build a basis, orthogonality also needs to be ensured between excited MP states of the same excitation manifold. Hence, the final ISR basis is obtained as

$$|\tilde{\Psi}_I^{(n)}\rangle = \sum_J |\Psi_J^{\#(n)}\rangle \left(S_{IJ}^{-\frac{1}{2}}\right)^{(n)}, \quad I = J \quad , \tag{2.25}$$

where S_{IJ} denotes the overlap matrix of the precursor states. Note, that I and J refer to the excitation manifold again, and not to specific excitations, since the exact orbital transitions can differ between I and J. Further note, that two different orthogonalization procedures have been used here. In the second step the Loewdin orthonormalization procedure has been applied, because of its beneficial properties, which ensure compactness of the Hamiltonian and normalization of the states. However, it requires a symmetric overlap matrix and can therefore not be applied in the first orthogonalization step, where instead the Gram-Schmidt procedure is applied. Nevertheless, since the Loewdin step is the last step, a compact representation of the Hamiltonian in a normalized basis is obtained. The working equations can then be derived from

$$M_{IJ} = \langle\tilde{\Psi}_I|\hat{H} - E_0|\tilde{\Psi}_J\rangle, \tag{2.26}$$

where a block of M within a given perturbation order is given as

$$M_{IJ}^{(n)} = \left(S_{IK}^{-\frac{1}{2}}\right)^{(k)} M_{KL}^{\#(l)} \left(S_{LJ}^{-\frac{1}{2}}\right)^{(m)}, \; n = k + l + m \, . \tag{2.27}$$

Note, that $M^{\#}$ denotes the shifted Hamiltonian in the precursor basis, which can be expanded in perturbation orders analogous to M. For the perturbative expansion of $S^{-\frac{1}{2}}$ one can make use of the

fact, that in zeroth order the relation $S_{IJ}^{(0)} = \delta_{IJ}$ holds and expand $S^{-\frac{1}{2}}$ in a Taylor-series. Therefore, S is substituted as

$$S = 1 + x \,. \tag{2.28}$$

Since $S_{IJ}^{(1)} = 0$, x includes all higher order terms, starting from second order. For instance the expansion up to second order of perturbation theory for $S_{IJ}^{-\frac{1}{2}}$ is given as

$$\left(S_{IJ}^{-\frac{1}{2}}\right)^{(2)} = \delta_{IJ} - \frac{1}{2} S_{IJ}^{(2)} \,. \tag{2.29}$$

This leaves a straightforward derivation for the working equations, which however becomes increasingly tedious for higher orders of perturbation theory. Up to second order the working equations are given as

$$M_{ia,jb}^{(0)} = \delta_{ij}\delta_{ab}(\epsilon_a - \epsilon_i), \tag{2.30}$$

$$M_{iajb,kcld}^{(0)} = \delta_{ik}\delta_{jl}\delta_{ac}\delta_{bd}(\epsilon_a + \epsilon_b - \epsilon_i - \epsilon_j), \tag{2.31}$$

$$M_{ia,jb}^{(1)} = -\langle aj||bi\rangle \,, \tag{2.32}$$

$$M_{ia,kcld}^{(1)} = (1 - P_{cd})\langle kl||id\rangle\,\delta_{ac} + (1 - P_{kl})\langle ak||cd\rangle\,\delta_{il}, \tag{2.33}$$

$$M_{iajb,kc}^{(1)} = (1 - P_{ab})\langle kb||ij\rangle\,\delta_{ac} + (1 - P_{ij})\langle ab||ci\rangle\,\delta_{jk}, \tag{2.34}$$

$$M_{ia,jb}^{(2)} = \frac{1}{4}\delta_{ij}\sum_{klc}(1 + P_{ab})\,t_{klac}\langle kl||bc\rangle + \frac{1}{4}\delta_{ab}\sum_{kcd}\left(1 + P_{ij}\right)t_{ikcd}\langle jk||cd\rangle - \frac{1}{2}\sum_{kc}\left(1 + P_{ij}P_{ab}\right)t_{ikac}\langle jk||bc\rangle \,, \tag{2.35}$$

where P_{ij} denotes the permutation operator between the indices i and j. Note, that for a consistent treatment of the matrix block $M_{ia,jb}$ needs to expanded up to the full perturbation order of the ADC method, i.e. for ADC(2) $M_{ia,jb}$ needs to be expanded up to second order. However, the block $M_{iajb,kcld}$ only needs to be expanded to the perturbation order of the ADC method minus two, and the blocks coupling $M_{ia,jb}$ and $M_{iajb,kcld}$ to the perturbation order of the ADC method minus one. Due to the compactness of the ADC method, the excitation space only grows, if the new diagonal block is at least of zeroth order. Therefore, ADC(0) and ADC(1) stay within the single excitation regime, while ADC(2) and ADC(3) remain in the double excitation regime.

2.5. Transition Densities within the Intermediate State Representation

As already mentioned in section 2.4, the ISR grants access to transition densities, and therefore also to properties, because the exact state can now be expanded in the ISR basis[50]

$$|\Psi_n\rangle = \sum_I \left|\tilde{\Psi}_I\right\rangle \left\langle\tilde{\Psi}_I \left|\Psi_n\right\rangle = \sum_I \left|\tilde{\Psi}_I\right\rangle X_{In}, \tag{2.36}$$

where X_{In} denotes the I-th element of the n-th ADC eigenvector. Working equations for arbitrary transition densities are then obtained by substituting the exact state with the expansion given in Eq. (2.36). For instance the transition density for a neutral single excitation is given as

$$\left\langle\Psi_f\right| a_p^\dagger a_q \left|\Psi_i\right\rangle = \sum_{IJ} X_{If}^\dagger \left\langle\tilde{\Psi}_I\right| a_p^\dagger a_q \left|\tilde{\Psi}_J\right\rangle X_{Ji} \,. \tag{2.37}$$

This is the key relation to obtaining properties within the ADC scheme, since the operator integral only needs to be contracted over the orbital indices of the corresponding density. For the example of a transition dipole moment from the ground state to an excited state, the relation reads

$$D_{0\to f} = \sum_{pq} d_{pq} \left\langle\Psi_f\right| a_p^\dagger a_q \left|\Psi_0\right\rangle = \sum_{pq} d_{pq} \sum_{IJ} X_{If}^\dagger \left\langle\tilde{\Psi}_I\right| a_p^\dagger a_q \left|\tilde{\Psi}_J\right\rangle X_{J0} \,. \tag{2.38}$$

Even though the access to properties is the standard application for transition densities, they are used later within the context of the excitonic renormatization method.

2.6. Configuration Interaction

As already mentioned in section 2.2, Configuration Interaction[18, 20], CI, is based on the variational principle. However, remaining in the one determinant basis only recovers HF. Hence, the basis needs to be expanded beyond the one determinant basis, which is the key difference between all methods based on the variational principle. If all singly excited determinants are taken into account, one refers to the method with CIS, singly and doubly excited determinants yield CISD, up to the complete basis, which is referred to as FCI. The wavefunction is then expanded linearly as

$$|\Psi_0\rangle = \left(1 + \sum_I c_I C_I\right) |\Phi_0\rangle \,, \tag{2.39}$$

where C_I refers to the excitation operator and c_I to the CI expansion coefficient of the excitation manifold I. Note, that the excited determinants are orthogonal to the ground state determinant. This ansatz can then be inserted into the variational principle, to obtain working equations for the expansion coefficients and the energy referred to the CI wavefunction. The diagonalization step of the Hamiltonian in the complete basis is obviously unpractical, so truncation schemes need to be employed, like the above mentioned CIS and CISD. However, truncating the linear expansion looses a property, which is called size consistency. Size consistency itself summarizes two properties, which are excitation energies independent of the system size as well as ground state energies linearly increasing with the system size. Obviously these two are very important properties, which is why CI is not a frequently used method.

2.7. Coupled Cluster

Coupled cluster[18, 20], CC, theory makes use of all the concepts already introduced in section 2.6, but uses a product ansatz, ensuring size consistency upon truncation,

$$|\Psi_0\rangle = \prod_I (1 + t_I C_I) |\Phi_0\rangle , \tag{2.40}$$

where t_I denotes the CC expansion coefficient, usually referred to as CC amplitudes. Introducing the cluster operator

$$T = \sum_I t_I C_I, \tag{2.41}$$

the wavefunction can be rewritten in an exponential form

$$|\Psi_0\rangle = e^T |\Phi_0\rangle . \tag{2.42}$$

Even though the CC amplitudes can still be solved for using the variational principle, the product ansatz massively increases the computational cost, since the CC amplitudes cannot be solved for independently. For instance in CCSD the singly excited CC amplitudes are connected to the doubly excited ones through the double excitation manifold, via $t_2 C_2 + \frac{1}{2} t_1 C_1 t_1 C_1$. Therefore, different schemes have been employed to obtain the CC amplitudes, with the most common one for standard CC being the projected CC scheme. This approach is obtained by multiplying with the inverse of the cluster expansion from the left on

$$H e^T |\Phi_0\rangle = E_0^{CC} e^T |\Phi_0\rangle , \tag{2.43}$$

yielding

$$e^{-T} H e^{T} \left|\Phi_0\right\rangle = E_0^{CC} \left|\Phi_0\right\rangle, \tag{2.44}$$

which is the eigenvalue problem for the so-called similarity transformed Hamiltonian $H' = e^{-T} H e^{T}$. H' is not hermitian anymore, while usually numerically only slightly deviating from the hermitian Hamiltonian, but provides the big advantage, that the energy and amplitude equations

$$\left\langle \Phi_0 \right| e^{-T} H e^{T} \left|\Phi_0\right\rangle = E_0^{CC} \tag{2.45}$$

$$\left\langle \Phi_I \right| e^{-T} H e^{T} \left|\Phi_0\right\rangle = 0 \quad , \quad I \neq 0 \tag{2.46}$$

are now decoupled. Again note, that the excited determinants are orthogonal to the ground state. Working equations are then generated by applying the Baker-Campbell-Hausdorff, BCH, expansion, which expands the H' as a series of nested commutators

$$H' = e^{-T} H e^{T} = H + [H, T] + \frac{1}{2}[[H, T], T] + \frac{1}{6}[[[H, T], T], T] + \frac{1}{24}[[[[H, T], T], T], T]. \tag{2.47}$$

Note, that this expansion naturally truncates at fourth order, since each commutator reduces maximum length of the Hamiltonian operator string, which is limited by the two particle operator, by one. Even though this expansion truncates at fourth order, it is usually truncated even further, since the full expansion scales as N^{10} with N referring to the system size. The Hamiltonian is then inserted in its normal ordered form, which is equal to subtracting the mean field contribution from the one particle and the two particle operator, easing up further evaluation of the commutators. Since the two particle operator also has a mean field contribution, of the form of an one particle operator, the normal ordered Hamiltonian H_N can be rewritten as

$$H_N = H - E_{HF} = F_N + V_N, \tag{2.48}$$

with F_N referring to the normal ordered Fock operator and V_N denoting the normal ordered two particle operator. Note, that the CC amplitudes are already in normal ordered form and therefore, if they appear to the left of the Hamiltonian without hermitian conjugation, they yield zero, since they are applied on the ground state determinant as deexcitation operator. Furthermore, all indices of the CC amplitudes need to be contracted with the Hamiltonian, since there are no CC amplitudes to the left of the Hamiltonian in hermitian conjugated form and due to the fact, that the operators

are sandwiched between ground state determinants in the energy equation. Hence, for the example of CCSD the energy correction one is left with

$$\begin{aligned}\left\langle \Phi_0 \right| H_N' \left| \Phi_0 \right\rangle &= \left\langle \Phi_0 \right| H_N t_1 C_1 + H_N t_2 C_2 + \frac{1}{2} H_N t_1 C_1 t_1 C_1 \left| \Phi_0 \right\rangle \\ &= t_1 \left\langle \Phi_0 \right| F_N C_1 \left| \Phi_0 \right\rangle + t_2 \left\langle \Phi_0 \right| V_N C_2 \left| \Phi_0 \right\rangle + \frac{1}{2} t_1 t_1 \left\langle \Phi_0 \right| V_N C_1 C_1 \left| \Phi_0 \right\rangle \\ &= \sum_{ia} f_{ia} t_i^a + \frac{1}{4} \sum_{ijab} \langle ij || ab \rangle \, t_{ij}^{ab} + \frac{1}{2} \sum_{ijab} \langle ij || ab \rangle \, t_i^a t_j^b .\end{aligned} \tag{2.49}$$

Note the similarity to the MP2 correlation energy, which gives the exact same result, if $t_1 = 0$ and $t_2 = -\frac{\langle ab||ij\rangle}{\epsilon_a + \epsilon_b - \epsilon_i - \epsilon_j}$, which is the same definition as for the t-amplitude of first order MP perturbation theory, apart from the minus sign. Since the connection between CC and MP[51] is required in the context of polaritonic unitary CC, it shall be lined out in more detail. As already explained, the connection lies within the amplitude equations, so the amplitude equations need to be evaluated. However, instead of evaluating the full CCSD amplitude equations a perturbation expansion scheme is applied, to only evaluate the first order amplitude equations, which then correspond to the first order MP amplitudes. Therefore, the CC amplitudes are expanded as

$$T = T^{(1)} + T^{(2)} + ... \tag{2.50}$$

and the Hamiltonian is separated as

$$H_N = F_N^{(0)} + V_N^{(1)}. \tag{2.51}$$

Now the first order single excitation CC amplitudes $t_1^{(1)}$ are obtained from

$$\begin{aligned}\left\langle \Phi_i^a \right| H_N'^{(1)} \left| \Phi_0 \right\rangle &= \left\langle \Phi_i^a \right| F_N \left| \Phi_0 \right\rangle + t_1^{(1)} \left\langle \Phi_i^a \right| F_N C_1 \left| \Phi_0 \right\rangle + t_2^{(1)} \left\langle \Phi_i^a \right| F_N C_2 \left| \Phi_0 \right\rangle \\ &= f_{ai} + \sum_c f_{ac} t_i^{c(1)} - \sum_k f_{ki} t_k^{a(1)} + \sum_{kc} f_{kc} t_{ik}^{ac(1)} \\ &= 0.\end{aligned} \tag{2.52}$$

Since this is a comparison to MP, which is based on a diagonalized Fock operator, one obtains

$$t_i^{a(1)} = -\frac{f_{ai} + \sum_{kc} f_{kc} t_{ik}^{ac(1)}}{\epsilon_a - \epsilon_i} = 0. \tag{2.53}$$

The analogous procedure for $t_2^{(1)}$ yields

$$\begin{aligned}\left\langle \Phi_{ij}^{ab} \right| H_N'^{(1)} \left| \Phi_0 \right\rangle &= \left\langle \Phi_{ij}^{ab} \right| V_N \left| \Phi_0 \right\rangle + t_2^{(1)} \left\langle \Phi_{ij}^{ab} \right| F_N C_2 \left| \Phi_0 \right\rangle \\ &= \langle ab| \, |ij\rangle + (1 + P_{ab}) \sum_c f_{bc} t_{ij}^{ac(1)} - (1 + P_{ij}) \sum_k f_{kj} t_{ik}^{ab(1)} \\ &= 0.\end{aligned} \tag{2.54}$$

Inserting the diagonal Fock operator yields

$$t_{ij}^{ab(1)} = -\frac{\langle ab| \, |ij\rangle}{\epsilon_a + \epsilon_b - \epsilon_i - \epsilon_j}. \tag{2.55}$$

Hence, one obtains exactly the amplitude equations, which match the CCSD energy to the MP2 energy. However, CCSD goes beyond MP2 with the remaining amplitude equations of higher perturbation order. Nevertheless, most CCSD programms use the MP2 amplitudes as a guess and therefore the results are equal in the zeroth iteration for CCSD. Furthermore, this similarity gives rise to CC approaches, which are partially treated using perturbation theory, as will be explored in this thesis within the context of polaritonic UCC2.

2.8. Unitary Coupled Cluster

As already discussed, the projected CC ansatz is not hermitian. However, recovering the hermiticity of the CC ansatz can already be achieved by choosing a unitary cluster expansion

$$|\Psi_0\rangle = e^u \, |\Phi_0\rangle \tag{2.56}$$

$$u = S - S^\dagger \tag{2.57}$$

$$S = \sum_I s_I C_I, \tag{2.58}$$

yielding a hermitian similarity transformed Hamiltonian $H' = e^{-u} H e^u$. This approach is called unitary CC[18], UCC, and is a similarity transformation to H' from the CC approach. Hence, the CC equations for determining the energy and amplitudes, Eq. (2.45) and (2.46) respectively, can also be applied to the UCC similarity transformed Hamiltonian. Therefore, H' expanded in the basis of the ground and excited determinants yields two fully decoupled blocks for the ground state and the excited states, like in the ADC approach. In fact, the UCC and ADC matrices are related by an

unitary transformation. In order to obtain the working equations for UCC, H' needs to be expanded in terms of H and u. In CC this is done via the BCH expansion, which naturally truncates in fourth order. However, this is not true for UCC, since every commutator conserves the number of second quantized operators for a unitary cluster operator. Nevertheless, a more favorable expansion has been found, where the normal ordered Hamiltonian is separated as in Eq. (2.51) and H'_N is rewritten as

$$H'_N = e^{-u} H_N e^u = e^U H_N = e^U F_N + e^U V_N = F_N + P(U)[F_N, u] + e^U V_N, \tag{2.59}$$

where the superoperator U has been introduced, which is defined as

$$Ux = [x, u], \tag{2.60}$$

and $P(U)$ defined as

$$P(U) = (e^U - 1)U^{-1}. \tag{2.61}$$

Multiplying H'_N with $P^{-1}(U)$ from the left one obtains

$$P^{-1}(U)(H'_N - F_N) = [F_N, u] + P^{-1}(U)e^U V_N. \tag{2.62}$$

The advantage of rewriting H'_N this way is twofold. First note, that F_N does not need to be iterated through the higher orders of H'_N, but only V_N. The second advantage is, that $P^{-1}(U)$ corresponds to the generative function for the Bernoulli numbers, which converge rapidly for lower orders and even result in zero for the third and fifth order contribution[52]. With the iterative part of H'_N summarized as V'_N and multiplying with the relation $1 = P^{-1}(U) - \sum_{n=1} \frac{B_n^-}{n!} U^n$, where B_n^- denotes the Bernoulli numbers with the negative convention, one obtains the generating function for H'_N as

$$H'_N = F_N + V'_N = F_N + [F_N, u] + P^{-1}(U)e^U V_N - \sum_{n=1} \frac{B_n^-}{n!} U^n V'_N. \tag{2.63}$$

This generating function can be simplified, since it is applied to the UCC amplitude equation, resulting in

$$\left\langle \Phi_I \right| H'_N \left| \Phi_0 \right\rangle = \langle \Phi_I | F_N | \Phi_0 \rangle + \left\langle \Phi_I \right| V'_N \left| \Phi_0 \right\rangle = \left\langle \Phi_I \right| V'_N \left| \Phi_0 \right\rangle = \left\langle \Phi_I \right| V'_{N,OD} \left| \Phi_0 \right\rangle, \tag{2.64}$$

where $V'_{N,OD}$ denotes the off-diagonal blocks of V'_N, because only those can couple the HF determinant to excited determinants. Similarly the diagonal blocks are referenced by $V'_{N,D}$, which are the only contributions required to iterate

$$V'^{(i+1)}_N = [F_N, u] + P^{-1}(U)e^U V_N - \sum_{n=1} \frac{B^-_n}{n!} U^n V'^{(i)}_{N,D}. \tag{2.65}$$

With the original V'_N rewritten as follows

$$V'_N = P(U)[F_N, u] + e^U V_N = (e^U - 1)F_N + e^U V_N = e^U(F_N + V_N) - F_N, \tag{2.66}$$

one can argue to start the iterative procedure with $V'^{(0)}_N = V_{N,D}$, since expanding e^U yields one in zeroth order, for which F_N cancels out and only V_N remains. Going through this iterative procedure once yields the following contributions

$$H'_N = F_N + V_N + [F_N, u] + \frac{1}{2}[V_N, u] + \frac{1}{2}[V_{N,D}, u], \tag{2.67}$$

with no further contributions for F_N appearing in higher orders. Using this formulation for H'_N yields the correlation energy of the UCCSD approach

$$E_0 = \frac{1}{4} \sum_{ijab} \langle ij| |ab\rangle s^{ab}_{ij}, \tag{2.68}$$

while the corresponding amplitude equations can be generated from the amplitude equations. However, in this thesis an ansatz based on UCC2 is extended, which is a simplification of the UCCSD approach. The UCC2 ansatz separates the normal ordered Hamiltonian in a perturbative ansatz, Eq. (2.51), while the UCC amplitudes are provided with the same perturbative order, as their corresponding amplitudes from MP perturbation theory. That means, that for instance in first order of perturbation theory only the doubly excited amplitude exists, since the singly excited amplitude is zero. Then all commutators from UCCSD are used for UCC2, which do not surpass a perturbative order of two. This results in the same energy equation, but significantly simplified amplitude equations. The working equations for the amplitudes of the UCC2 ansatz with a diagonal fock matrix and V_D summarized into V are then given as

$$\begin{aligned}\left\langle \Phi_i^a \right| H_N'^{(1)} \left| \Phi_0 \right\rangle &= s_1^{(2)} \left\langle \Phi_i^a \right| F_N C_1 \left| \Phi_0 \right\rangle + s_2^{(1)} \left\langle \Phi_i^a \right| V_N C_2 \left| \Phi_0 \right\rangle \\ &= (\epsilon_a - \epsilon_i) s_i^{a(2)} + \frac{1}{2} \sum_{jbc} \langle aj||bc\rangle \, s_{ij}^{bc(1)} - \frac{1}{2} \sum_{jkb} \langle jk||ib\rangle \, s_{jk}^{ab(1)} \\ &= 0,\end{aligned} \tag{2.69}$$

and

$$\begin{aligned}\left\langle \Phi_{ij}^{ab} \right| H_N'^{(1)} \left| \Phi_0 \right\rangle &= \left\langle \Phi_{ij}^{ab} \right| V_N \left| \Phi_0 \right\rangle + s_2^{(1)} \left\langle \Phi_{ij}^{ab} \right| F_N C_2 \left| \Phi_0 \right\rangle + s_2^{(1)} \left\langle \Phi_{ij}^{ab} \right| V_N C_2 \left| \Phi_0 \right\rangle \\ &= \langle ab||ij\rangle + (\epsilon_a + \epsilon_b - \epsilon_i - \epsilon_j) s_{ij}^{ab(1)} \\ &+ \frac{1}{2} \sum_{kl} \langle kl||ij\rangle \, s_{kl}^{ab(1)} + \frac{1}{2} \sum_{cd} \langle ab||cd\rangle \, s_{ij}^{cd(1)} + (1 - P_{ij})(1 - P_{ab}) \sum_{kc} \langle kb||cj\rangle \, s_{ik}^{ac(1)} \\ &= 0.\end{aligned} \tag{2.70}$$

Note, that this approach does not just yield less equations to determine the amplitudes, but also has decoupled amplitudes. Hence, the doubly excited equations can be iterated to yield $s_2^{(1)}$, which is independent of $s_1^{(2)}$, and therefore provides a significant speed-up compared to UCCSD.

2.9. Semiempirical methods

Semiempirical methods have always been important in quantum chemistry, since most practically relevant problems require computations on large systems, where the high scaling of the presented post-HF methods makes these computations impossible. However, there has been tremendous progress over the last decades in terms of floating point operations per second of the hardware, parallel computing and linear algebra algorithms, as well as approaches to reduce the computational scaling of quantum chemical methods, sometimes even down to quasi linear scaling[23, 53], and to reduce the size of the basis set, by introducing a correction for the truncated basis[54, 55]. Especially these new low scaling approaches are able to handle also large systems, but only if the system provides highly local densities for ground state computations and highly local transition densities for excited state computations. This is not true for many practically relevant systems, which is why semiempirical methods are still widely used today. In this thesis semiempirical methods and their

concepts are not required for theoretical developments, but only for computations, and therefore shall only be shortly outlined.

2.9.1. Density Functional Theory

Density functional theory[20], DFT, is based on the Hohenberg-Kohn theorems, which state, that the wavefunction of the ground state is bijectively mapped onto the electron density of the ground state and that the variational principle also applies to the electron density. The electronic energy of the system is then given as

$$E[p(r)] = T[p(r)] + V_{ne}[p(r)] + V_{ee}[p(r)] + V_{xc}[p(r)], \tag{2.71}$$

where T, V_{ne}, V_{ee} and V_{xc} denote the kinetic, nuclear electron attraction, Coulomb electron electron repulsion and exchange correlation energy functional. The advantage over wavefunction based methods is the low dimensionality of $p(r)$, which is three, compared to the high dimensionality of the wavefunction, which still yields a significant speed-up after evaluating the electron density over a grid. However, the method has major issues, since for the kinetic energy functional only the functional for the free electron gas is known for more than two electrons, which favors non-chemically bound solutions over bound ones, while V_{xc} is completely unknown. Nevertheless, V_{xc} can be reasonably well approximated with the local density approximation, LDA, or the generalized gradient approximation, GGA, which both involve empirical parameters. Nowadays T is mostly handled by reintroducing orbitals and using the kinetic energy term from the wavefunction based Hamiltonian. This approach significantly reduces the speed of the method, but is still much faster than HF, while providing results of proper accuracy now. Since the empirical parameters in V_{xc} need to be fitted, DFT works very well for organic molecules build from light atoms, because they only require small variations in the empirical parameters. A lot of practically relevant molecules fall under this category, which is why DFT is widely used, but its performance is rather poor, when leaving the realm of organic molecules. Using Eq. (2.19), this approach can be extended to yield excited states as well, using only the random phase approximation, RPA. However, usually only one block of the 2 x 2 RPA block matrix is used for time-dependent DFT, TDDFT, which is the so-called Tamm-Dancoff approximation. In most cases, RPA accuracy can then be reobtained by applying a cheap dispersion correction. TDDFT has the same limitations as DFT, in terms of molecular systems, but also performs poor on charge transfer states, which are described well by HF. Therefore, most DFT and TDDFT calculations nowadays are hybrid calculations, where the final Hamiltonian is build from a linear combination of HF and DFT Hamiltonian.

2.9.2. Force Fields

Force-field[20, 56], FF, approaches are probably the crudest of approximations to the actual Hamiltonian, since they neither use wavefunctions, nor electron densities, but parametrizations for internal coordinates. For instance bond lengths and angles are parametrized by harmonic oscillators, which for bond lenghts are very similar to the anharmonic oscillator around the equilibrium geometry. Dihedral angles are parametrized by smooth functions, showing minima when atoms are the furthest apart and maxima where they are closest to each other. Non-binding interactions are also taken into account, e.g. using the classical dipole-dipole interaction to describe van-der-Waals interactions. This approach is by far the fastest of all quantum chemical methods, but still gives reasonable results for geometries, relative energies of conformers and sometimes even properties, which is why they are widely used for initial screenings and geometry optimizations. Obviously this approach cannot be extended to excited states though. It shall be noted here, that in terms of speed machine learning algorithms greatly surpass the speed of force fields, but for large systems the generalization to other systems is usually not given, which is why nowadays machine learning algorithms are only applied to specific molecules, which they were trained for.

2.9.3. Extended Tight Binding

Recently also tight-binding methods have a renaissance. The method most widely applied here is the extended tight binding method, XTB, optimized for geometries, frequencies and non-binding interactions, GFN-XTB[21]. XTB can be thought of an intermediate method between FFs and DFT, since it is based on the tight-binding energy functional perturbatively expanded as

$$E[p(r)] = E^{(0)}[p_0(r)] + E^{(1)}[p_0(r), \delta p(r)] + E^{(2)}[p_0(r), (\delta p(r))^2] + E^{(3)}[p_0(r), (\delta p(r))^3] + ..., \tag{2.72}$$

where $p_0(r)$ is the initial tight-binding electron density. $E^{(0)}$ is described by a Lennard-Jones potential also including dispersion, which can be thought of as a tight-binding version of a force field. The force field is then perturbed by density fluctuations, leading to anisotropic corrections to $p_0(r)$. Extended up to infinite order, the full density is recovered. Since the energy functionals are then plugged into a DFT machinery, the fully expanded XTB ansatz yields DFT. For instance for the GFN2-XTB method, which is the most widely used GFN-XTB method, Eq. (2.72) is truncated after the third order. This approach has the advantage, that only small perturbations to the non-iterated tight-binding density need to be iterated, which can be transformed to terms, which are much faster evaluated, than the full density in DFT. This approach has then been numerically proven to provide

close to DFT accuracy for geometries, frequencies and non-binding interactions, at significantly lower computational cost. Therefore, GFN-XTB enables fast prescreening at almost DFT accuracy in principle for all energies and properties, since it is a density based methods. GFN-XTB also grants access to excited states and the only atom specific parameters, which need to be fitted, are global parameters. Hence, other than DFT or FFs, GFN-XTB can easily be applied to the whole periodic system of elements.

2.10. Non-Relativistic Quantum Electrodynamics

2.10.1. Deriviation of the Pauli-Fierz Hamiltonian

In order to derive a practical Hamiltonian for polaritonic systems in chemistry, the standard Hamiltonian from electrodynamics will be canonically quantized and transformed into a compact equation[57]. Canonical quantization of a variable, q, yields its conjugated momenta, p, from the rules of Lagrangian mechanics

$$p_{conj} = \frac{\partial L}{\partial \dot{q}} \tag{2.73}$$

$$q_{conj} = \frac{\partial L}{\partial \dot{p}}, \tag{2.74}$$

where $\dot{q}$ refers to the time derivative of q and L denotes the Langrangian from classical electrodynamics

$$L = \sum_a \frac{1}{2} m_a \dot{r}_a^2 + \frac{\epsilon_0}{2} \int (E^2(r) + c^2 B^2(r)) d^3 r + \sum_a (q_a \dot{r}_a \cdot A(r_a) - q_a U(r_a)). \tag{2.75}$$

One needs to sum over all particles a, which shall be dropped in the following for brevity along with the dependencies r and t of the fields. Furthermore, U and A denote a scalar field and a vector field, respectively, which are utilized to define the electric, E, and magnetic field, B as

$$E = -\dot{A} - \nabla U \tag{2.76}$$

$$B = \nabla \times A. \tag{2.77}$$

The Hamiltonian can then be obtained from

$$H = p_{conj}\dot{r} - L. \tag{2.78}$$

Choosing q in Eq. (2.73) as r yields the conjugate momentum

$$p_{cong} = \frac{\partial L}{\partial \dot{r}} = m\dot{r} + qA \tag{2.79}$$

and with p denoting the momentum without a vector field applied, one obtains

$$H = \frac{1}{2m}(p - qA)^2 - \frac{\epsilon_0}{2}\int (E^2 + c^2B^2)d^3r - (q\dot{r}\cdot A - qU). \tag{2.80}$$

In order to recover the standard Hamiltonian used in quantum mechanics, without electrodynamic fields, the fields will be decomposed into a longitudinal and a transversal part, which separates the scalar field contribution from the vector field contribution. However, this decomposition requires locality, which is not given, due to the spatial derivatives, so the reciprocal space is utilized here, which one obtains through Fourier transformation. The fields are then defined in reciprocal space as

$$\mathfrak{B} = ik \times \mathfrak{A} \tag{2.81}$$

$$\mathfrak{E} = -\dot{\mathfrak{A}} - ik\mathfrak{U} \tag{2.82}$$

and the longitudinal $V_\parallel$ and transversal fields $V_\perp$ are then defined as

$$\nabla \times V_\parallel(r) = ik \times \mathfrak{V}_\parallel(k) = 0 \tag{2.83}$$

$$\nabla V_\perp(r) = ik\mathfrak{V}_\perp(k) = 0. \tag{2.84}$$

Decomposing the fields then shows, that the magnetic field is purely transversal, while in the electric field the scalar field contribution is purely longitudinal. In fact, also the remaining vector field contribution in the electric field is transversal, when the Coulomb gauge is applied. With $\mathfrak{E} = \mathfrak{E}_\parallel + \mathfrak{E}_\perp$ and $\mathfrak{E}_\parallel \cdot \mathfrak{E}_\perp = 0$, as well as the Parseval-Plancherel identity

$$\int E \cdot E d^3r = \int \mathfrak{E}^* \cdot \mathfrak{E} d^3k, \tag{2.85}$$

one obtains

$$\left(\frac{\epsilon_0}{2}\int \left(E^2 + c^2B^2\right) d^3r\right)_\perp = \frac{\epsilon_0}{2}\int \left(E_\perp^2 + c^2B^2\right) d^3r = \frac{\epsilon_0}{2}\int \left(\mathfrak{E}_\perp^2 + c^2\mathfrak{B}^2\right) d^3k \tag{2.86}$$

and

$$\begin{aligned}\left(\frac{\epsilon_0}{2}\int\left(E^2+c^2B^2\right)d^3r\right)_{\parallel} &= \frac{\epsilon_0}{2}\int|\mathfrak{E}_{\parallel}(k)|^2d^3k = \frac{\epsilon_0}{2}\int E_{\parallel}(r)^2d^3r\\ &= \frac{1}{8\pi\epsilon_0}\int\int\frac{p(r)p(r')}{|r-r'|}d^3rd^3r'\\ &= \sum_{\alpha}\frac{q_{\alpha}^2}{2\epsilon_0(2\pi)^3}\int\frac{d^3k}{|k|^2}+\frac{1}{8\pi\epsilon_0}\sum_{\alpha\neq\beta}\frac{q_{\alpha}q_{\beta}}{r_{\alpha}-r_{\beta}}\\ &= V_{Coul}.\end{aligned} \tag{2.87}$$

Recovering the coulomb potential is crucial, since now the standard Hamiltonian can be excluded as a separate term for the derivation of polaritonic methods, since the methods are already developed for it. For the next step the following intermediates are used

$$\alpha_{\epsilon}(k) = -\frac{i}{2N}\left(\mathfrak{E}_{\perp}(k) - c\kappa\times\mathfrak{B}(k)\right) \tag{2.88}$$

$$\beta_{\epsilon}(k) = -\frac{i}{2N}\left(\mathfrak{E}_{\perp}(k) + c\kappa\times\mathfrak{B}(k)\right) = -\alpha_k^*(-k), \tag{2.89}$$

with $N = \sqrt{\frac{\hbar\omega}{2\epsilon_0}}$ and κ denoting the unit vector of k. These are the eigenfunctions of the equations of motion of the transversal fields without a current of charged particles, which is why they are vectors orthogonal to k, indicated by the index ϵ. The Lagrangian can be rewritten as

$$L = \frac{1}{2}m\dot{r}^2 - V_{Coul} + \int\left(\frac{\epsilon_0}{2}\left(\dot{\mathfrak{A}}^2 - c^2(ik\times\mathfrak{A})^2\right) + \mathrm{j}\cdot\mathfrak{A}\right)d^3k, \tag{2.90}$$

where j is the electric current in reciprocal space. With the conjugated momentum to $\mathfrak{A}$ given as

$$\mathfrak{Z} = \frac{\partial L}{\partial\dot{\mathfrak{A}}} = \frac{\partial\int\frac{\epsilon_0}{2}\dot{\mathfrak{A}}^2d^3k}{\partial\dot{\mathfrak{A}}} = \epsilon_0\dot{\mathfrak{A}} = -\epsilon_0\mathfrak{E}_{\perp} \tag{2.91}$$

and the fact that

$$c\kappa\times\mathfrak{B} = ic\kappa\times k\times\mathfrak{A} = ic\mathfrak{A}, \tag{2.92}$$

one can rewrite Eq. (2.88) as

$$\alpha_{\epsilon}(k) = \sqrt{\frac{\epsilon_0}{2\hbar\omega}}\left(\omega\mathfrak{A}_{\epsilon} + \frac{i}{\epsilon_0}\mathfrak{Z}_{\epsilon}\right). \tag{2.93}$$

This formulation can now be used to rewrite the Hamiltonian as

$$H = \frac{1}{2m}(p - qA)^2 + V_{Coul} + \int \frac{\hbar\omega}{2} \sum_{\epsilon} \left(\alpha_\epsilon(k)^* \alpha_\epsilon(k) + \alpha_\epsilon(k)\alpha_\epsilon(k)^* \right) d^3k. \tag{2.94}$$

This relation can easier be understood by the fact, that j is proportional to $\mathfrak{E}_\perp$ and therefore also to $\mathfrak{Z}$. One can already expect the additional part to the standard quantum chemical Hamiltonian to be described by a harmonic oscillator, which significantly simplifies further derivations for polaritonic quantum chemical methods. Now the actual quantization is performed, which is known for the standard Hamiltonian, where spatial and momentum operators obey the anti-commutation relations. Furthermore, $\mathfrak{A}$ and its conjugated momentum are quantized, but since these are fields interacting via photons, i.e. bosons, they need to obey the commutation relations

$$\left[\mathfrak{A}_n(k), \mathfrak{Z}_m(k')\right] = 0 \tag{2.95a}$$

$$\left[\mathfrak{A}_n(k), \mathfrak{Z}_m^\dagger(k')\right] = i\hbar\delta_{mn}\delta(k - k'). \tag{2.95b}$$

All other commutators are zero. From these commutation relations on obtains

$$\left[\mathfrak{A}_\epsilon(k), \mathfrak{Z}_{\epsilon'}(k')\right] = i\hbar\delta_{\epsilon\epsilon'}\delta(k + k') \tag{2.96a}$$

$$\left[\mathfrak{A}_\epsilon(k), \mathfrak{Z}_{\epsilon'}^\dagger(k')\right] = i\hbar\delta_{\epsilon\epsilon'}\delta(k - k'). \tag{2.96b}$$

With the other commutators still giving zero. From these one obtains

$$\left[a_\epsilon(k), a_{\epsilon'}^\dagger(k')\right] = \delta_{\epsilon\epsilon'}\delta(k - k'), \tag{2.97}$$

where the other two commutation relations yield zero. Using these commutation relations, the integral part can be brought into the common quantum harmonic oscillator representation

$$H = \frac{1}{2m}(p - qA)^2 + V_{Coul} + \sum_i \hbar\omega_i \left(a^\dagger a + \frac{1}{2} \right). \tag{2.98}$$

Since in principle an explicit interaction with the spin and not just the charge of the electrons and cores could be relevant, this contribution shall be investigated by introducing an *ad hoc* interaction term as

$$H_1^S = -\sum_\alpha g_\alpha \frac{q_\alpha}{2m_\alpha} S_\alpha \cdot B(r_\alpha), \tag{2.99}$$

where g_α denotes the Lande factor. Since $B = \nabla \times A \sim kA$ one obtains

$$\frac{H_1^S}{H_1} \simeq \frac{q\hbar B/m}{qAp/m} \simeq \frac{\hbar kA}{pA} = \frac{\hbar k}{p}. \tag{2.100}$$

Since bound electrons in molecules are considered along with photons in the optical and long-UV energy regime, the relation is very small, and the coupling of the particle spins to the magnetic field can be neglected. As already mentioned, the Coulomb gauge has been applied, to separate E and B into longitudinal and transversal contributions, which is a degree of freedom, due to the non-uniqueness of the Lagrangian. One can switch representations between Lagrangians, by adding a total time-derivative

$$L'(x, \dot{x}) = L(x, \dot{x}) + \frac{d}{dt}F(x, t) = L(x, \dot{x}) + \dot{x}\frac{\partial F}{\partial x} + \frac{\partial F}{\partial t}, \tag{2.101}$$

yielding the new conjugated momentum

$$p_{L'} = p_L + \frac{\partial F}{\partial x}. \tag{2.102}$$

The spatial operators remains the same. This swap between representations can be achieved by an unitary transformation, with the unitary operator

$$T = e^{\frac{i}{\hbar}F}, \tag{2.103}$$

so that

$$\hat{x}^{(2)} = T\hat{x}^{(1)}T^\dagger \tag{2.104a}$$

$$\hat{p}^{(2)} = T\hat{p}^{(1)}T^\dagger \tag{2.104b}$$

$$\left|\Psi^{(2)}\right\rangle = T\left|\Psi^{(1)}\right\rangle. \tag{2.104c}$$

From these transformations, and the fact, that the Schrödinger equation is only valid for representation two with L' or representation one with L it follows from
$i\hbar\frac{d}{dt}\left|\Psi^{(2)}\right\rangle = H_{L'}^{(2)}\left|\Psi^{(2)}\right\rangle$, that

$$H_{L'}^{(2)} = TH_L^{(1)}T^\dagger - \frac{\partial F}{\partial t}. \tag{2.105}$$

With the vector field given as

$$A(r_\alpha) = \sum_i \sqrt{\frac{\hbar}{2\epsilon_0 \omega_i L^3}} \left(a_i \epsilon_i e^{+ik_i r_\alpha} + a_i^\dagger \epsilon_i e^{-ik_i r_\alpha} \right) \tag{2.106}$$

and the dipole approximation, $|k_i r_\alpha| << 1$, A becomes time-independent. Note, that ϵ_i describes the polaritzation of photon i. One can now get rid of A completely by a unitary transformation, which is defined as

$$T p_\alpha T^\dagger = p_\alpha + q_\alpha A(0). \tag{2.107}$$

By defining $\lambda_i = \frac{i}{\sqrt{2\epsilon_0 \epsilon_r \hbar \omega_i L^3}} \epsilon_i \cdot d$, where d denotes the dipole operator, the resulting transformation can be written as

$$T = exp\left(\sum_i (\lambda_i^* a_i - \lambda_i a_i^\dagger) \right). \tag{2.108}$$

Since the transformation is time-independent, the last term in eq. (2.105) is zero. With $T a_i T^\dagger = a_i + \lambda_i$ and $T a_i^\dagger T^\dagger = a_i^\dagger + \lambda_i^*$ one obtains the transformed Hamiltonian as

$$H' = \sum_\alpha \frac{p_\alpha^2}{2m_\alpha} + V_{Coul} + \sum_i \hbar \omega_i \left(\left(a_i^\dagger a_i + \frac{1}{2} \right) + (\lambda_i a_i^\dagger + \lambda_i^* a_i) + \lambda_i^* \lambda_i \right). \tag{2.109}$$

This is known as the Pauli-Fierz Hamiltonian, from which quantum chemical methods can rather straightforwardly be expanded to polaritonic quantum chemical methods, since the Hamiltonian can be seen as the standard quantum chemical Hamiltonian where a perturbative term is added.

2.10.2. Linear response of the Pauli-Fierz Hamiltonian

In order to obtain the linear response, the representation of the Hamiltonian is changed first, which eases up the photonic perturbation and the evaluation of the final integrals[41]. Therefore, the bosonic field operators are given in terms of photonic displacement coordinates q, analogously to the harmonic oscillator

$$a = \frac{1}{\sqrt{2}} \left(q + \frac{\partial}{\partial q} \right) = \frac{1}{\sqrt{2}} \left(q - i\omega p_q \right) \tag{2.110}$$

$$a^\dagger = \frac{1}{\sqrt{2}} \left(q - \frac{\partial}{\partial q} \right) = \frac{1}{\sqrt{2}} \left(q + i\omega p_q \right), \tag{2.111}$$

which transforms the Hamiltonian to

$$H = T + V_{Coul} + \frac{1}{2}\sum_{\alpha}\left(p_{\alpha}^2 + \omega_{\alpha}^2(q_{\alpha} - \frac{\lambda_{\alpha}}{\omega_{\alpha}}R)^2\right). \tag{2.112}$$

Here p_q denotes the conjugated momentum to q, R the total dipole moment of the system, and T the kinetic part of the standard Hamiltonian. The perturbation, H_{ext}, is then given by an external electromagnetic potential v, disturbing the matter system, and a photonic current j, disturbing the light system

$$H_{ext}(t) = V_{ext}(t) + J_{ext}(t) = \sum_{i} v(r_i, t) + \sum_{\alpha}\frac{j_{\alpha}(t)}{\omega_{\alpha}}q_{\alpha}. \tag{2.113}$$

Note, that the photonic perturbation has this form, since j needs to be introduced before unitarily transforming the Hamiltonian from the Coulomg gauge to the Pauli-Fierz Hamiltonian, which provides the so-called length gauge. Now the linear response is obtained via the standard procedure, where the Born series is terminated after first order

$$\Psi_I(t) \simeq \Psi_I(0) - \frac{i}{\hbar}\int_{t_0}^{t} dt' H_{ext,I}(t')\Psi_I(t), \tag{2.114}$$

which is then used to calculate the change in the expectation value of an arbitrary operator, O, due to the time-dependent external perturbation in the interaction picture as

$$\delta\langle O(t)\rangle = \langle\Psi(t)|\, O\,|\Psi(t)\rangle - \langle\Psi_0|\, O\,|\Psi_0\rangle = -\frac{i}{\hbar}\int_{t_0}^{t} dt' \left\langle\Psi_0\right|\left[O_I(t), H_{ext,I}(t')\right]\left|\Psi_0\right\rangle. \tag{2.115}$$

The responses χ are then obtained as

$$\delta\chi = -\frac{i}{\hbar}\int_{t_0}^{t} dt' \int dr' \langle\Psi_0|\left[X_I, Y_I\right]|\Psi_0\rangle = -\frac{i}{\hbar}\Theta(t-t')\left\langle\Psi_0\right|\left[X_I, \tilde{X}_I\right]\left|\Psi_0\right\rangle, \tag{2.116}$$

with $X = \{n(r,t), q_{\alpha}(t)\}$, $Y = \{V_{ext}(r',t'), J_{ext}(t')\}$ and $\tilde{X} = \{n(r,t), \frac{1}{\omega_{\alpha}}q_{\alpha}(t)\}$. This yields four responses, better known as propagators, which can be thought of as the response of the matter system to the matter system, the response of the photonic system to the matter system, as well as both responses to the photonic system. In Lehmann representation the final responses are

$$\chi_n^n(r, r', \omega) = \frac{1}{\hbar}\lim_{\eta\to 0^+}\sum_{k}\left(\frac{f_k(r)f_k^*(r')}{\omega - \Omega_k + i\eta} - \frac{f_k(r')f_k^*(r)}{\omega + \Omega_k + i\eta}\right) \tag{2.117a}$$

$$\chi^{n}_{q_\alpha}(r,\omega) = \frac{1}{\hbar}\lim_{\eta\to 0^+}\sum_k \frac{1}{\omega_\alpha}\left(\frac{f_k(r)g^*_{\alpha,k}}{\omega-\Omega_k+i\eta} - \frac{g_{\alpha,k}f^*_k(r)}{\omega+\Omega_k+i\eta}\right) \tag{2.117b}$$

$$\chi^{q_\alpha}_{n}(r',\omega) = \frac{1}{\hbar}\lim_{\eta\to 0^+}\sum_k \left(\frac{g_{\alpha,k}f^*_k(r')}{\omega-\Omega_k+i\eta} - \frac{f_k(r')g^*_{\alpha,k}}{\omega+\Omega_k+i\eta}\right) \tag{2.117c}$$

$$\chi^{q_\alpha}_{q_{\alpha'}}(\omega) = \frac{1}{\hbar}\lim_{\eta\to 0^+}\sum_k \frac{1}{\omega_{\alpha'}}\left(\frac{g_{\alpha,k}g^*_{\alpha',k}}{\omega-\Omega_k+i\eta} - \frac{g_{\alpha',k}g^*_{\alpha,k}}{\omega+\Omega_k+i\eta}\right), \tag{2.117d}$$

where $f_k(r) = \langle\Psi_0|\, n(r)\, |\Psi_k\rangle$, which is the transition moment known from standard linear response theory, and $g_{\alpha,k} = \langle\Psi_0|\, q_\alpha\, |\Psi_k\rangle$. Hence, the response to the matter system from the matter perturbation is the same as for standard linear response theory, apart from the different energy eigenvalues in Ω_k, which is important, since now polaritonic methods depending on the response, or propagator, e.g. DFT and ADC, are only extensions to the non-polaritonic methods, instead of completely different methods. The same holds for the evaluation of properties from propagators, e.g. see section 2.5, where the non-polaritonic approach can be considered a good zeroth order approximation to the consistent polaritonic procedure. This response will then be applied molecules in cavities and is visualized in Figure 2.1.

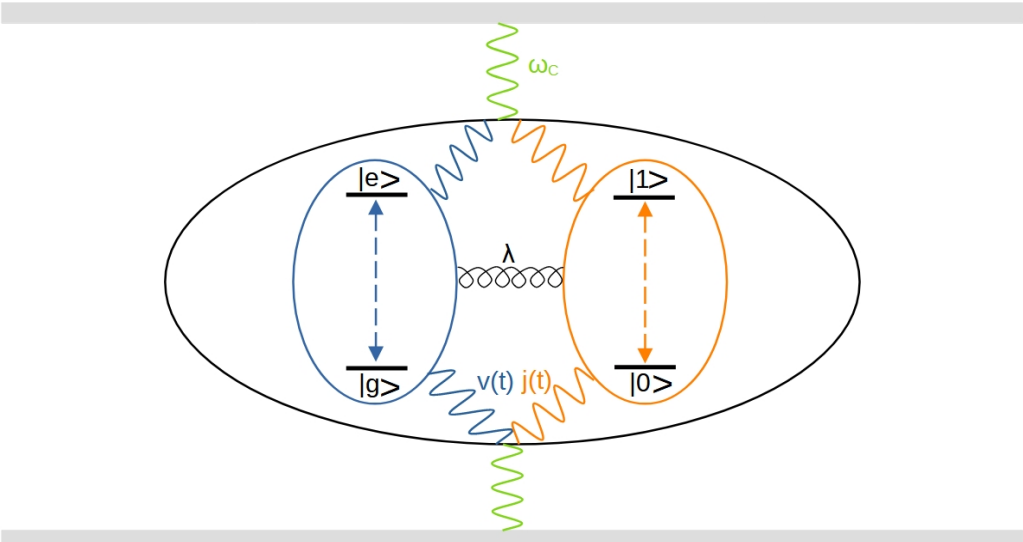

Figure 2.1.: Visualization of the polaritonic linear response of a 2 x 2 light-matter system in a cavity, which is coupled by the constant λ, determined by the experimental setup. The black ellipsoid depicts the polaritonic system, interacting with the cavity photon of frequency ω_C.

2.11. Polaritonic Hartree-Fock

2.11.1. Transforming to a Hamiltonian with an origin invariant mean-field

Before the mean field of the Pauli-Fierz Hamiltonian is determined[45], the Pauli-Fierz Hamiltonian will be rewritten as

$$H = H_e + \omega b^\dagger b - \sqrt{\frac{\omega}{2}}(\lambda \cdot d)(b^\dagger + b) + \frac{1}{2}(\lambda \cdot d)^2. \tag{2.118}$$

Note, that λ has been multiplied with $\sqrt{2\hbar\omega}$ and the dipole operator has been factored out, while i was factored into the polaritzation vector, since now it is a real constant given by the experimental setup, as $\lambda = \frac{1}{\sqrt{\epsilon_0 \epsilon_r L^3}}\epsilon$. Also since for the derivation of polaritonic methods fermionic and bosonic second quantized operators are required, the bosonic second quantized operators are now denoted by b. Finally $H_e = \sum_\alpha \frac{p_\alpha^2}{2m_\alpha} + V_{Coul}$ abbreviates the non-polaritonic Hamiltonian and the sum over all photons has been dropped too, so only photons of one wavelength are taken into account. Note, that this Hamiltonian still has an issue, since it is not origin invariant, due to the nuclear contribution, d_N, in the dipole operator

$$d = \sum_{pq} d_{pq} a_p^\dagger a_q + d_N. \tag{2.119}$$

Note, that the Hamiltonian is origin invariant, if the system has no global charge. If the system has a global charge, the center of the global charge can also be set to the origin and not moved from there, which suffices for most practically relevant calculations. However, in order to properly deal with systems providing a global charge the Hamiltonian will be transformed again to provide an origin invariant mean-field. The expectation value of the Hamiltonian is given as

$$\langle H \rangle = E_{HF} + \omega b^\dagger b - \sqrt{\frac{\omega}{2}}(\lambda \cdot \langle d \rangle)(b^\dagger + b) + \frac{1}{2}\left\langle (\lambda \cdot d)^2 \right\rangle, \tag{2.120}$$

where E_{HF} denotes the non-QED HF energy and by substituting $X = \sqrt{\frac{\omega}{2}}(\lambda \cdot \langle d \rangle)$ the expectation value reduces to

$$\langle H \rangle = E_{HF} + \omega b^\dagger b - x(b^\dagger + b) + \frac{x^2}{\omega}. \tag{2.121}$$

Now a unitary transformation is applied to the Hamiltonian, with the transformation operator (2.108), with the new constant z, which yields

$$\langle H \rangle = E_{HF} + \omega b^\dagger b - x(b^\dagger + b) + \frac{x^2}{\omega} + \omega(z b^\dagger + z^* b + z^* z) - x(z + z^*). \tag{2.122}$$

Choosing $z = \frac{x}{\omega}$ grants

$$\langle H \rangle = E_{HF} + \omega b^\dagger b. \tag{2.123}$$

Hence, an origin invariant mean-field energy is obtained, by applying this transformation to the Pauli-Fierz Hamiltonian, yielding the Hamiltonian, which is used throughout this thesis, as

$$H = H_e + \omega b^\dagger b - \sqrt{\frac{\omega}{2}}(\lambda \cdot (d - \langle d \rangle))(b^\dagger + b) + \frac{1}{2}(\lambda \cdot (d - \langle d \rangle))^2. \tag{2.124}$$

2.11.2. Polaritonic Hartree-Fock for the transformed Hamiltonian in the photonic vacuum

Since HF is derived for the ground state, the natural choice is to choose the fermionic system in the standard ground state determinant and the bosonic system in the vacuum. The basis is then build from the tensor product of the fock space with the photonic number states. Note, that the photonic number states are eigenfunctions of the harmonic oscillator, since the pure bosonic system is exactly determined by a harmonic oscillator, but explicit bosonic states are never required, since in the second quantized basis the bosonic field operators are the known ladder operators of the harmonic oscillator. Building the expectation value of the Hamiltonian with the tensor product of the ground state determinant and the photonic vacuum, for which the notation $|\Phi_I\rangle \otimes |n\rangle = \left|\Phi_{I,n}\right\rangle$ is used, gives

$$\begin{aligned} \left\langle \Phi_{0,0} \right| H \left| \Phi_{0,0} \right\rangle &= \left\langle \Phi_{0,0} \right| H_e + \omega b^\dagger b - \sqrt{\frac{\omega}{2}}(\lambda \cdot (d - \langle d \rangle))(b^\dagger + b) + \frac{1}{2}(\lambda \cdot (d - \langle d \rangle))^2 \left| \Phi_{0,0} \right\rangle \\ &= \left\langle \Phi_0 \right| H_e + \frac{1}{2}(\lambda \cdot (d - \langle d \rangle))^2 \left| \Phi_0 \right\rangle. \end{aligned} \tag{2.125}$$

Hence, H_e is shifted by a purely electronic contribution, containing a two and a one particle contribution, and evaluated in the purely fermionic basis. Therefore, the electronic contributions in H_e are merely shifted, so the polaritonic HF method, QED-HF, can be obtained with established methods. In order to do so, the shift to H_e is brought into normal order

$$\frac{1}{2}\sum_{pqrs}(\lambda \cdot d_{pr})(\lambda \cdot d_{qs}) a_p^\dagger a_r a_q^\dagger a_s = \frac{1}{2}\sum_{pqrs}(\lambda \cdot d_{pr})(\lambda \cdot d_{qs}) a_p^\dagger a_q^\dagger a_s a_r + \frac{1}{2}\sum_{pqr}(\lambda \cdot d_{pr})(\lambda \cdot d_{rq}) a_p^\dagger a_q, \tag{2.126}$$

using the fermionic commutation relations. Since the two particle field operator string is evaluated analogously to the electron repulsion integrals, one obtains the polaritonic Fock operator as

$$\begin{aligned} F_{pq} &= F_{pq,e} + \Big(\sum_i (\lambda \cdot d_{pq})(\lambda \cdot d_{ii}) - \sum_i (\lambda \cdot d_{pi})(\lambda \cdot d_{iq}) + \frac{1}{2} \sum_r (\lambda \cdot d_{pr})(\lambda \cdot d_{rq}) \\ &= F_{pq,e} + \frac{1}{2}\Big(- \sum_i (\lambda \cdot d_{pi})(\lambda \cdot d_{iq}) + \sum_a (\lambda \cdot d_{pa})(\lambda \cdot d_{aq})\Big) c_p^\dagger c_q, \end{aligned} \tag{2.127}$$

and the QED-HF energy as

$$E_{QED-HF} = E_{HF} + \frac{1}{2} \left\langle (\lambda \cdot (d - \langle d \rangle))^2 \right\rangle = E_{HF} + \frac{1}{2} \sum_{i,a} (\lambda \cdot d_{ia})^2. \tag{2.128}$$

Note, that to the nuclear repulsion energy the term $\frac{1}{2}(\lambda \cdot (\langle d \rangle))^2$ is added, which is a constant on the diagonal of the QED-Fock operator. It is further important to note, that the mean-field energy is origin invariant, but the QED-Fock operator is not. This can be seen by separating d into a diagonal part, which is origin dependent, $\langle d \rangle$ and the remainder d', which is origin independent, $d = \langle d \rangle + d'$. This way the QED-Fock operator can be separated into an origin invariant part and the non-invariant part

$$F_{pq} = F_{pq,origin-invariant} - (\lambda \cdot \langle d \rangle)(\lambda \cdot d'_{ij}) - \frac{1}{2}(\lambda \cdot \langle d \rangle)^2 \delta_{ij} + (\lambda \cdot \langle d \rangle)(\lambda \cdot d'_{ab}) + \frac{1}{2}(\lambda \cdot \langle d \rangle)^2 \delta_{ab}, \tag{2.129}$$

which partially cancels against the constant on the diagonal $\frac{1}{2}(\lambda \cdot (\langle d \rangle))^2$, yielding

$$F_{pq} = F_{pq,origin-invariant} - (\lambda \cdot \langle d \rangle)(\lambda \cdot d'_{ij}) + (\lambda \cdot \langle d \rangle)(\lambda \cdot d'_{ab}) + (\lambda \cdot \langle d \rangle)^2 \delta_{ab}. \tag{2.130}$$

2.12. Excitonic Renormalization

The excitonic renormalization method[28], XR, is a fragmentation approach, i.e. a super-system is divided in subsystems, which a referred to as fragments. These fragments are calculated separately and then the interaction betwenn the fragments is determined. A crucial difference of XR to other fragmentation approaches is, that the basis is constructed from the states $|\psi_i\rangle$ from all N fragments, in contrast to building the basis from determinants. The basis is then constructed from the globally antisymmetrized tensor product of all states from all fragments

$$|\Psi_I\rangle = |\psi_{i_1}\psi_{i_2}\cdots\psi_{i_N}\rangle, \tag{2.131}$$

where $I = (i_1, i_2, \cdots i_N)$ tracks the states and their corresponding fragments. Note, that these states are not orthonormal. However, by introducing a biorthogonal complement basis $\{\left|\Psi^I\right\rangle\}$, obeying $\left\langle\Psi^I\middle|\Psi_J\right\rangle = \delta_{IJ}$, a basis similar to the CC basis is constructed, which is also not orthonormal, but biorthogonal. This enables the introduction of second quantized operatos, the so-called fluctuation operators, as

$$\hat{\tau}^{j_m}_{k_m}\left|\psi_{i_1}\cdots\psi_{i_m}\cdots\psi_{i_N}\right\rangle = \delta_{j_m i_m}\left|\psi_{i_1}\cdots\psi_{k_m}\cdots\psi_{i_N}\right\rangle, \tag{2.132}$$

providing the following commutation relations

$$[\hat{\tau}^j_i, \hat{\tau}^l_k] = \delta_{jk}\hat{\tau}^l_i - \delta_{il}\hat{\tau}^k_j. \tag{2.133}$$

This ansatz enables separation of short and long range correlation, since the short range correlation is already covered by the states, which are now used to solve for the long range correlation. Furthermore, this leads to the possibility of truncation of the state space from each fragment, since correlated states are used as the fragment basis, which can already contain all the relevant correlation in very few states, instead of orbitals. The comparison of an excitation within the fluctuation operator basis and the second quantized basis acting on determinants is visualized in Figure 2.2.

Using the fluctuation operator basis, the Hamiltonian can be rewritten without approximation as

$$\begin{aligned}\hat{\mathcal{H}} = &\sum_m \sum_{\substack{I=(i_m)\\J=(j_m)}} \langle\Psi^I|\hat{H}_1|\Psi_J\rangle\hat{\tau}^{j_m}_{i_m} + \sum_{m_1<m_2}\sum_{\substack{I=(i_{m_1},i_{m_2})\\J=(j_{m_1},j_{m_2})}} \langle\Psi^I|\hat{H}_2|\Psi_J\rangle\hat{\tau}^{j_{m_1}}_{i_{m_1}}\hat{\tau}^{j_{m_2}}_{i_{m_2}}\\
&+ \sum_{m_1<m_2<m_3}\sum_{\substack{I=(i_{m_1},i_{m_2},i_{m_3})\\J=(j_{m_1},j_{m_2},j_{m_3})}} \langle\Psi^I|\hat{H}_3|\Psi_J\rangle\hat{\tau}^{j_{m_1}}_{i_{m_1}}\hat{\tau}^{j_{m_2}}_{i_{m_2}}\hat{\tau}^{j_{m_3}}_{i_{m_3}}\\
&+ \sum_{m_1<m_2<m_3<m_4}\sum_{\substack{I=(i_{m_1},i_{m_2},i_{m_3},i_{m_4})\\J=(j_{m_1},j_{m_2},j_{m_3},j_{m_4})}} \langle\Psi^I|\hat{H}_4|\Psi_J\rangle\hat{\tau}^{j_{m_1}}_{i_{m_1}}\hat{\tau}^{j_{m_2}}_{i_{m_2}}\hat{\tau}^{j_{m_3}}_{i_{m_3}}\hat{\tau}^{j_{m_4}}_{i_{m_4}},\end{aligned} \tag{2.134}$$

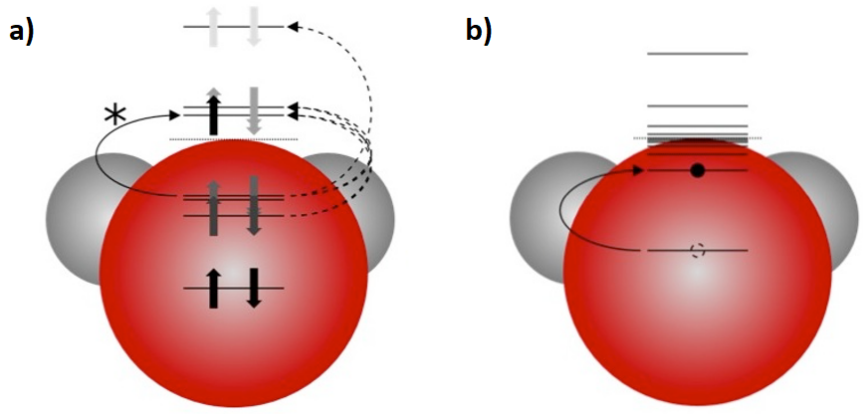

Figure 2.2.: Comparison between two second quantized operator bases, where a) shows a single excitation in the fluctuation operator basis and b) shows the corresponding excitation in the determinant basis. Both are shown in the orbital picture.

with $\hat{H}_i$ denoting the i body fragment contribution from the Hamiltonian. Since the Hamiltonian has at maximum four second quantized operators, it can only interact with four particles, which is why $\hat{\mathcal{H}} = \sum_{i=1}^{4} \hat{H}_i$, and therefore the expansion of the Hamiltonian in the fluctuation operator basis naturally truncates after the four fragment contribution. The i body fragment contributions to the Hamiltonian are then given by the single particle Hamiltonian

$$\hat{H} = \sum_{pqrs} h_q^p a_p^\dagger a^q + \sum_{pqrs} v_{rs}^{pq} a_p^\dagger a_q^\dagger a^s a^r, \tag{2.135}$$

where $h_q^p = \langle \Phi^p | \hat{h} | \Phi_q \rangle$ and $v_{rs}^{pq} = \frac{1}{4} \langle \Phi^p \Phi^q | \hat{v} | \Phi_r \Phi_s \rangle$, where the second quantized operators of each term need to act on particles of exactly i different fragments. Note, that these second quantized operators act on the orbitals of the single fragments $\{|\Phi_p\rangle\}$ and their biorthogonal complements $\{|\Phi^p\rangle\}$. Hence, only creation operators from one basis obey anticommutation relations with annihilation operators from the other basis, such that

$$[a_p^\dagger, a^q] = \delta_{pq}, \quad [a_p^\dagger, a_q^\dagger] = 0, \quad [a^p, a^q] = 0. \tag{2.136}$$

This suffices to evaluate the matrix elements in Eq. (2.134). The evaluation of the one fragment term is trivial, since it is only evaluated in the basis of one fragment, which is assumed to be orthogonal. Note, that in the following all states of a single fragment are assumed to be orthonormal. Therefore, it yields the diagonalized matrix of the method used to calculate the states for the individual fragment. The two fragment term can be evaluated as

$$\begin{aligned}\langle \psi^{i_1}\psi^{i_2}|\hat{H}_2|\psi_{j_1}\psi_{j_2}\rangle &= \langle h_2^1\rangle + \langle h_1^2\rangle + \langle v_{12}^{12}\rangle \\ &+\langle v_{21}^{11}\rangle + \langle v_{22}^{12}\rangle + \langle v_{12}^{22}\rangle + \langle v_{11}^{21}\rangle \\ &+\langle v_{22}^{11}\rangle + \langle v_{11}^{22}\rangle. \end{aligned} \tag{2.137}$$

Working equations can then be obtained by building the states from the vacuum states and fermionic field operators, as well as making use of the fact, that also the biorthogonal complements of the super-system are build from tensor products. The first term on the right hand side can then be evaluated as

$$\langle h_2^1\rangle = \sum_{p_1 q_2} h_{q_2}^{p_1} \left\langle \left| \hat{\psi}^{i_1}\hat{\psi}^{i_2}...\hat{\psi}^{i_N} a_{p_1}^{\dagger} a^{q_2} \hat{\psi}_{j_N}...\hat{\psi}_{j_2}\hat{\psi}_{j_1} \right| \right\rangle . \tag{2.138}$$

In order to evaluate the expectation value, the state operators need to be brought into their orbital representation. This is achieved by the relations

$$\hat{\psi}_{i_m}|\rangle = \left|\psi_{i_m}\right\rangle = \sum_{P_m} z_{i_m}^{P_m} \left|\Phi_{P_m}\right\rangle = \sum_{P_m} z_{i_m}^{P_m}\hat{\Phi}_{P_m}|\rangle \tag{2.139}$$

$$\langle|\hat{\psi}^{i_m} = \left\langle \psi^{i_m}\right| = \sum_{P_m} \bar{z}_{P_m}^{i_m} \left\langle \Phi^{P_m}\right| = \sum_{P_m} \bar{z}_{P_m}^{i_m} \langle|\hat{\Phi}^{P_m}, \tag{2.140}$$

where z is the coefficient vector building the corresponding state from the orbital basis of the fragment and $\bar{z}$ denotes its inverse. This yields

$$
\begin{aligned}
\langle h_2^1 \rangle &= \sum_{p_1 q_2} h_{q_2}^{p_1} \left\langle \left| \hat{\psi}^{i_1} \hat{\psi}^{i_2} \ldots \hat{\psi}^{i_N} a_{p_1}^\dagger a^{q_2} \hat{\psi}_{j_N} \ldots \hat{\psi}_{j_2} \hat{\psi}_{j_1} \right| \right\rangle \\
&= \sum_{p_1 q_2} h_{q_2}^{p_1} \sum_P \left\langle \left| \hat{\Phi}^{P_1} \hat{\Phi}^{P_2} \ldots \hat{\Phi}^{P_N} a_{p_1}^\dagger a^{q_2} \hat{\Phi}_{Q_N} \ldots \hat{\Phi}_{Q_2} \hat{\Phi}_{Q_1} \right| \right\rangle \prod_{m=1}^{N} \bar{z}_{P_m}^{i_m} z_{j_m}^{Q_m} \\
&= \sum_{p_1 q_2} h_{q_2}^{p_1} \sum_P \left\langle \left| \hat{\Phi}^{P_1} \hat{\Phi}^{P_2} a_{p_1}^\dagger a^{q_2} \hat{\Phi}_{Q_2} \hat{\Phi}_{Q_1} \right| \right\rangle \left\langle \left| \hat{\Phi}^{P_3} \ldots \hat{\Phi}^{P_N} \hat{\Phi}_{Q_N} \ldots \hat{\Phi}_{Q_3} \right| \right\rangle \prod_{m=1}^{N} \bar{z}_{P_m}^{i_m} z_{j_m}^{Q_m} \\
&= \sum_{p_1 q_2} h_{q_2}^{p_1} \sum_P \left\langle \left| \hat{\Phi}^{P_1} \hat{\Phi}^{P_2} a_{p_1}^\dagger a^{q_2} \hat{\Phi}_{Q_2} \hat{\Phi}_{Q_1} \right| \right\rangle \prod_{m=1}^{2} \bar{z}_{P_m}^{i_m} z_{i_m}^{P_m} \delta_{i_{3\ldots N} j_{3\ldots N}} \\
&= (-1)^{n_{i_2}} \sum_{p_1 q_2} h_{q_2}^{p_1} \sum_P \left\langle \left| \hat{\Phi}^{P_1} a_{p_1}^\dagger \hat{\Phi}_{Q_1} \right| \right\rangle \left\langle \left| \hat{\Phi}^{P_2} a^{q_2} \hat{\Phi}_{Q_2} \right| \right\rangle \prod_{m=1}^{2} \bar{z}_{P_m}^{i_m} z_{i_m}^{P_m} \delta_{i_{3\ldots N} j_{3\ldots N}} \\
&= (-1)^{n_{i_2}} \sum_{p_1 q_2} h_{q_2}^{p_1} \left\langle \left| \hat{\psi}^{i_1} a_{p_1}^\dagger \hat{\psi}_{j_1} \right| \right\rangle \left\langle \left| \hat{\psi}^{i_2} a^{q_2} \hat{\psi}_{j_2} \right| \right\rangle \delta_{i_{3\ldots N} j_{3\ldots N}} \\
&= (-1)^{n_{i_2}} \sum_{p_1 q_2} h_{q_2}^{p_1} \left\langle \psi^{i_1} \right| a_{p_1}^\dagger \left| \psi_{j_1} \right\rangle \left\langle \psi^{i_2} \right| a^{q_2} \left| \psi_{j_2} \right\rangle \delta_{i_{3\ldots N} j_{3\ldots N}} \\
&= (-1)^{n_{i_2}} \sum_{p_1 q_2} h_{q_2}^{p_1} \left\langle \psi_{i_1} \right| a_{p_1}^\dagger \left| \psi_{j_1} \right\rangle \left\langle \psi_{i_2} \right| a^{q_2} \left| \psi_{j_2} \right\rangle \delta_{i_{3\ldots N} j_{3\ldots N}} \\
&= (-1)^{n_{i_2}} \sum_{p_1 q_2} h_{q_2}^{p_1} \left\langle \psi_{i_1} \right| a_{p_1}^\dagger \left| \psi_{j_1} \right\rangle \left\langle \psi_{i_2} \right| a_{q_2} \left| \psi_{j_2} \right\rangle \delta_{i_{3\ldots N} j_{3\ldots N}} \\
&= (-1)^{n_{i_2}} \sum_{p_1 q_2} h_{q_2}^{p_1} \rho_{p_1} \rho^{q_2} \delta_{i_{3\ldots N} j_{3\ldots N}},
\end{aligned}
\tag{2.141}
$$

where the density, ρ, has been introduced and n_{i_2} denotes the number of electrons in the state i_2. $\langle h_1^2 \rangle$ can then be evaluated simply by applying symmetry considerations. In the following the Kronecker delta for the remaining state space will be dropped for brevity. The other expectation values can be evaluated analogously to

$$
\langle v_{12}^{12} \rangle = 4 \sum_{p_1 q_2 r_1 s_2} v_{r_1 s_2}^{p_1 q_2} \rho_{p_1}^{r_1} \rho_{q_2}^{s_2} \tag{2.142}
$$

$$
\langle v_{21}^{11} \rangle = 2(-1)^{n_{i_2}} \sum_{p_1 q_1 r_2 s_1} v_{r_2 s_1}^{p_1 q_1} \rho_{p_1 q_1}^{s_1} \rho^{r_2} \tag{2.143}
$$

$$
\langle v_{22}^{11} \rangle = \sum_{p_1 q_1 r_2 s_2} v_{r_2 s_2}^{p_1 q_1} \rho_{p_1 q_1} \rho^{s_2 r_2}. \tag{2.144}
$$

Hence, all that remains from the supersystem is a global phase, and the fragment Hamiltonian can be evaluated from just biorthogonalized atomic integrals and densities evaluated on single

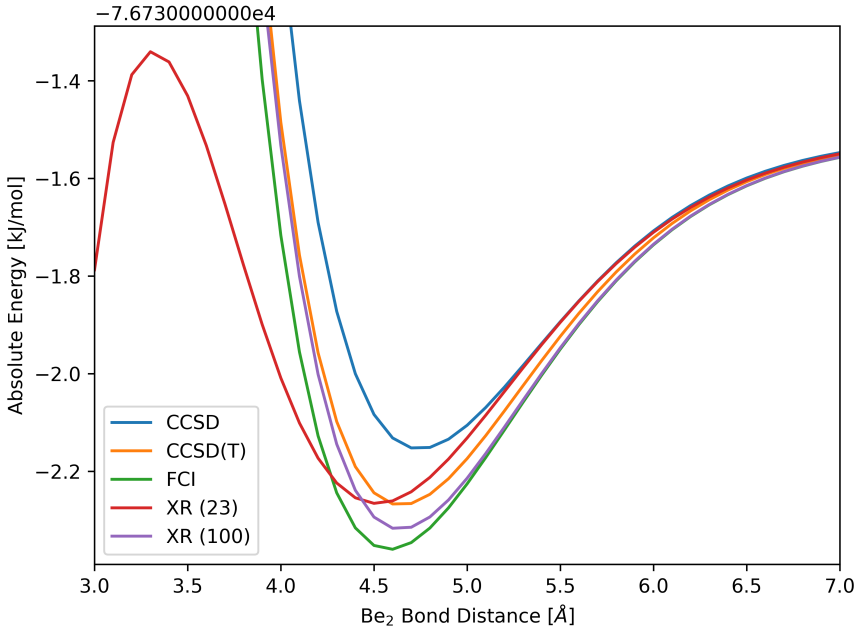

Figure 2.3.: Comparison of the Dissoziation curves of Be_2 in the 6-31G basis set. XR(n) denotes, that n FCI states have been used from the monomers. Note, that these states were optimized with respect to lowering the effective rank of the pseudo density, which builds the dimer ground state at FCI level. This procedure is described in more detail in the literature[29].

fragments. This is extremely powerful, since all correlation for the full system only needs to be evaluated for single fragments, which makes this approach in principle scale as the number of interactions after which the Hamiltonian is cut off, k, and the number of fragments N, as $\binom{N}{N-k}$. However, the numerical performance of this approach is rather poor if applied to a truncated state space, as shown in Figure 2.3.

This is due to the fact, that large non-hermitian terms can appear, e.g. core orbitals overlapping with unoccupied orbitals from an other fragment, because biorthogonality is only ensured for the full state space. This issue becomes more critical for short Be_2 bond lengths, as can be seen in Figure 2.3. The curve then seems to provide qualitatively wrong behaviour at short distances, but it shall be noted, that this can also be an artifact of the Be_2 system, which shows an additional even deeper minimum at a lower bond distance for FCI, if a large basis set is used. Using a less truncated state space on the other hand provides very good results, providing overall much higher accuracy than CCSD(T), but using this many states introduces a very large prefactor, so CCSD(T) will probably be faster even up to medium sized molecules, even though the XR approach only scales as N^4 in CPU time and memory. Hence, XR is required to achieve good accuracy for small state spaces in order to be of practical relevance. Ensuring biorthogonality in the truncated state space,

in the following denoted with a tilde, requires explicit biorthogonalization between the truncated spaces of the fragments required for the i body terms of the Hamiltonian. This is ensured by the super-system wavefunction for the truncated space $\left|\bar{\Psi}^{\tilde{I}}\right\rangle$, which obeys $\langle\bar{\Psi}^{\tilde{I}}|\Psi_{\tilde{J}}\rangle = \delta_{\tilde{I}\tilde{J}}$. Analogous to the biorthogonalization procedure, $\left|\bar{\Psi}^{\tilde{I}}\right\rangle$ can be obtained as

$$\langle\bar{\Psi}^{\tilde{I}}| = \sum_{\tilde{J}} \bar{S}^{\tilde{I}\tilde{J}}\langle\Psi_{\tilde{J}}|. \tag{2.145}$$

Using this a new, non-terminating, expansion of the Hamiltonian is obtained as

$$\begin{aligned}\hat{\tilde{\mathcal{H}}} &= \tilde{H}_0 + \sum_m \sum_{\substack{\tilde{i}_m \\ \tilde{j}_m}} \tilde{H}^{\tilde{i}_m}_{\tilde{j}_m}\, \hat{\tau}^{\tilde{j}_m}_{\tilde{i}_m} + \sum_{m_1<m_2} \sum_{\substack{\tilde{i}_{m_1},\tilde{i}_{m_2} \\ \tilde{j}_{m_1}\tilde{j}_{m_2}}} \tilde{H}^{\tilde{i}_{m_1}\tilde{i}_{m_2}}_{\tilde{j}_{m_1}\tilde{j}_{m_2}}\, \hat{\tau}^{\tilde{j}_{m_1}}_{\tilde{i}_{m_1}} \hat{\tau}^{\tilde{j}_{m_2}}_{\tilde{i}_{m_2}} \\ &\quad + \cdots + \sum_{\substack{\tilde{i}_{m_1},\cdots\tilde{i}_{m_N} \\ \tilde{j}_{m_1},\cdots\tilde{j}_{m_N}}} \tilde{H}^{\tilde{i}_{m_1}\cdots\tilde{i}_{m_N}}_{\tilde{j}_{m_1}\cdots\tilde{j}_{m_N}}\, \hat{\tau}^{\tilde{j}_{m_1}}_{\tilde{i}_{m_1}} \cdots \hat{\tau}^{\tilde{j}_{m_N}}_{\tilde{i}_{m_N}},\end{aligned} \tag{2.146}$$

with the matrix elements

$$\tilde{H}_0 = \langle|\hat{\boldsymbol{\mathcal{H}}}|\rangle = 0 \tag{2.147}$$

$$\tilde{H}^{\tilde{i}_m}_{\tilde{j}_m} = \langle\bar{\Psi}^{(\tilde{i}_m)}|\hat{\boldsymbol{\mathcal{H}}}|\Psi_{(\tilde{j}_m)}\rangle - \tilde{H}_0\, \delta_{\tilde{i}_m\tilde{j}_m} \tag{2.148}$$

$$\begin{aligned}\tilde{H}^{\tilde{i}_{m_1}\tilde{i}_{m_2}}_{\tilde{j}_{m_1}\tilde{j}_{m_2}} &= \langle\bar{\Psi}^{(\tilde{i}_{m_1},\tilde{i}_{m_2})}|\hat{\boldsymbol{\mathcal{H}}}|\Psi_{(\tilde{j}_{m_1},\tilde{j}_{m_2})}\rangle \\ &\quad - \tilde{H}^{\tilde{i}_{m_1}}_{\tilde{j}_{m_1}}\, \delta_{\tilde{i}_{m_2}\tilde{j}_{m_2}} - \tilde{H}^{\tilde{i}_{m_2}}_{\tilde{j}_{m_2}}\, \delta_{\tilde{i}_{m_1}\tilde{j}_{m_1}} - \tilde{H}_0\, \delta_{\tilde{i}_{m_1}\tilde{j}_{m_1}}\delta_{\tilde{i}_{m_2}\tilde{j}_{m_2}}.\end{aligned} \tag{2.149}$$

Truncating this expansion after the dimer interaction and evaluating the overlap and the Hamiltonian elements by brute force using FCI monomer states yields FCI accuracy for the dimer, even if the state space is massively truncated, as can be seen from Figure 2.4.

Hence, the dimer interaction is completely recovered. This approach is denoted as XR". However, this approach is not practical, since evaluating all terms by brute force is extremely demanding in terms of CPU time and memory. Nevertheless, once the XR matrix is build, quantum chemical methods can be easily derived to obtain the lowest eigenvalues, since the Hamiltonian is expanded in the second quantized fluctuation operator basis. For instance the CC variant for the dimer XR Hamiltonian results in a formal scaling of N^3 with the system size and N^4 with the number of states per fragment[29]. Note, that the number of states within each fragment is very small after truncation, so the XR-CC method can be evaluated at the cost of a mean-field calculation, roughly

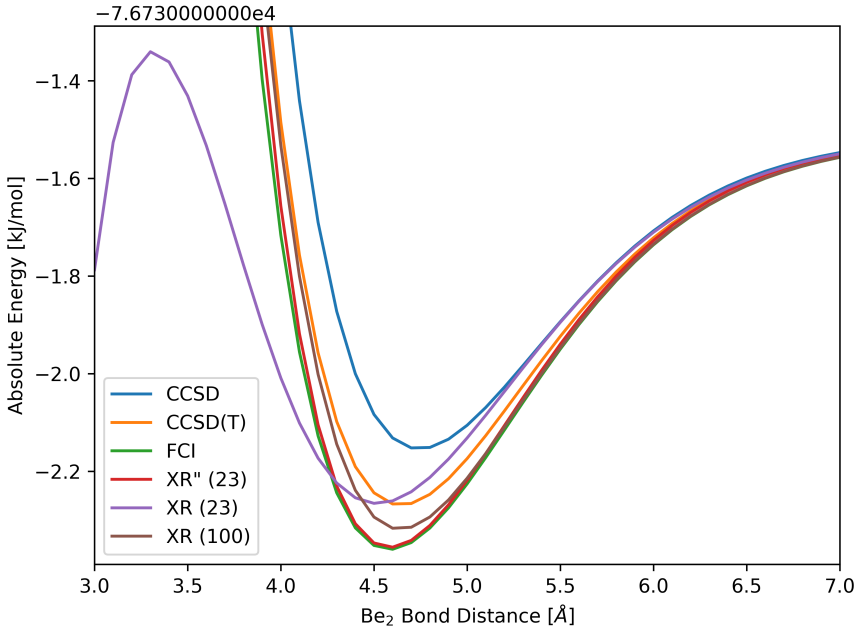

Figure 2.4.: Comparison of the methods shown in Figure 2.3 against the XR" method.

speaking. This can in principle already be applied to large clusters of small atoms and molecules, but in order to calculate chemically relevant systems three things need to be taken care of. First of all the brute force evaluation of the terms needs to be brought into a form similar to the non-hermitian ansatz, then densities other than FCI densities need to be used for the fragments and finally an algorithm needs to be developed, which is capable of calculating the almost optimal states, without building the density matrix of the full dimer.

3. Results and Discussion

3.1. Polaritonic Perturbation Theory

3.1.1. Computational Details

The newly developed polaritonic perturbation theory methods presented in the following were carried out with a development version of the adcc program package 0.15.14[58], which is located at https://github.com/BauerMarco. The QED-CCSD-1 and QED-HF calculations were conducted utilizing the Hilbert plugin 0.1[59] for the Psi4 program package 1.6[60]. For standard/non-polaritonic HF calculations the Psi4 program package was used. All calculations have been performed either on the hydrogenfluoride molecule, or in section 3.1.3 on pyrrole, using the cc-pVDZ basis set, as implemented in the Psi4 program package. The density-fitted implementations of the Hilbert package the JK-fitted cc-pVDZ basis set has been used. The bond-length of hydrogenfluoride was chosen as 0.917 Å and the bond-vector is always aligned with the polarization of the field. Pyrrole has been optimized using the Orca programm package 5.0.1[61] with the same basis sets and the resolution of identity variant of MP2. For the potential energy surfaces the N-H distance has been scanned in steps of 0.1 Angstroms from 0.7 to 4.5 Angstroms, along with the symmetrically sampled angle α around the N-H bond axis in the equilibrium geometry towards the normal axis of the aromatic plane, which was sampled with 10 datapoints in the interval $[-\frac{\pi}{2}, \frac{\pi}{2}]$. For simplicity the state space was reduced to the electronic ground state with a single photonic excitation and the electronic second excited state in the photonic vacuum. Note, that this state provides a different symmetry, than the states in the energetic vicinity and therefore also orthogonal transition dipole moments. Aligning the polarization of the cavity photon with the transition dipole moment can therefore be expected to yield negligible interactions to other states.The quantum dynamical simulations on these surfaces have then been carried out by Federico Mellini, using the multi-configurational time-dependent Hartree method as implemented in the Heidelberg MCTDH programm package 86[62], after fitting the surfaces with the potfit algorithm and interpolating using the chnpot algorithm as implemented in the same programm package. A complex absorbing potential has been introduced as well at a N-H distance of 2.2 Angstrom, to account for the loss of population through the conical intersection.

3.1.2. Polaritonic Møller-Plesset Perturbation Theory

In order to determine polaritonic MP, QED-MP, the Hamiltonian needs to be split analogous to section 2.3. This leads to two choices now, namely setting H_0 either to the non-polaritonic Fock operator, yielding QED-MP, or to the polaritonic Fock operator, yielding QED(np-HF)-MP. Both variants shall be examined in the following[63].

QED-MP

Using the polaritonic Fock operator for H_0 yields a diagonal H_0, since the eigenstates from it are used to span the Fock space. Hence, one obtains

$$H_0 = \sum_p \epsilon_p c_p^\dagger c_p + \omega b^\dagger b, \tag{3.1}$$

for the polaritonic mean-field in the photonic vacuum. Generalizing the two particle contribution of the purely electronic dipole term in the Hamiltonian, Eq. (2.124), to

$$\frac{1}{4} D_{pqrs} a_p^\dagger a_q^\dagger a_s a_r = \frac{1}{4} \left((\lambda \cdot d_{pr})(\lambda \cdot d_{qs}) - (\lambda \cdot d_{ps})(\lambda \cdot d_{qr}) \right) a_p^\dagger a_q^\dagger a_s a_r, \tag{3.2}$$

yields the the perturbation to the polaritonic mean-field as

$$\begin{aligned} H_1 = & - \sum_{pqk} \langle pk||qk\rangle \, a_p^\dagger a_q + \frac{1}{4} \sum_{pqrs} \langle pq||rs\rangle \, a_p^\dagger a_q^\dagger a_s a_r + \frac{1}{2} \sum_{pqrs} (\lambda \cdot d_{pr})(\lambda \cdot d_{qs}) a_p^\dagger a_q^\dagger a_s a_r \\ & - \sum_{pqk} (\lambda \cdot d_{pq})(\lambda \cdot \langle d \rangle \, \delta_{pq}) a_p^\dagger a_q + \sum_{pqk} (\lambda \cdot d_{pk})(\lambda \cdot d_{kq}) a_p^\dagger a_q \\ & - \sqrt{\frac{\omega}{2}} \sum_{pq} (\lambda \cdot (d_{pq} - \langle d \rangle_e \, \delta_{pq}))(b^\dagger + b) a_p^\dagger a_q \\ = & - \sum_{pqk} (\langle pk||qk\rangle + D_{pkqk}) a_p^\dagger a_q + \frac{1}{4} \sum_{pqrs} (\langle pq||rs\rangle + D_{pqrs}) a_p^\dagger a_q^\dagger a_s a_r \\ & - \sqrt{\frac{\omega}{2}} \sum_{pq} (\lambda \cdot (d_{pq} - \langle d \rangle \, \delta_{pq}))(b^\dagger + b) a_p^\dagger a_q. \end{aligned} \tag{3.3}$$

Hence, the purely electronic additional component to H_e in H_{PF} only leads to a shift of the electronic repulsion integrals, ERIs. Therefore only the term coupling electronic to photonic field requires explicit evaluation, since the other terms yield the standard MP working equations, see section 2.3, with shifted ERIs. With the energies defined as Eq. (2.11), and the zeroth order wavefunction only containing the photonic vacuum, see section 2.11.2, the coupling term yields

zero, and the standard MP working equations are obtained with shifted ERIs and eigenenergies of the QED-Fock operator. Hence, the zeroth and first order energies are found to be

$$E_0^{(0)} = \sum_i \epsilon_i \tag{3.4}$$

and

$$E_0^{(1)} = -\frac{1}{2} \sum_{ij} (\langle ij||ij\rangle + D_{ijij}). \tag{3.5}$$

The first order energy contribution can then be transformed to

$$\begin{aligned}
E_0^{(1)} &= -\frac{1}{2} \sum_{ij} (\langle ij||ij\rangle + D_{ijij}) \\
&= -\frac{1}{2} \sum_{ij} (\langle ij||ij\rangle + \big((\lambda \cdot d_{ii})(\lambda \cdot d_{jj}) - (\lambda \cdot d_{ij})(\lambda \cdot d_{ji})\big)) \\
&= -\frac{1}{2} \sum_{ij} (\langle ij||ij\rangle + \big((\lambda \cdot \langle d\rangle)^2 - (\lambda \cdot d_{ij})^2\big)) \\
&= -\frac{1}{2} \sum_{ij} (\langle ij||ij\rangle + \big((\lambda \cdot \langle d\rangle)^2 - (\lambda \cdot (d'_{ij} + \langle d\rangle))^2\big)) \\
&= -\frac{1}{2} \sum_{ij} (\langle ij||ij\rangle - 2(\lambda \cdot d'_{ij})(\lambda \cdot \langle d\rangle) - (\lambda \cdot d'_{ij})^2).
\end{aligned} \tag{3.6}$$

The origin dependent term here exactly cancels the origin dependent contribution in the occupied-occupied block of the QED-Fock operator, Eq. (2.130), and since the occupied orbitals are summed up, the first order QED-MP energy is origin invariant. This needs to be true, since the first order QED-MP energy is required to recover the QED-HF energy, which is by definition of the Hamiltonian origin invariant. However, the zeroth order energy and the higher order energies of QED-MP are not origin invariant, but the deviation is rather small, since the zeroth order contribution is cancelled by the first order contribution, so it comes into play at second order of perturbation theory. The higher order QED-MP wavefunctions, which are required for the higher order QED-MP energies are then obtained from Eq. (2.12), where the excitation class now summarizes electronic and photonic excitation classes. The resulting first order QED-MP wavefunction is then obtained as

$$\begin{aligned}\left|\Psi_0^{(1)}\right\rangle = &\sqrt{\frac{\omega}{2}}\sum_{ia}\frac{(\lambda\cdot d_{ia})}{\epsilon_a-\epsilon_i+\omega}\left|\Psi_{i,1}^{a}\right\rangle \\ &-\frac{1}{4}\sum_{ijab}\frac{\langle ab||ij\rangle + D_{abij}}{\epsilon_a+\epsilon_b-\epsilon_i-\epsilon_j}\left|\Psi_{ij,0}^{ab}\right\rangle,\end{aligned} \tag{3.7}$$

which yields the second order energy correction

$$E_0^{(2)} = -\frac{1}{4}\sum_{ijab}\frac{(\langle ij||ab\rangle + D_{ijab})^2}{\epsilon_a+\epsilon_b-\epsilon_i-\epsilon_j} - \frac{\omega}{2}\sum_{ia}\frac{(\lambda\cdot d_{ia})^2}{\epsilon_a-\epsilon_i+\omega}. \tag{3.8}$$

Note the additional term in the first order wavefunction, which has a contribution from the singly excited electronic determinant and a single excitation in the photon number space. This term yields the second term in the second order energy correction, which can be interpreted as a correction to the QED-HF energy, since if $\omega = \epsilon_a - \epsilon_i$, it is equal to minus one half times the additional energy of the Pauli-Fierz Hamiltonian to the standard Hamiltonian in Eq. (2.128). Also note, that for large ω the second order QED-MP correlation energy goes to minus infinity. However, as will be shown later, this overshoots the correlation energy of the corresponding polaritonic CCSD version, QED-CCSD-1[45, 64], only for large coupling strengths and photon energies far beyond the near-UV region, where the dipole approximation made in the Pauli-Fierz Hamiltonian breaks down anyway, see section 2.10.

QED(np-HF)-MP

Choosing the standard Fock operator for H_0 yields the perturbation

$$\begin{aligned}H_1 = &-\sum_{pqk}(\langle pk||qk\rangle + D_{pkqk})c_p^\dagger c_q \\ &+\frac{1}{4}\sum_{pqrs}(\langle pq||rs\rangle + D_{pqrs})c_p^\dagger c_q^\dagger c_s c_r \\ &-\sqrt{\frac{\omega}{2}}\sum_{pq}(\lambda\cdot(d_{pq}-\langle d\rangle_e\,\delta_{pq}))(b^\dagger+b)c_p^\dagger c_q \\ &+\frac{1}{2}\sum_{pqc}(\lambda\cdot d_{pc})(\lambda\cdot d_{cq})c_p^\dagger c_q \\ &-\frac{1}{2}\sum_{pqk}(\lambda\cdot d_{pk})(\lambda\cdot d_{kq})c_p^\dagger c_q + \frac{1}{2}(\lambda\cdot\langle d\rangle_e)^2.\end{aligned} \tag{3.9}$$

Using Eq. (2.11) yields the same zeroth order energy as for standard MP, while the first order energy is given as

$$\begin{aligned} E_0^{(1)} = &-\frac{1}{2}\sum_{ij}(\langle ij|\,|ij\rangle + D_{ijij}) + \frac{1}{2}(\lambda\cdot\langle d\rangle_e)^2 \\ &+\frac{1}{2}\sum_{ia}(\lambda\cdot d_{ia})(\lambda\cdot d_{ai}) - \frac{1}{2}\sum_{ij}(\lambda\cdot d_{ij})(\lambda\cdot d_{ji}). \end{aligned} \tag{3.10}$$

With Eq. (3.2) the shift in the ERI can be evaluated as

$$\begin{aligned} -\frac{1}{2}D_{ijij} &= -\frac{1}{2}\Big((\lambda\cdot d_{ii})(\lambda\cdot d_{jj}) - (\lambda\cdot d_{ij})(\lambda\cdot d_{ji})\Big) \\ &= -\frac{1}{2}(\lambda\cdot\langle d\rangle_e)^2 + \frac{1}{2}(\lambda\cdot d_{ij})(\lambda\cdot d_{ji}), \end{aligned} \tag{3.11}$$

which can be utilized to rewrite the first order energy correction as follows

$$E_0^{(1)} = -\frac{1}{2}\sum_{ij}\langle ij|\,|ij\rangle + \frac{1}{2}\sum_{ia}(\lambda\cdot d_{ia})(\lambda\cdot d_{ai}). \tag{3.12}$$

This can now be used to show, that the first order energy is again equal to Eq. (2.128)

$$E_0^{(0)} + E_0^{(1)} = E_{HF} + \frac{1}{2}\sum_{ia}(\lambda\cdot d_{ia})^2. \tag{3.13}$$

The first order wavefunction is the same as Eq. (3.7) plus an additional contribution, which is

$$\begin{aligned} &\frac{1}{2}\left|\Psi_{i,0}^a\right\rangle\left(\sum_k\frac{(\lambda\cdot d_{ak})(\lambda\cdot d_{ki})}{\epsilon_a-\epsilon_i} - \sum_c\frac{(\lambda\cdot d_{ac})(\lambda\cdot d_{ci})}{\epsilon_a-\epsilon_i}\right) \\ &= \frac{1}{2}t_{ia,0}\left|\Psi_{i,0}^a\right\rangle, \end{aligned} \tag{3.14}$$

which yields the second order energy correction as

$$E_0^{(2)} = -\frac{1}{4}\sum_{ijab}\frac{(\langle ij||ab\rangle + D_{ijab})^2}{\epsilon_a+\epsilon_b-\epsilon_i-\epsilon_j} - \frac{\omega}{2}\sum_{ia}\frac{(\lambda\cdot d_{ia})^2}{\epsilon_a-\epsilon_i+\omega} - \frac{1}{4}\sum_{ia}(t_{ia,0})^2(\epsilon_a-\epsilon_i). \tag{3.15}$$

Numerical results

As already pointed out in section 2.7, a connection between CC and MP exists, which can be used to test the implementation and compare numerical results of QED-MP and QED(np-HF)-MP, since an independent implementation for the corresponding polaritonic CC approach exists. This polaritonic CC approach is called QED-CCSD-1 and uses the QED-HF reference, while otherwise following the derivation in section 2.7 using the Hamiltonian from Eq. (2.124) and the same tensor product basis as used here. However, the initial guess of the QED-CCSD-1 method only uses the photonic vacuum. Hence, the shifted ERI contribution in the second order energy correction has to be equal to the correlation energy of the QED-CCSD-1 guess. This comparison along with the full correlation energies of QED-CCSD-1, QED-MP and QED(np-HF)-MP are shown in Figure 3.1.

Note, that the QED-Fock operator in the QED-HF implementation differs slightly from Eq. (2.127), since the quadratic term in Eq. (2.124) is treated different, which does however not affect QED-PT, but only QED(np-HF)-PT. This leads to a numerical inconsistency for QED(np-HF)-MP, and later also QED(np-HF)-ADC, which however can be considered negligibly small. Now one can see, that for all coupling strengths and photon energies the difference between the correlation energy of the initial guess of QED-CCSD-1 and the shifted ERI contribution in QED-MP is on the order of the Cholesky treshhold of $10^{-9} a.u.$. This test ensures, that most of the implementation is correct, since the shift of the ERIs also depends on $\lambda \cdot d$. It shall also be noted, that the additional term in the second order correlation energy in QED(np-HF)-MP compared to QED-MP recovers most of the mean-field correction from QED-HF compared to HF. As indicated by the correlation energy of QED-CCSD-1, this difference is negligible for small coupling strengths, since it is much smaller than the correlation energy, but fully iterating the mean-field in the QED-HF approach can be expected to have non-negligible impact on the accuracy for strong coupling strengths. It can also be seen, that the additional contribution in the QED-MP2 correlation energy corrects the QED-MP2 energy from the initial guess of QED-CCSD-1 toward the fully iterated QED-CCSD-1. For QED-MP2 the correction from the initial guess to the fully iterated QED-CCSD-1 is only overshooted, i.e. it starts to diverge, at $\lambda = 0.06$ and $\lambda = 0.10$ with $\omega = 1.6 a.u.$ and $\omega = 0.9 a.u.$, respectively. Therefore, divergence of the additional term in the QED-MP2 correlation energy is only expected for hard UV cavity photons, where the dipole approximation starts to break down anyway, even for strong coupling strengths. Hence, for practical calculations in the strong coupling regime QED-MP is recommended. For small coupling strengths the difference in the absolute energy between the full QED-MP2 and the full QED(np-HF)-MP2 approach are much smaller than the purely electronic correlation energy, and therefore both approaches can be considered as equally accurate. This also indicates, that for small coupling strengths field free references can be used in general, which also

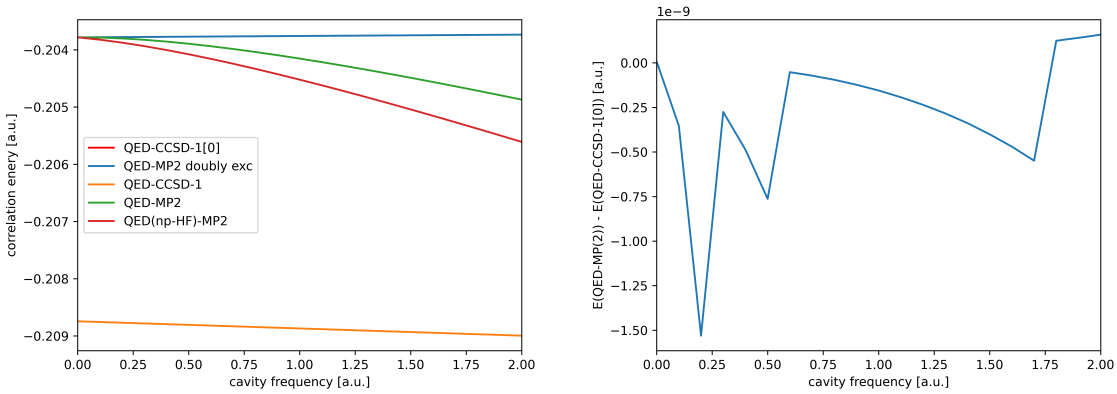

(a) $\lambda = 0.02$ **(b)** $\lambda = 0.02$

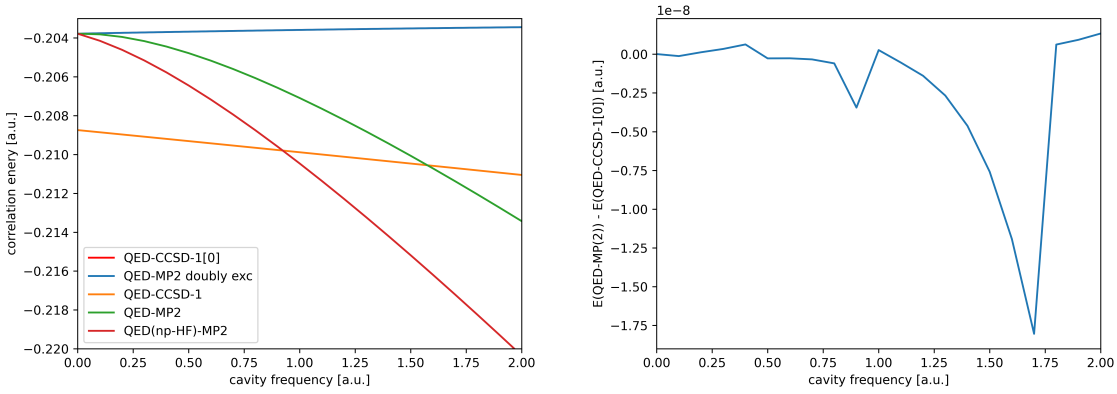

(c) $\lambda = 0.06$ **(d)** $\lambda = 0.06$

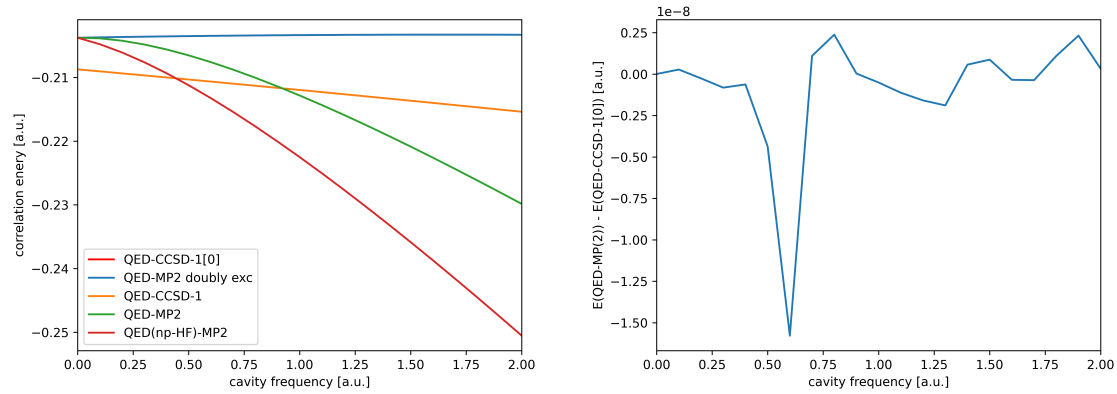

(e) $\lambda = 0.10$ **(f)** $\lambda = 0.10$

Figure 3.1.: a), c) and e) Show the comparison of the correlation energies of hydrogenfluoride computed at the level of QED-MP2, "QED-MP2 doubly exc", which is only the adapted standard MP2 contribution, QED(np-HF)-MP2, QED-CCSD-1 and its initial guess QED-CCSD-1[0]. b), d) and f) visualize the difference between "QED-MP2 doubly exc" and QED-CCSD-1[0]. The HF, QED-HF and QED-CCSD-1 calculations have been carried out using Cholesky decomposition of the ERIs.

motivates building the polaritonic matrix using field free states and calculating the polaritonic couplings from them, according to the Pauli-Fierz Hamiltonian. By now this is the most common approach to polaritonic states, since no new non-adiabatic coupling elements need to be derived, while still being reasonably accurate for weak coupling strengths, making it especially useful for dynamic simulations. This ansatz will be discussed in more detail later. In the strong coupling regime QED-MP2 was shown to be reasonably accurate, while outscaling QED-CCSD-1, since the scalings are the same as for the corresponding non-polaritonic methods, and is therefore the recommended method for medium up to large sized molecules. It shall be noted here, that since QED(np-HF)-MP uses an origin invariant reference, it is origin invariant through all orders of perturbation theory, as can be seen for the second order contribution, where only the $t_{ia,0}$-amplitude provides origin dependent terms, which cancel themselves out, since the nuclear contribution is the same on all diagonal elements, independent of whether they appear in the purely occupied or the purely virtual block of the dipole matrix. Nevertheless, since this is only necessary for very few applications, QED-MP is preferred, since these methods only need to be applied for intermediate and high coupling strengths, where QED-MP is more accurate, while also due to the additional contribution from $\left|\Psi^a_{i,0}\right\rangle$ in the first order wavefunction of QED(np-HF)-MP, the corresponding ADC variant contains significantly more terms, which makes it slower and much more tedious to derive.

3.1.3. Polaritonic Algebraic Diagrammatic Construction Theory

As already examined in section 3.1.2, two formulations for polaritonic MP can be thought of as natural polaritonic expansions MP, depending on the partitioning of the Hamiltonian. Since ADC depends on MP, see section 2.4, two formulations of ADC can be carried out, depending on which polaritonic MP is chosen as reference. Following the derivation presented in section 2.4, with the polaritonic Hamiltonian and the polaritonic MP reference, requires the extension of the ISR basis. Using the previous notation for the matter-field tensor product states, the polaritonic ADC matrix in the adapted ISR basis is given as

$$\left\langle \tilde{\Psi}_{I,N} \right| H - E_0 \left| \tilde{\Psi}_{J,M} \right\rangle, \tag{3.16}$$

where the ISR basis is build from the adapted electronically and photonically excited basis, used to expand the wavefunctions of the corresponding MP method, Eqs. (3.7) and (3.14)[63].

QED-ADC

The QED-MP method and the corresponding partitioning of the Hamiltonian lead to the QED-ADC method. The adapted polaritonic ISR basis is then build from the adapted polaritonic precursor states

$$\left|\Psi^{\#}_{I,0}\right\rangle^{(0)} = C_I \left|\Psi^{(0)}_{0,0}\right\rangle \tag{3.17a}$$

$$\left|\Psi^{\#}_{I,0}\right\rangle^{(1)} = C_I \left|\Psi^{(1)}_{0,0}\right\rangle \tag{3.17b}$$

$$\left|\Psi^{\#}_{I,1}\right\rangle^{(0)} = C_I \left|\Psi^{(0)}_{0,1}\right\rangle \tag{3.17c}$$

$$\begin{aligned}\left|\Psi^{\#}_{I,1}\right\rangle^{(1)} &= C_I \left|\Psi^{(1)}_{0,1}\right\rangle - \left|\Psi^{(0)}_{0,0}\right\rangle \left\langle\Psi^{(0)}_{0,0}\right| C_{I,1} \left|\Psi^{(0)}_{0,0}\right\rangle^{(1)} \\ &= C_I \left|\Psi^{(1)}_{0,1}\right\rangle - \sqrt{\frac{\omega}{2}} \frac{(\lambda \cdot d_{ia})}{\epsilon_a - \epsilon_i + \omega} \left|\Psi^{(0)}_{0,0}\right\rangle .\end{aligned} \tag{3.17d}$$

Note, that the orthogonolization is carried out with respect to the photonic excitations as well. Further note, that the precursor states have already been truncated, because in principle the photonic excitations go up to infinity. These photonically higher excited states are equal to those given here, with the difference, that for a photonic excitation of N the second term in Eq. (3.17d) is multiplied with a factor of $\sqrt{N}$. However, this would yield in an infinitely large matrix with a band structure, which provides a width of one, since a photonic excitation of N only interacts with photonic excitations of $N - 1$ and $N + 1$ in QED-ADC(1). The implicit coupling to even higher and lower photonic excitations is very small, i.e. for Hydrogenfluoride, where the cavity field is aligned with the bond vector, the first bright excitation which is intermediately strong coupled to the singly excited photon field, including double photon excitations alters the excitation energies by up to a few meV. This error is almost two orders of magnitude smaller than the mean absolute error, MAE, of even ADC(2) and ADC(3) and therefore negligible. Note, that this error might become significant for some systems at very strong couplings for QED-ADC(1), however, for QED-ADC(2) the doubly excited photon number space is included and the influence of triply excited photon number states on couplings based on the photonic ground and first excited state are significantly smaller. Hence, for practically relevant calculations restricting the photon number state space to a maximum of two

will lead to negligible errors. Nevertheless, for practical reasons QED-ADC(0) and QED-ADC(1) will be restricted to singly excited photon number states, yielding the QED-ADC(1) matrix as

$$\begin{pmatrix} \left\langle \tilde{\Psi}_{I,0} \right| H - E_0 \left| \tilde{\Psi}_{J,0} \right\rangle & \left\langle \tilde{\Psi}_{I,0} \right| H - E_0 \left| \tilde{\Psi}_{J,1} \right\rangle \\ \left\langle \tilde{\Psi}_{I,1} \right| H - E_0 \left| \tilde{\Psi}_{J,0} \right\rangle & \left\langle \tilde{\Psi}_{I,1} \right| H - E_0 \left| \tilde{\Psi}_{J,1} \right\rangle \end{pmatrix}. \tag{3.18}$$

For the Loewdin orthogonalization the inverse square root is then required, which is given by

$$S^{-\frac{1}{2}}_{I,N;J,M} = \delta_{I,N;J,M} - \frac{1}{2} S^{(2)}_{I,N;J,M} \tag{3.19}$$

up to second order, because the zeroth and first order of the overlap matrix are given by $\delta_{I,N;J,M}$ and 0, respectively. This simplifies the QED-ADC(0) and QED-ADC(1) matrix to

$$\begin{pmatrix} \left\langle \Psi^{\#}_{I,0} \right| H - E_0 \left| \Psi^{\#}_{J,0} \right\rangle & \left\langle \Psi^{\#}_{I,0} \right| H - E_0 \left| \Psi^{\#}_{J,1} \right\rangle \\ \left\langle \Psi^{\#}_{I,1} \right| H - E_0 \left| \Psi^{\#}_{J,0} \right\rangle & \left\langle \Psi^{\#}_{I,1} \right| H - E_0 \left| \Psi^{\#}_{J,1} \right\rangle \end{pmatrix}. \tag{3.20}$$

The zeroth order contributions are then given by

$$\left\langle \Psi^{\#}_{I,0} \right| H - E_0 \left| \Psi^{\#}_{J,0} \right\rangle^{(0)} = \delta_{ij}\delta_{ab}(\epsilon_a - \epsilon_i) \tag{3.21a}$$

$$\left\langle \Psi^{\#}_{0,1} \right| H - E_0 \left| \Psi^{\#}_{0,1} \right\rangle^{(0)} = \omega \tag{3.21b}$$

$$\left\langle \Psi^{\#}_{I,1} \right| H - E_0 \left| \Psi^{\#}_{J,1} \right\rangle^{(0)} = \delta_{ij}\delta_{ab}(\epsilon_a - \epsilon_i + \omega), \tag{3.21c}$$

while the first order contributions are

$$\begin{aligned} &\left\langle \Psi^{\#}_{I,0} \right| H - E_0 \left| \Psi^{\#}_{J,0} \right\rangle^{(1)} = \left\langle \Psi^{\#}_{I,1} \right| H - E_0 \left| \Psi^{\#}_{J,1} \right\rangle^{(1)} \\ &= -(\langle aj| \, |bi\rangle + D_{ajbi}) \end{aligned} \tag{3.22a}$$

$$\left\langle \Psi^{\#}_{I,1} \right| H - E_0 \left| \Psi^{\#}_{J,0} \right\rangle^{(1)} = -\sqrt{\frac{\omega}{2}}(\delta_{ij}(\lambda \cdot d_{ab}) - \delta_{ab}(\lambda \cdot d_{ij})) \tag{3.22b}$$

$$\left\langle \Psi^{\#}_{0,1} \right| H - E_0 \left| \Psi^{\#}_{J,0} \right\rangle^{(1)} = -\sqrt{\frac{\omega}{2}}(\lambda \cdot d_{jb}) \tag{3.22c}$$

$$\left\langle \Psi^{\#}_{I,0} \right| H - E_0 \left| \Psi^{\#}_{J,1} \right\rangle^{(1)} = -\sqrt{\frac{\omega}{2}}(\delta_{ij}(\lambda \cdot d_{ab}) - \delta_{ab}(\lambda \cdot d_{ij})) \tag{3.22d}$$

$$\left\langle \Psi^{\#}_{I,0} \right| H - E_0 \left| \Psi^{\#}_{0,1} \right\rangle^{(1)} = -\sqrt{\frac{\omega}{2}}(\lambda \cdot d_{ai}). \tag{3.22e}$$

Note, that in principle new QED-HF and QED-MP solutions are required here for the electronic ground state with a single photonic excitation, since $\omega b^\dagger b$ is part of the mean-field. However, these mean-field terms do not couple with the electronic space. Hence, the QED-HF and therefore also the QED-MP solution stay the same, apart from the energy of the photon number state, which is simply added to the total energy. For the QED-ADC(2) working equations the matrix then has to be extended to the doubly excited photon number states, because the explicitly couple to the photonic vacuum now, i.e. they are not zero anymore. Furthermore, the second order expansion of the squared inverse of the overlap matrix is not diagonal anymore. Carrying out the evaluation yields the working equations as

$\left\langle \tilde{\Psi}_{I,0} \right| H - E_0 \left| \tilde{\Psi}_{J,0} \right\rangle$:

$$\begin{aligned} \left\langle \tilde{\Psi}^a_{i,0} \right| H - E_0 \left| \tilde{\Psi}^b_{j,0} \right\rangle^{(2)} = \frac{\omega}{4} \Bigg(& \delta_{ij}(1 + P_{ab}) \sum_k t_{kb,1}(\lambda \cdot d_{ka}) \\ & + \delta_{ab}(1 + P_{ij}) \sum_c t_{jc,1}(\lambda \cdot d_{ic}) - (1 + P_{ij}P_{ab}) t_{ia,1}(\lambda \cdot d_{jb}) \Bigg) \end{aligned} \tag{3.23}$$

$\left\langle \tilde{\Psi}_{I,1} \right| H - E_0 \left| \tilde{\Psi}_{J,0} \right\rangle$:

$$\left\langle \tilde{\Psi}_{0,1} \right| H - E_0 \left| \tilde{\Psi}^b_{j,0} \right\rangle^{(2)} = \sqrt{\frac{\omega}{2}} \sum_{kc} t_{jkbc}(\lambda \cdot d_{kc}) \tag{3.24}$$

$$\begin{aligned} \left\langle \tilde{\Psi}^a_{i,1} \right| H - E_0 \left| \tilde{\Psi}^b_{j,0} \right\rangle^{(2)} = \sqrt{\frac{\omega}{2}} \Bigg(& \delta_{ij} \sum_{kc} t_{kc,1} \langle ka || cb \rangle \\ & + \delta_{ab} \sum_{kc} t_{kc,1} \langle kj || ic \rangle + \sum_k t_{ka,1} \langle jk || ib \rangle + \sum_c t_{ic,1} \langle ja || bc \rangle \Bigg) \end{aligned} \tag{3.25}$$

$$\begin{aligned} & \left\langle \tilde{\Psi}^a_{i,1} \right| H - E_0 \left| \tilde{\Psi}^{bc}_{jk,0} \right\rangle^{(1)} = \\ & - \sqrt{\frac{\omega}{2}} (1 - P_{jk})(1 - P_{bc}) \delta_{ij} \delta_{ab} (\lambda \cdot d_{kc}) \end{aligned} \tag{3.26}$$

$\left\langle \tilde{\Psi}_{I,2} \right| H - E_0 \left| \tilde{\Psi}_{J,0} \right\rangle$:

$$\begin{aligned}\left\langle \tilde{\Psi}^a_{i,2} \right| H - E_0 \left| \tilde{\Psi}^b_{j,0} \right\rangle^{(2)} = -\frac{\omega}{2}\sqrt{2}\Bigg(\delta_{ab}\delta_{ij} \sum_{kc} t_{kc,1}(\lambda \cdot d_{kc}) \\ - \delta_{ij} \sum_{k} t_{ka,1}(\lambda \cdot d_{kb}) - \delta_{ab} \sum_{k} t_{ic,1}(\lambda \cdot d_{jc}) \Bigg).\end{aligned} \tag{3.27}$$

The remaining non-zero blocks are either hermitian conjugates, or both photon number states of a block need to be increased by one, yielding an additional global factor to the block, given by the bosonic field operators. This is due to the fact, that the bosonic field operators are essentially ladder operators of the harmonic oscillator, where e.g. a deexcitation from one to zero yields an additional factor of $\sqrt{1}$, hence not affecting the result, while a deexcitation from the second to the first excited state yields an additional factor of $\sqrt{2}$. It shall be noted, that as for QED-MP the first order method, i.e. QED-ADC(1), is origin-invariant, since all origin-dependent terms in D_{ajbi} cancel with the origin dependent terms in $\delta_{ij}\delta_{ab}(\epsilon_a - \epsilon_i)$. Hence, higher order QED-ADC method only contain origin-dependent terms from second order and higher, which makes them rather small.

QED(np-HF)-ADC

The QED(np-HF)-MP method and the corresponding partitioning of the Hamiltonian lead to the QED(np-HF)-ADC method. This yields the same zeroth order precursor states as in section 3.1.3, but the first order precursor states now read

$$\left| \Psi^{\#}_{I,0} \right\rangle^{(1)} = C_I \left| \Psi^{(1)}_{0,0} \right\rangle - \frac{1}{2} t^{(1)}_{ia,0} \left| \Psi^{(0)}_{0,0} \right\rangle \tag{3.28a}$$

$$\left| \Psi^{\#}_{I,1} \right\rangle^{(1)} = C_I \left| \Psi^{(1)}_{0,1} \right\rangle - \sqrt{\frac{\omega}{2}} \frac{(\lambda \cdot d_{ia})}{\epsilon_a - \epsilon_i + \omega} \left| \Psi^{(0)}_{0,0} \right\rangle - \frac{1}{2} t^{(1)}_{ia,0} \left| \Psi^{(0)}_{0,1} \right\rangle . \tag{3.28b}$$

Note, that this basis has been truncated for the same reason as discussed in section 3.1.3, while also the same procedure can be applied to obtain higher photon number states. Hence, the QED(np-HF)-ADC matrix has the same band structure as the corresponding QED-ADC method. Since the zeroth order precursor states are equal to those in section 3.1.3, the working equations in zeroth order are also the same, apart from the fact, that the orbital energies are now obtained from standard HF, instead of QED-HF. The first order equations are also equal for the off-diagonal blocks, where off-diagonal refers to the photon number states, but the new diagonal blocks are

$$\begin{aligned}\left\langle \Psi^{\#}_{I,0} \right| H - E_0 \left| \Psi^{\#}_{J,0} \right\rangle^{(1)} &= -(\langle aj| \, |bi\rangle + D_{ajbi}) \\ &- \frac{1}{2}\delta_{ij} t^{(1)}_{ab,0}(\epsilon_a - \epsilon_b) + \frac{1}{2}\delta_{ab} t^{(1)}_{ij,0}(\epsilon_i - \epsilon_j)\end{aligned} \tag{3.29}$$

and

$$\begin{aligned}\left\langle \Psi^{\#}_{I,1} \right| H - E_0 \left| \Psi^{\#}_{J,1} \right\rangle^{(1)} &= -(\langle aj| \, |bi\rangle + D_{ajbi}) \\ &- \frac{1}{2}\delta_{ij} t^{(1)}_{ab,0}(\epsilon_a - \epsilon_b) + \frac{1}{2}\delta_{ab} t^{(1)}_{ij,0}(\epsilon_i - \epsilon_j) + \delta_{ij}\delta_{ab}\omega.\end{aligned} \tag{3.30}$$

As already mentioned in section 3.1.2, the first order QED(np-HF)-MP wavefunction contains an additional contribution from a singly electronically excited determinant in the photonic vacuum. This additional contribution increased the amount of additional terms in QED(np-HF)-ADC(1) only very slightly with respect to QED-ADC(1), but significantly increases the amount of terms for the corresponding second order matrices. Hence, QED(np-HF)-ADC was only derived up to first order. Note, that the higher excited photon number state blocks can also be evaluated with the same procedure examined in section 3.1.3. It shall also be noted, that QED(np-HF)-ADC is origin invariant through all orders of perturbation theory, like its corresponding ground state.

Testing

As can be seen from section 2.4 the ADC(1) matrix is equal to the CIS matrix, without the ground state. Since a polaritonic CIS method[65], QED-CIS, exists, which is based on the QED-HF reference, the QED-ADC(1) method can be tested, because like for the non-polaritonic methods these methods are equal apart from their ground state contributions. Hence, the QED-CIS matrix without the ground state and the ground to excited state coupling blocks, needs to yield the same eigenvalues as QED-ADC(1). This has been tested to be true to numerical precision. However, no method exists, which should yield similar results to the QED-ADC(2) matrix, so the QED-ADC(2) method can only be tested on its implementation and not its derivation. A detailed explanation for this testing procedure can be found in section 3.1.3. For numerical comparison QED-ADC(1), QED-ADC(2) and QED(np-HF)-ADC(1) have been applied to Hydrogenfluoride again, where the setup of the calculation was analogous to the one in section 3.1.2. These numerical results are visualized in Figure 3.2.

Note, that for better comparison the first order methods have been computed with doubly excited photon number states, as is required for the second order method. All methods yield qualitatively

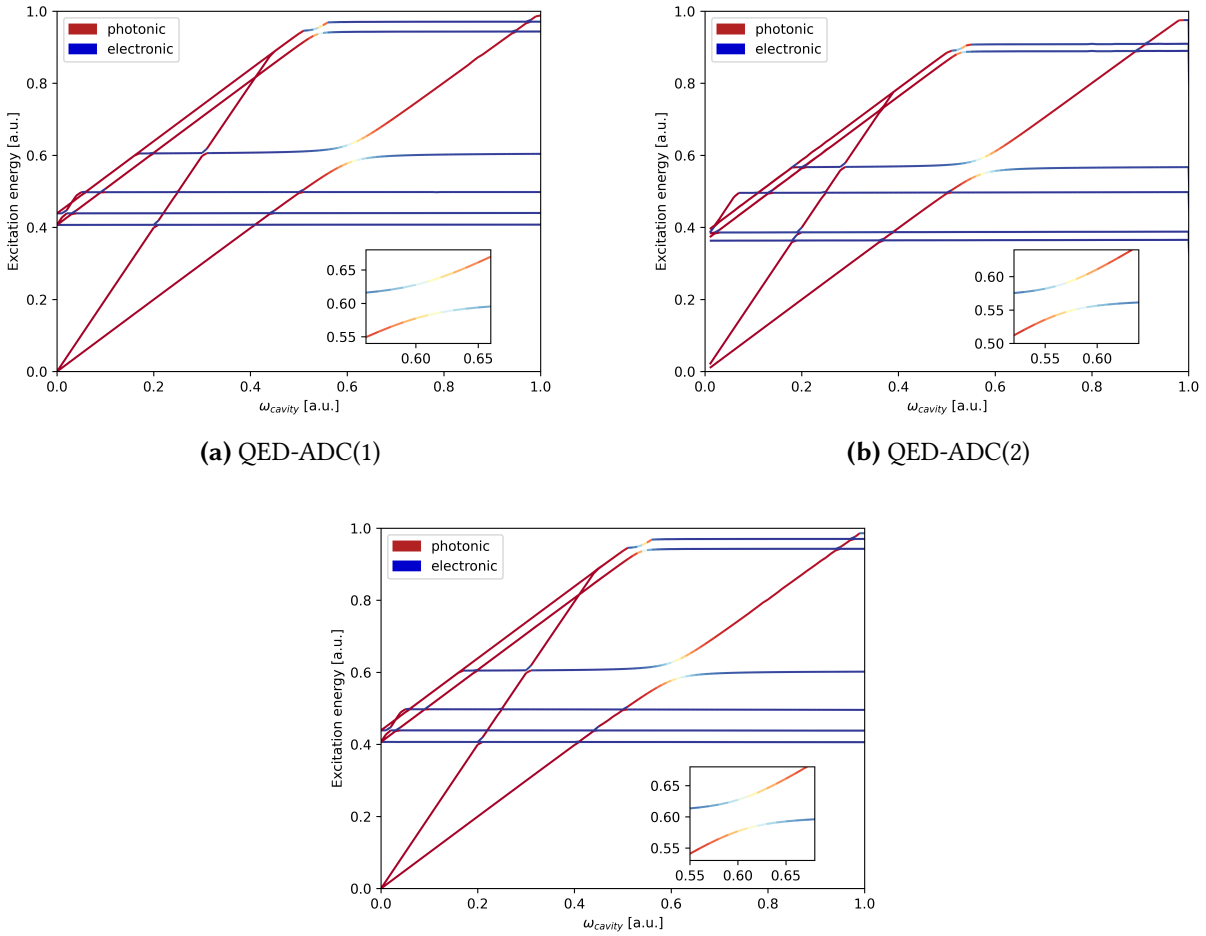

(a) QED-ADC(1)

(b) QED-ADC(2)

(c) QED(np-HF)-ADC(1)

Figure 3.2.: Excitation energies of the 11 energetically lowest excited states of Hydrogenfluoride computed at different levels of theory for a coupling strength of $\lambda = 0.05$ against the energy of the cavity photon. Polariton formation is shown in the insets. Note, that all methods include the doubly excited photon number space. Furthermore, the electronic and photonic character is determined by the norm of the corresponding part of the QED-ADC vector.

equal results, which are also qualitatively equal to published scans generated from equation of motion variant of QED-CCSD-1[45], apart from the doubly excited photon number states, which are not included in the literature approach. The insets show the polariton with the largest Rabi-splitting, which is roughly 1 eV. For this rather large splitting QED-ADC(1), Figure 3.2a, and QED(np-HF)-ADC(1), Figure 3.2c, deviate by only 22 meV for the upper and less for the lower polariton. This shows, that even for intermediate coupling strengths QED-ADC(1) and QED(np-HF)-ADC(1) yield differences in energy, which are roughly one order of magnitude smaller than the MAE of ADC(2). This is in line with the result from section 3.1.2, emphasizing that taking the full mean-field of

the Pauli-Fierz Hamiltonian does indeed become important for intermediate to strong couplings, but is negligible for weak to intermediate couplings. This is concluded on the fact, that an error in relative energy of one order of magnitude less than the MAE of a method can be considered a significant contribution already, while the intermediate coupling strength is not clearly defined either. Note, that the above mentioned deviation of 22 meV is compromised though, see section 3.1.2, and therefore actually might slightly deviate, if the Hamiltonian was treated consistently in the QED-HF calculation. Furthermore, given this small deviation, as well as the small number of additional terms in QED(np-HF)-ADC(1) compared to QED-ADC(1), which has been tested already, the QED(np-HF) family of perturbation methods can be considered tested as well.

QED-npADC

Since no method exists, providing contributions similar to QED-ADC(2), a different testing procedure needs to be applied here. Here, a unitary transformation is applied to the QED-ADC(2) matrix, so it is build from different contributions now, similar to the field free approach described in section 3.1.2. The most simple way to do this, is using the states, which are closest to the QED-ADC(2) states, but still remain in the photonic vacuum. These are given by diagonalizing the non-polaritonic Hamiltonian with the squared dipole term of the Pauli-Fierz Hamiltonian. Doing this with QED-ADC requires solving QED-HF and using these orbitals with the shifted ERIs, see section 3.1.2, in the standard MP and ADC methods. In the next step the dipole and perturbation, i.e. full Hamiltonian minus mean-field Hamiltonian, operators need to be evaluated using the ISR and the previously obtained ADC states, including the photonic vacuum field, according to the procedure described in section 2.5. This alters the working equations of just the diagonal blocks of the QED-ADC(1) matrix, i.e. the blocks with the same photonic excitation in the bra and the ket state. As can be seen from section 3.1.3, the second order QED-ADC contribution does not provide such contributions, apart from those appearing in standard ADC(2). Note, that additional contribution to the diagonal singles singles block in the photonic vacuum of QED-ADC(2) originates from the coupling term in the Hamiltonian and not from the squared dipole term. Hence, only the zeroth and first order diagonal blocks are changed, which are entirely build from the same working equations as standard ADC with the shifted ERIs, apart from a trivial contribution on the diagonal, which is 0 in the electronic, ω in the singly excited photonic and 2ω in the doubly excited photonic block. Hence, the unitary transformation diagonalizes the blocks on the diagonal of the QED-ADC(1) matrix and transforms the off-diagonal blocks accordingly. Apart from the term mentioned above the same is true for the QED-ADC(2) matrix. This way the transformed QED-ADC(2) matrix is obtained from calculating the ADC(2) states with the polaritonic vacuum contribution included, evaluating

the dipole and the perturbation operator in the ISR basis using these states and then using the eigenvalues corresponding to the states as diagonal for the QED-ADC(2) matrix in the photonic vacuum. The same diagonal is added with ω for the singly excited photonic diagonal of the QED-ADC(2) and the same procedure yields the diagonal for the doubly excited photonic diagonal, where 2ω needs to added. The remaining terms are obtained from using the new dipole and perturbation matrices in the full second order working equations, as well as for the first order working equations, where ISR states of different photonic excitations are coupled. This can be seen as a test for the implementation, since all terms need to be reimplemented, due to how the implementation of other ADC and therefore also QED-ADC methods is structured in the adcc package. Furthermore, the matrix then needs to be build explicitly, instead of using the matrix vector product implementation used in adcc, which is then pipelined into a subspace solver. This new formulation of the QED-ADC matrix is called QED-npADC and was tested to be equal to QED-ADC in first and second order to numerical precision. Note, that this approach provides all purely electronic terms, without couplings to photonic number states of different excitation, on its diagonal by definition. Further note, that the additional contribution in second order to the diagonal block is small, and that the couplings between different photonic excitations are not much bigger than the diagonal elements. Therefore, significant couplings only appear in the energetic vicinity of an other state, and even then only alter the states in their energetic vicinity. This is true for all polaritonic methods, but in the QED-npADC approach these energies are located on the diagonal in good approximation. Therefore, the QED-npADC matrix can be truncated to only those states in the energetic vicinity of the coupling of interest, which are just a few states for most practically relevant examples, even in the strong coupling regime. The heavily truncated QED-npADC method can then be compared to the inset of Figure 3.2b, yielding differences of less than 50 meV. This comparison is also visualized in Figure 3.3.

Hence, truncated QED-npADC is a very good approximation to QED-ADC, while significantly lowering memory requirements as well as CPU time, because the most expensive step is the calculation of non-polaritonic ADC, if only a few states are taken into account. Considering up to doubly excited photon number states this reduces the size of the ADC matrix by a factor of 3 in each dimension. Furthermore, the convergence rate is drastically increased, because the Davidson solver converges faster with smaller coupling elements, since the diagonal of the matrix then becomes more dominant. In QED-ADC the most dominant coupling contributions scale linear with $\sqrt{\omega}$ and λ, and can reach large values if the transition dipole moment is large. If the cavity photon is then in resonance with a transition with a large dipole moment, which is the most common use case for polaritonic applications, the convergence speed of the Davidson solver applied to QED-ADC is drastically reduced. This is circumvented with the QED-npADC method. Finally the

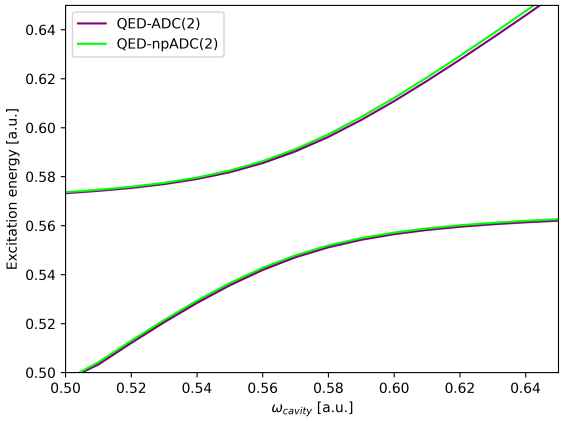

Figure 3.3.: Inset of Figure 3.2b compared to the same states calculated with QED-npADC(2), with only the eleven lowest states in energy.

QED-npADC method shall be compared to the similar approaches found in literature, as already mentioned in section 3.1.2. In these approaches field free states are computed and then used with the corresponding transition dipole moments and energies, to build the polaritonic matrix according to the polaritonic Hamiltonian. This approach is equal to QED-npADC(1), if the literature approaches would use states obtained from a method, which treats the electronic Hamiltonian and the vacuum field contribution in a consistent manner. However, only field free states are used. Therefore, these literature approaches can, but usually do not, achieve a consistent treatment of the polaritonic Hamiltonian through first order of perturbation theory. Hence, the QED-npADC(2) approach goes beyond these literature approaches, since it is consistent through second order of perturbation theory, while still using a truncated state space. This is especially useful, since the truncated QED-npADC matrix can be considered a good approximation to the diabatic representation of QED-ADC, which is required for most quantum dynamical simulations. It shall also be noted, that it outscales all other currently available polaritonic *ab initio* methods, for instance QED-CCSD-1, which scales as N^6, because it scales as N^5, like its non-polaritonic version. Bringing QED-ADC into the form of QED-npADC and truncating the state space is also advantageous for further derivations, like gradients. The advantage for deriving gradients is, that the derivatives for the diagonal elements are already known, if they are known for just QED-HF, since the diagonal is build from the eigenvalues of the standard ADC method with the vacuum coupling included. This yields a different Fock operator, but the perturbation operator is then given by Eq. (3.3) without the term coupling the bosonic with the electronic field. This is the same perturbation operator as used to derive standard MP and ADC, apart from a shift of the ERIs. Hence, all working equations, e.g. gradients, are

the same, after the ERIs were shifted. Hence, QED-npADC gradients can be obtained by only determining the gradients of the dipole operator and the ERIs. An other advantage is, that the ground state does not appear in the QED-npADC matrix. This yields trivial access to lossy cavities. This can be seen from the Lindbladian of a lossy cavity, which can be given as

$$\dot{\rho} = -\frac{i}{\hbar}[H, \rho] + \gamma b\rho b^\dagger - \frac{\gamma}{2}(b^\dagger b\rho + \rho b^\dagger b), \tag{3.31}$$

where γ is the parameter determining the loss rate. If no states are contained in the QED-npADC matrix, which have non-zero overlap after applying either b or $b^\dagger$, the term $\gamma b\rho b^\dagger$ yields zero[65, 66]. In the most common use case ω or 2ω is set equal to an electronic transition, so all states in the energetic vicinity can be expected to either have different electronic states or different photon occupation number. Using only these states, which are the relevant states, yields a set of states, providing no overlap after applying a bosonic field operator. This simplifies the Lindbladian to

$$\dot{\rho} = -\frac{i}{\hbar}[\tilde{H}, \rho], \tag{3.32}$$

where

$$\tilde{H} = H - i\frac{\gamma}{2} b^\dagger b. \tag{3.33}$$

Hence, this yields the Pauli-Fierz Hamiltonian with a shifted omega $\tilde{\omega} = \omega - i\frac{\gamma}{2}$ and can therefore be evaluated in a wavefunction based formalism, instead of using a density matrix based formalism. Hence, lossy cavities can be accounted for by simply adding an imaginary term to the energy of the cavity photon. This is not possible, if the state space cannot be truncated.

Photodissociation Dynamics of Pyrrole in a Photonic Cavity

In order to emphasize the impact of the choice of method on the accuracy of the result, the photodissociation dynamics of Pyrrole coupled to a photonic cavity are investigated in the following. Therefore the two methods presented in theis thesis shall be investigated, which yield a "quasi-diabatic" representation. These methods are QED-npADC(2) and its corresponding first order ansatz, for which two flavors are considered. One of the first order variants uses completely field-free states, i.e. states, which are computed by standard ADC(2), while the second one uses ADC(2) states, which additionally treat the squared dipole term of the Pauli-Fierz Hamiltonian, which is purely fermionic, in a consistent manner. The first order variants are therefore referred to as field-free and full-field, respectively. Note, that for the full field variant the orbitals are obtained from the polaritonic Fock operator, while the corresponding MP and ADC results can be obtained from the

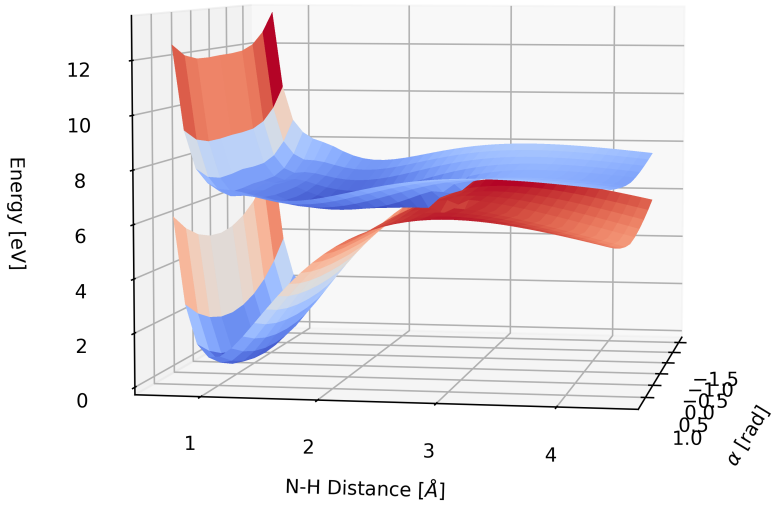

Figure 3.4.: Potential energy surfaces of the ground and second excited state in the photonic vacuum without polaritonic coupling of Pyrrole.

standard implementations with adapted ERIs, see Eq. (3.3). The potential energy surfaces were then calculated over two degrees of freedom with no polaritonic coupling, which are visualized in Figure 3.4 and agree very well with the surfaces published in literature[67], as well as with coupling constants of $\lambda = 0.001$, $\lambda = 0.01$ and $\lambda = 0.1$, with $\lambda = \frac{1}{\sqrt{2\hbar\omega\epsilon_0\epsilon_r V}}$, which are referred to as intermediate, strong and ultra strong, respectively. Subsequent dynamical simulation then yields the evolution of the population of the wavepacket after initial excitation at the Frank-Condon point, which are visualized in Figure 3.5.

As can be seen all variants show only minor deviations for the intermediate coupling. For strong coupling QED-npADC(2) is still very close to the non-polaritonic result, while the field-free variant already shows a Rabi-Oscillation and slower decay of the population. At the ultra strong coupling QED-npADC(2) shows a single Rabi-Oscillation and therefore shows slower decay than the non-polaritonic result, while the field-free variant lost roughly 40 % of its population after 20 femtosecond and then shows stable Rabi-Oscillations, which is qualitatively different from all other variants. Note, that the populations do not add up to one, due to the complex absorbing potential. Further note, that the full-field variant was left out in Figures 3.5a and 3.5b, since it barely deviates from QED-npADC(2), and even for the ultra strong coupling only slightly deviates from QED-npADC(2). The slower decay rates of the field-free variant compared to QED-npADC(2)

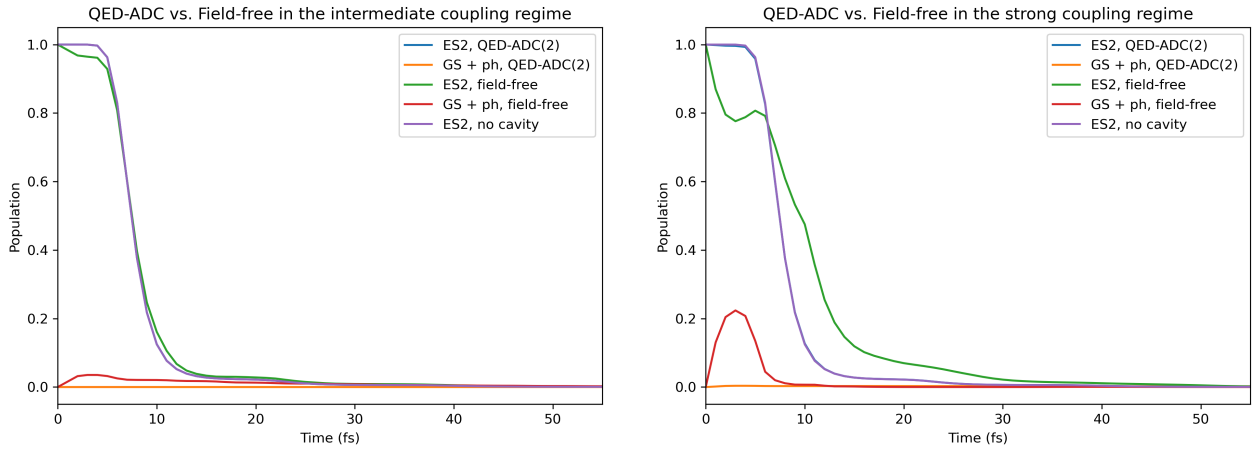

(a) $\lambda = 0.001$ **(b)** $\lambda = 0.01$

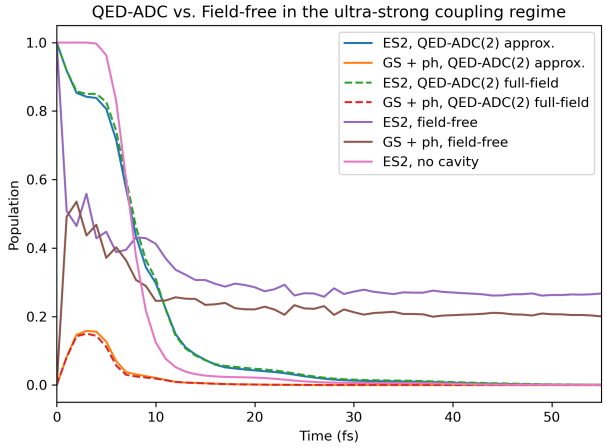

(c) $\lambda = 0.1$

Figure 3.5.: Evolution of the population dynamics of a wavepacket prepared at the Frank-Condon point of the excited surface for different coupling strengths. These figures were kindly provided by Federico Mellini.

and the full-field variant originate in the destabilization of the ground state through the quadratic component of the Pauli-Fierz Hamiltonian, as can be seen e.g. in Eq. 2.128. This penalty to the energy is then balanced by a new set of orbitals and states, which provide smaller transition dipole moments. This balancing is completely neglected by the field-free variant, leading to overestimation of the Rabi-Splitting. The deviation can be expected to be severe at lower coupling strengths too for system, which provide either larger transition dipole moments or smaller gradients at the Frank-Condon point of the excited state. Deviations can also be caused by interactions with other states in the energetic vicinity. Under these circumstances QED-npADC(2) is also expected to further deviate from the full-field variant in the strong coupling limit. Hence, considering that the field-free

variant can lead to major errors and even qualitatively wrong predictions in the strong coupling limit, as well as the negligible additional effort, which is required to compute the full-field and the QED-npADC(2) result, the QED-npADC(2) method should be used over the full-field and especially the field-free variant even for small coupling strengths, when computing polaritonic potential energy surfaces. However, for future investigations on properties and gradients the full-field variant should be considered of the most interest, since it only slightly deviates from QED-npADC(2), while not requiring additional derivation and implementation of densities and gradients for the diagonal elements of the "quasi-diabatic" representation.

3.1.4. Polaritonic Unitary Coupled Cluster

In order to derive QED-UCC2 we utilize the Bernoulli expansion, established in chapter 2.8. The the new mean-field and perturbation are chosen as the QED-Fock operator, $\tilde{F}$, and H_{PF} minus the QED-Fock operator as the perturbation, $\tilde{V}$.

$$\tilde{F} = F + \Omega \tag{3.34}$$

$$\tilde{V} = V + C, \tag{3.35}$$

where F is the polaritonic Fock operator in the photonic ground state (i.e. without Ω), $\Omega = \omega b^\dagger b$, V denotes the antisymmetrized two electron integrals with the additional shift from the D_{pqrs} object, and C is the term from H_{PF}, which couples the bosonic to the fermionic system. Note, that we use the transformed variant of H_{PF}. The Bernoulli expansion then yields the same result, as for the non-polaritonic Hamiltonian, if and only if the mean-field is still block-diagonal and the perturbation can be separated into a non-block-diagonal part and a block-diagonal part, where the latter is always zero for an amplitude equation. The first condition is true, since we provide a diagonal QED-Fock operator, after having converged the QED-SCF equations. The second condition is still fulfilled for V as in the non-polaritonic case, i.e. the non-diagonal part for V are the $\langle oo||vv\rangle$-type integrals, where o and v denote occupied and virtual orbital indices, respectively. In order to define the non-diagonal part of C we need to extend the purely electronic orbital basis to the polaritonic orbital basis, where the ground state is still defined by the electronic and photonic ground state, $\left|\Phi_{0,0}\right\rangle$, but the excited determinants can also have photonic excitations, e.g. $\left|\Phi_{ia,1}\right\rangle$. The non-diagonal terms have to obey the following equation

$$\left\langle \Phi_{I,X} \right| \tilde{V}'_{OD} \left| \Phi_{0,0} \right\rangle = 0 \tag{3.36}$$

where $\tilde{V}'$ denotes the perturbation from the Bernoulli expansion. $\tilde{V}'$ only contains terms with at max one V' and therefore only one C. Note, that the bosonic field operators introduce no antisymmetry to the result, but yield symmetric results. Since we also obtain other terms, than just the trivial solution $\tilde{V}'_{OD} = 0$, the whole antisymmetry is embedded into the electronic part only. The electronic part provides the same field operators as F and therefore C can be separated into an off-diagonal part and a block-diagonal part analogous to F. However, the dipole operator is not block-diagonal, so $C_{OD} \neq 0$. With the adapted Bernoulli expansion for the Pauli-Fierz Hamiltonian at hand, we now define the polaritonic UCC cluster operator as

$$u = S - S^\dagger \tag{3.37}$$

$$S = \sum_I s_I C_I + \left(\tilde{\omega} + \sum_I \tilde{s}_I C_I \right) b^\dagger + \left(\tilde{\tilde{\omega}} + \sum_I \tilde{\tilde{s}}_I C_I \right) b^\dagger b^\dagger. \tag{3.38}$$

Note, that up to two bosonic excitations are taken into account for polaritonic UCC2, because in polaritonic ADC(2) they directly couple to the photonic vacuum blocks. Furthermore, polaritonic ADC(2) only provides amplitudes up to two fermionic excitations, so the fermionic excitation manifold is also restricted to two. The same restrictions are valid for the QED-ADC(2) and therefore also the QED-UCC2 matrix. The expansion of the similarity transformed QED-UCC2 Hamiltonian then yields the analogous result to UCC2

$$H'_{PF} = H_{PF} + [F + \Omega, u] + \frac{1}{2}[V + C, u] + \frac{1}{2}[(V + C)_D, u]. \tag{3.39}$$

Note, that C and Ω are already in normal ordered form. Further note, that s_2 and $\tilde{s}_1$ appear in the first order wavefunction of QED-MP1 and are therefore of first order, while the other amplitudes provide a perturbation order of two. For a diagonal polaritonic Fock operator and $\tilde{V}_D$ summarized into $\tilde{V}$ the QED-UCC2 energy and amplitudes can then be calculated as

$$\begin{aligned}
\left\langle \Phi_{0,0} \right| H'_{PF} \left| \Phi_{0,0} \right\rangle &= E_{QED\text{-}HF} + \frac{1}{4} \sum_{ijab} \langle ij| |ab\rangle \, s_{ij}^{ab(1)} + \left\langle \Phi_{0,0} \right| [\Omega, u] + \frac{1}{2}[C, u] + \frac{1}{2}[C_D, u] \left| \Phi_{0,0} \right\rangle \\
&= E_{QED\text{-}HF} + \frac{1}{4} \sum_{ijab} \langle ij| |ab\rangle \, s_{ij}^{ab(1)} + \left\langle \Phi_{0,0} \right| \frac{1}{2}[C, u] \left| \Phi_{0,0} \right\rangle \\
&= E_{QED\text{-}HF} + \frac{1}{4} \sum_{ijab} \langle ij| |ab\rangle \, s_{ij}^{ab(1)} - \sqrt{\frac{\omega}{2}} \sum_{ia} \lambda \cdot d_{ia} \tilde{s}_i^{a(1)}
\end{aligned} \tag{3.40}$$

and

$$\begin{aligned}\left\langle \Phi^a_{i,0}\right| H'_{PF} \left|\Phi_{0,0}\right\rangle &= s_1^{(2)} \left\langle \Phi^a_{i,0}\right| FC_1 \left|\Phi_0\right\rangle + s_2^{(1)} \left\langle \Phi^a_{i,0}\right| VC_2 \left|\Phi_0\right\rangle + \tilde{s}_1^{(1)} \left\langle \Phi^a_{i,0}\right| CC_1 \left|\Phi_0\right\rangle \\ &= (\epsilon_a - \epsilon_i) s_i^{a(2)} + \frac{1}{2}\sum_{jbc} \langle aj||bc\rangle\, s_{ij}^{bc(1)} - \frac{1}{2}\sum_{jkb} \langle jk||ib\rangle\, s_{jk}^{ab(1)} \\ &\quad - \sqrt{\frac{\omega}{2}}\left(\sum_c \lambda \cdot d_{ac}\tilde{s}_i^{c(1)} - \sum_k \lambda \cdot d_{ki}\tilde{s}_k^{a(1)}\right) \\ &= 0,\end{aligned} \tag{3.41}$$

$$\begin{aligned}\left\langle \Phi^a_{i,1}\right| H'_{PF} \left|\Phi_{0,0}\right\rangle &= \left\langle \Phi^a_{i,1}\right| C \left|\Phi_{0,0}\right\rangle + s_2^{(1)} \left\langle \Phi^a_{i,1}\right| CC_2 \left|\Phi_{0,0}\right\rangle + \tilde{s}_1^{(1)} \left\langle \Phi^a_{i,1}\right| \Omega C_1 \left|\Phi_{0,0}\right\rangle \\ &\quad + \tilde{s}_1^{(1)} \left\langle \Phi^a_{i,1}\right| FC_1 \left|\Phi_{0,0}\right\rangle + \tilde{s}_1^{(1)} \left\langle \Phi^a_{i,1}\right| VC_1 \left|\Phi_{0,0}\right\rangle \\ &= -\sqrt{\frac{\omega}{2}}(\lambda \cdot d_{ia}) - \frac{1}{2}\sqrt{\frac{\omega}{2}}\sum_{kc} \lambda \cdot d_{kc} s_{ik}^{ac(1)} + (\epsilon_a - \epsilon_i + \omega)\tilde{s}_i^{a(1)} + \sum_{kc} \langle ak||ic\rangle\, \tilde{s}_k^{c(1)} \\ &= 0,\end{aligned} \tag{3.42}$$

$$\begin{aligned}\left\langle \Phi^a_{i,2}\right| H'_{PF} \left|\Phi_{0,0}\right\rangle &= \tilde{s}_1^{(1)} \left\langle \Phi^a_{i,2}\right| CC_1 \left|\Phi_{0,0}\right\rangle + \tilde{\tilde{s}}_1^{(2)} \left\langle \Phi^a_{i,2}\right| \Omega C_1 \left|\Phi_{0,0}\right\rangle + \tilde{\tilde{s}}_1^{(2)} \left\langle \Phi^a_{i,2}\right| FC_1 \left|\Phi_{0,0}\right\rangle \\ &= -\sqrt{\omega}\left(\sum_c \lambda \cdot d_{ac}\tilde{s}_i^{c(1)} - \sum_k \lambda \cdot d_{ki}\tilde{s}_k^{a(1)}\right) + \sqrt{2}(\epsilon_a - \epsilon_i + 2\omega)\tilde{\tilde{s}}_i^{a(2)} \\ &= 0,\end{aligned} \tag{3.43}$$

$$\begin{aligned}\left\langle \Phi^{ab}_{ij,0}\right| H'_{PF} \left|\Phi_{0,0}\right\rangle &= \left\langle \Phi^{ab}_{ij,0}\right| V \left|\Phi_0\right\rangle + s_2^{(1)} \left\langle \Phi^{ab}_{ij,0}\right| FC_2 \left|\Phi_0\right\rangle + s_2^{(1)} \left\langle \Phi^{ab}_{ij,0}\right| VC_2 \left|\Phi_0\right\rangle + \tilde{s}_1^{(1)} \left\langle \Phi^{ab}_{ij,0}\right| CC_1 \left|\Phi_0\right\rangle \\ &= \langle ab||ij\rangle + (\epsilon_a + \epsilon_b - \epsilon_i - \epsilon_j) s_{ij}^{ab(1)} + \frac{1}{2}\sum_{kl} \langle kl||ij\rangle\, s_{kl}^{ab(1)} + \frac{1}{2}\sum_{cd} \langle ab||cd\rangle\, s_{ij}^{cd(1)} \\ &\quad + (1 - P_{ij})(1 - P_{ab}) \sum_{kc} \langle kb||cj\rangle\, s_{ik}^{ac(1)} - \sqrt{\frac{\omega}{2}}\frac{1}{2}(1 - P_{ab})(1 - P_{ij})\lambda \cdot d_{ai}\tilde{s}_j^{b(1)} \\ &= 0,\end{aligned} \tag{3.44}$$

$$\begin{aligned}\left\langle \Phi^{ab}_{ij,1}\right| H'_{PF} \left|\Phi_{0,0}\right\rangle &= s_2^{(1)} \left\langle \Phi^{ab}_{ij,1}\right| CC_2 \left|\Phi_{0,0}\right\rangle + \tilde{s}_2^{(2)} \left\langle \Phi^{ab}_{ij,1}\right| \Omega C_2 \left|\Phi_{0,0}\right\rangle \\ &+ \tilde{s}_2^{(2)} \left\langle \Phi^{ab}_{ij,1}\right| FC_2 \left|\Phi_{0,0}\right\rangle + \tilde{s}_1^{(1)} \left\langle \Phi^{ab}_{ij,1}\right| VC_1 \left|\Phi_{0,0}\right\rangle \\ &= -\sqrt{\frac{\omega}{2}} \left((1-P_{ab}) \sum_c \lambda \cdot d_{bc} s_{ij}^{ac(1)} + (1-P_{ij}) \sum_k \lambda \cdot d_{ki} s_{jk}^{ab(1)} \right) \\ &+ (\epsilon_a + \epsilon_b - \epsilon_i - \epsilon_j + \omega) \tilde{s}_{ij}^{ab(2)} + (1-P_{ij}) \sum_c \langle ab||ic\rangle \, \tilde{s}_j^{c(1)} + (1-P_{ab}) \sum_k \langle bk||ij\rangle \, \tilde{s}_k^{a(1)} \\ &= 0,\end{aligned} \tag{3.45}$$

$$\begin{aligned}\left\langle \Phi^{ab}_{ij,2}\right| H'_{PF} \left|\Phi_{0,0}\right\rangle &= \tilde{s}_1^{(1)} \left\langle \Phi^{ab}_{ij,2}\right| CC_1 \left|\Phi_{0,0}\right\rangle + \tilde{\tilde{s}}_2^{(2)} \left\langle \Phi^{ab}_{ij,2}\right| \Omega C_2 \left|\Phi_{0,0}\right\rangle + \tilde{\tilde{s}}_2^{(2)} \left\langle \Phi^{ab}_{ij,2}\right| FC_2 \left|\Phi_{0,0}\right\rangle \\ &= -\sqrt{\omega}(1-P_{ij})(1-P_{ab}) \lambda \cdot d_{ai} \tilde{s}_j^{b(1)} + \sqrt{2}(\epsilon_a + \epsilon_b - \epsilon_i - \epsilon_j + 2\omega) \tilde{\tilde{s}}_{ij}^{ab(2)} \\ &= 0,\end{aligned} \tag{3.46}$$

where d denotes the shifted dipole matrix. Note, that since the QED-UCC2 matrix is a unitary transform of the QED-ADC(2) matrix, where the electronic ground state is decoupled from the excited states even if they contain photonic excitations, one obtains $\left\langle \Phi_{0,1}\right| H'_{PF} \left|\Phi_{0,0}\right\rangle = 0$ and $\left\langle \Phi_{0,2}\right| H'_{PF} \left|\Phi_{0,0}\right\rangle = 0$. Since those are the only blocks, where $\tilde{\omega}$ and $\tilde{\tilde{\omega}}$ could have contributions, they do not appear in the working equations. As can be seen now, Eqs. (3.41), (3.43), (3.45) and (3.46) determine $s_1^{(2)}$, $\tilde{\tilde{s}}_1^{(2)}$, $\tilde{s}_2^{(2)}$ and $\tilde{\tilde{s}}_2^{(2)}$ without iteration, respectively. The remaining two equations can be reformulated into working equations

$$\tilde{s}_i^{a(1)} = \frac{\sqrt{\frac{\omega}{2}}(\lambda \cdot d_{ia}) + \frac{1}{2}\sqrt{\frac{\omega}{2}} \sum_{kc} \lambda \cdot d_{kc} s_{ik}^{ac(1)} - \sum_{kc} \langle ak||ic\rangle \, \tilde{s}_k^{c(1)}}{\epsilon_a - \epsilon_i + \omega} \tag{3.47}$$

$$\begin{aligned}s_{ij}^{ab(1)} = -\Bigg(&\langle ab||ij\rangle + \frac{1}{2} \sum_{kl} \langle kl||ij\rangle \, s_{kl}^{ab(1)} + \frac{1}{2} \sum_{cd} \langle ab||cd\rangle \, s_{ij}^{cd(1)} + (1-P_{ij})(1-P_{ab}) \sum_{kc} \langle kb||cj\rangle \, s_{ik}^{ac(1)} \\ &- \sqrt{\frac{\omega}{2}} \frac{1}{2} (1-P_{ab})(1-P_{ij}) \lambda \cdot d_{ai} \tilde{s}_j^{b(1)} \Bigg) (\epsilon_a + \epsilon_b - \epsilon_i - \epsilon_j)^{-1},\end{aligned} \tag{3.48}$$

which are the only two amplitudes contributing to the QED-UCC2 energy, and since they only depend on each other, no further amplitudes need to be iterated. The initial guess is once again set

up by restricting the working equations to the first order contributions, which yields the QED-MP2 equations. This can be implemented in a straightforward manner, since the QED-MP(2) class can be inherited here, so the energy equation as well as all required amplitudes are already available and set to their initial guess. Using a homebrew DIIS solver, the amplitudes can then be iterated. Utilizing the same setup used to obtain Figure 3.1 and including QED-UCC(2) yields Figure 3.6.

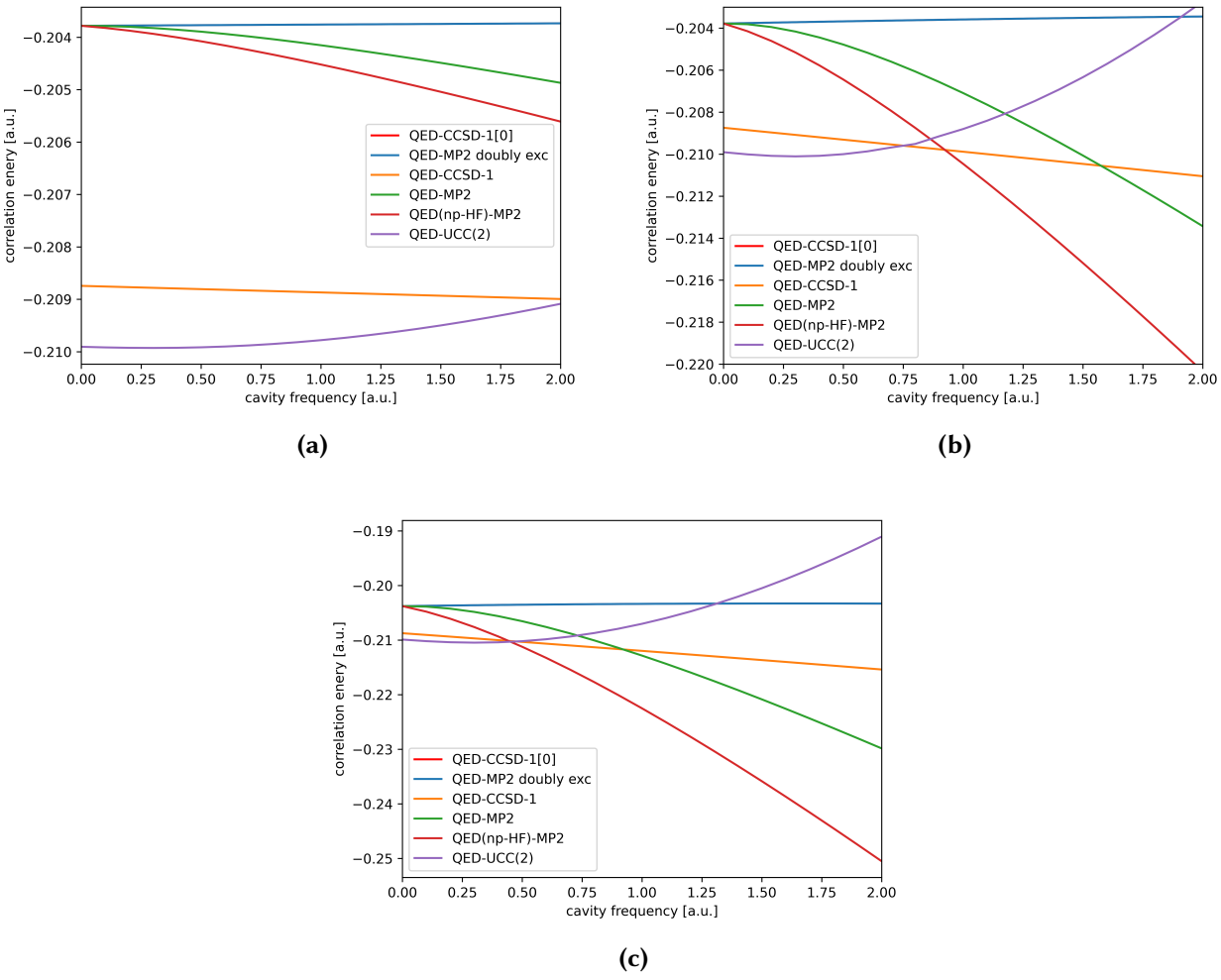

Figure 3.6.: Comparison of QED-UCC(2) against the results shown in Figure 3.1, where also a), b) and c) are calculated with the same coupling constant.

As can be seen from Figure 3.6, QED-UCC(2) slightly overestimates the correlation energy of QED-CCSD-1 for small ω, and with increasing ω is corrected towards the QED-CCSD-1 correlation energy. However, as QED-MP(2) starts to diverge, see section 3.1.2, QED-UCC(2) also diverges, but in the opposite direction. Hence, QED-UCC(2) is valid for roughly the same range of coupling strength and cavity photon energy as QED-MP(2). In section 3.1.2 it was explained in detail, that this range

suffices for all practically relevant calculations, so QED-UCC(2) can also be used for in principle all practically relevant systems. Note, that QED-UCC(2) also outscales QED-CCSD-1, while yielding very similar correlation energies within this practically relevant range, which makes QED-UCC(2) a highly favorable polaritonic ground state method. Furthermore, QED-UCC(2) can also be used as a polaritonic ground state to QED-ADC(2), since both share the same amplitudes. However, QED-UCC(2) uses a perturbation expansion around the reference determinant, which makes it non-variational, while also its performance highly depends on how good of an approximation the determinant is to the exact wavefunction. This problem arises already from the non-polaritonic comparison of QED-CCSD-1 and QED-UCC(2). This is a major issue for multi reference calculations, even if only two determinants are relevant. In these multi reference regimes QED-CCSD-1 is therefore favorable over QED-UCC(2) and QED-MP(2). Nevertheless, it shall be mentioned, that even though QED-UCC(2) usually fails at producing qualitatively correct dissoziation curves, it damps most of the divergence of QED-MP(2), just like in the non-polaritonic regime.

3.2. Excitonic Renormalization

3.2.1. Computational Details

The numerical results in this section have been computed using the programm package described in section 3.2.7. The system under consideration is the Beryllium dimer using the 6-31G basis set as implemented in the psi4 programm package[60]. If not noted otherwise, all densities are included, which can be build from neutral and singly charged excitations at the FCI level of theory.

3.2.2. Approximating the Brute Forced Excitonic Renormalization Method

As already mentioned in section 2.12, the biggest impairment is the explicit orthogonalization of the truncated state space, which is currently determined by brute force. One can write the overlap matrix from Eq. (2.145) for the two-fragment contribution as

$$(S_{\tilde{I}\tilde{J}})_{mn} = \left\langle \Psi_{i_m}\Psi_{i_n} \middle| \Psi_{j_m}\Psi_{j_n} \right\rangle = \sum_{P_m P_n Q_m Q_n} \left(\bar{z}^i_P z^Q_j\right)_m \left(\bar{z}^i_P z^Q_j\right)_n \left\langle \phi_{P_m}\phi_{P_n} \middle| \phi_{Q_m}\phi_{Q_n} \right\rangle . \tag{3.49}$$

Note, that the factors on the left run only over one fragment index and therefore only need to be evaluated once for each fragment. This is rather computationally cheap, but the overlap of two-fragment determinants is not decoupled. This term can be rewritten as a determinant of monomer overlaps

$$\left\langle \phi_{P_m}\phi_{P_n} \middle| \phi_{Q_m}\phi_{Q_n} \right\rangle = \begin{pmatrix} \left\langle \Phi_{P_m} \middle| \Phi_{Q_m} \right\rangle & \left\langle \Phi_{P_m} \middle| \Phi_{Q_n} \right\rangle \\ \left\langle \Phi_{P_n} \middle| \Phi_{Q_m} \right\rangle & \left\langle \Phi_{P_n} \middle| \Phi_{Q_n} \right\rangle \end{pmatrix}. \tag{3.50}$$

Nevertheless, $S_{\tilde{I}\tilde{J}}$ requires evaluating a determinant the size of the sum of two orbital spaces in each dimension for all combinations of states of all dimer combinations of fragments. This results in a very high scaling is therefore not a practically applicable approach. Note, that the same has to be done for the Hamiltonian, which is even more expensive. Hence, an approximation needs to be found, which lowers this scaling. One could think of either truncating the orbital basis for each state to only the most dominant contributions, which however still requires numerical computation of all orbital dimer overlaps, or approximating $\left\langle \phi_{P_m}\phi_{P_n} \middle| \phi_{Q_m}\phi_{Q_n} \right\rangle$ with an algebraic scheme. As can be seen from Eq. (3.50), the latter can be achieved by approximating the overlap of two non-orthogonal determinants. In the trivial case of orthogonal determinants the overlap yields the Kronecker delta. If they differ by only one dimension, then the result is given by a Kronecker delta, where two indices yield an additional result of a 2x2 matrix, which is not equal to the identity matrix, so the overlap matrix has two off-diagonal elements unequal to zero and two diagonal elements unequal to one. Determining these four values is obviously much cheaper, than evaluating the full overlap matrix by brute force. For two arbitrary determinants, which are equal to each other apart from one dimension, which is orthogonal to all other states in the same determinant, this requires at least biorthogonalizing the differing dimension. Assuming the differing dimension is orbital p and taking into account, that the other orbitals are already biorthogonal, this operation is done by

$$\langle \Phi_A | \Phi_B \rangle = \left\langle \Phi^A \middle| (a_p^\dagger - a^{p\dagger}) a_p \middle| \Phi_B \right\rangle. \tag{3.51}$$

As can be seen here, biorthogonal creation operators are required, which is indicated by a hermitian conjugation of the annihilation operation, however, since they are not hermitian and creation as well as annihilation operators of the same representation, i.e. "normal" or biorthogonal complement, are relevant, the creation operators are from now on abbreviated with a c. As can be seen from Eq. (3.51), this procedure can be applied up to arbitrary number of different orbitals. This is also true for states in the fluctuation operator basis as well as super-system states, which define the full wavefunction in XR. Hence, the overlap of two super-system states can be rewritten as

$$\langle \Psi_I | \Psi_J \rangle = \langle \Psi^I | \hat{S} | \Psi_J \rangle \tag{3.52}$$

with

$$\begin{aligned}
\hat{S} &= 1 + \sum_{p} (\hat{c}_p - \hat{c}^p)\hat{a}_p \\
&\quad + \sum_{p<q} (\hat{c}_p - \hat{c}^p)(\hat{c}_q - \hat{c}^q)\hat{a}_q\hat{a}_p + \cdots && (3.53) \\
&= 1 + \sum_{pq} \sigma_{pq}\, \hat{c}_p \hat{a}^q \\
&\quad + \frac{1}{2} \sum_{pqrs} \sigma_{pq}\sigma_{rs}\, \hat{c}_p \hat{c}_r \hat{a}^s \hat{a}^q + \cdots && (3.54) \\
&= \hat{S}^{[0]} + \hat{S}^{[1]} + \hat{S}^{[2]} + \cdots && (3.55)
\end{aligned}$$

and

$$\sigma_{pq} \in \boldsymbol{\sigma} = \mathbf{s} - \mathbf{1} \tag{3.56}$$

$$s_{pq} = \langle \phi_p | \phi_q \rangle \in \mathbf{s}. \tag{3.57}$$

Note, that in $\hat{S}$ the corrections for different numbers of states have been separated, in order to expand $\hat{S}$ in a series around the trivial case of completely orthogonal states. The series was then reformulated using the relation

$$\hat{a}_p = \sum_{q} s_{pq} \hat{a}^q. \tag{3.58}$$

From this expansion working equations can be generated analogous to Eq. (2.141), yielding dimer overlaps as

$$\left\langle \Psi^{i_1}\Psi^{i_2}\right| \hat{S}^{[0]} \left|\Psi_{j_2}\Psi_{j_1}\right\rangle = \left\langle \Psi^{i_1}\Psi^{i_2} \right|\Psi_{j_2}\Psi_{j_1}\rangle = \delta_{IJ} \tag{3.59}$$

$$\begin{aligned}\left\langle \Psi^{i_1}\Psi^{i_2}\right| \hat{S}^{[1]} \left|\Psi_{j_2}\Psi_{j_1}\right\rangle &= \left\langle \Psi^{i_1}\Psi^{i_2}\right| \sum_{p_1 q_2} \sigma_{p_1 q_2}\, \hat{c}_{p_1} \hat{a}^{q_2} \left|\Psi_{j_2}\Psi_{j_1}\right\rangle + \left\langle \Psi^{i_1}\Psi^{i_2}\right| \sum_{p_2 q_1} \sigma_{p_2 q_1}\, \hat{c}_{p_2} \hat{a}^{q_1} \left|\Psi_{j_2}\Psi_{j_1}\right\rangle \\ &= (-1)^{n_2}(1 - P_{12}) \sum_{p_1 q_2} \sigma_{p_1 q_2}\rho_{p_1}\rho^{q_2}\end{aligned} \tag{3.60}$$

$$\left\langle \Psi^{i_1}\Psi^{i_2}\right| \hat{S}^{[2]} \left|\Psi_{j_2}\Psi_{j_1}\right\rangle = \frac{1}{2}(1 + P_{12}) \sum_{p_1 q_2 r_1 s_2} \sigma_{p_1 q_2}\sigma_{r_1 s_2}\rho_{p_1 r_1}\rho^{q_2 s_2} - \sum_{p_1 q_2 r_2 s_1} \sigma_{p_1 q_2}\sigma_{r_2 s_1}\rho^{s_1}_{p_1}\rho^{q_2}_{r_2} \tag{3.61}$$

$$\left\langle \Psi^{i_1}\Psi^{i_2}\right| \hat{S}^{[3]} \left|\Psi_{j_2}\Psi_{j_1}\right\rangle \approx (-1)^{n_2}\frac{1}{2}(1 - P_{12}) \sum_{p_1 q_2 r_1 s_2 t_2 u_1} \sigma_{p_1 q_2}\sigma_{r_1 s_2}\sigma_{t_2 u_1}\rho^{u_1}_{p_1 r_1}\rho^{s_2 q_2}_{t_2} \tag{3.62}$$

$$\begin{aligned}\left\langle \Psi^{i_1}\Psi^{i_2}\right| \hat{S}^{[4]} \left|\Psi_{j_2}\Psi_{j_1}\right\rangle \approx{}& \frac{1}{4} \sum_{p_1 q_2 r_1 s_2 t_2 u_1 v_2 w_1} \sigma_{p_1 q_2}\sigma_{r_1 s_2}\sigma_{t_2 u_1}\sigma_{v_2 w_1}\rho^{u_1 w_1}_{p_1 r_1}\rho^{s_2 q_2}_{v_2 t_2} \\ &- \frac{1}{6}(1 - P_{12}) \sum_{p_1 q_2 r_1 s_2 t_1 u_2 v_2 w_1} \sigma_{p_1 q_2}\sigma_{r_1 s_2}\sigma_{t_1 u_2}\sigma_{v_2 w_1}\rho^{w_1}_{p_1 r_1 t_1}\rho^{u_2 s_2 q_2}_{v_2}.\end{aligned} \tag{3.63}$$

Note, that the field operators of $\hat{S}$ can refer to a state of any fragment involved, so they need to be swapped to preserve the normal ordering, introducing an additional factor of minus one. Furthermore, as throughout the whole, orthogonal fragment states are assumed, and therefore $\sigma_{p_1 q_1} = 0$. Therefore, $\hat{S}^{[n]}$ requires densities of a field operator string with a maximum length of n, and since densities describing for instance triple ionization yield negligible contributions, $\hat{S}$ converges rather quickly. As a numerical example, neglecting triple ionization and electron attachment and expanding $\hat{S}$ up to fourth order yields a difference matrix with a Frobenius norm on the order of 10^{-4} by subtracting it from the exact overlap matrix, at the equilibrium geometry of the Beryllium dimer, which is visualized in Figure 3.7.

In fact each order lowers the error by roughly one order of magnitude. Note, that this is the same system, which was already considered in literature, where only neutral and singly charged Beryllium atoms were considered, which yielded FCI accuracy. In this system only double ionization/attachment is possible, which is in line with at least partially dropping three body density contributions. Hence, by truncating the expansion of $\hat{S}$ at low order yields a cheap and precise approximation to the overlap, which can be extended to exact accuracy by further expanding $\hat{S}$. The same expansion can be applied to the Hamiltonian term, which yields

$$\left\langle \Psi_{i_1}\Psi_{i_2}\right| H \left|\Psi_{j_2}\Psi_{j_1}\right\rangle = \left\langle \Psi^{i_1}\Psi^{i_2}\right| \hat{S}H \left|\Psi_{j_2}\Psi_{j_1}\right\rangle = \left\langle \Psi^{i_1}\Psi^{i_2}\right| (\hat{S}^{[0]} + \hat{S}^{[1]} + \hat{S}^{[2]} + ...)H \left|\Psi_{j_2}\Psi_{j_1}\right\rangle. \tag{3.64}$$

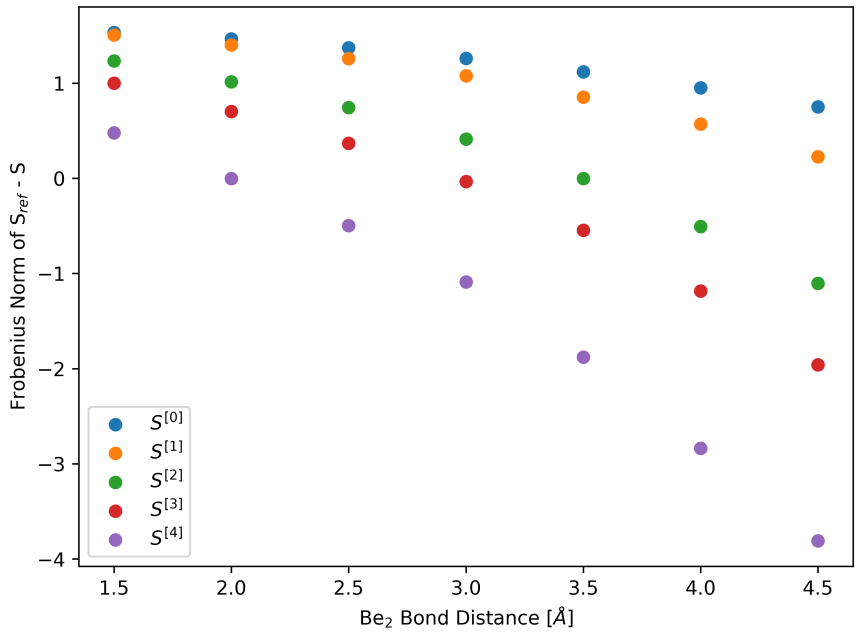

Figure 3.7.: Convergence behaviour for the expansion in $\hat{S}$ for the dissociation of the Beryllium dimer.

Using algebraic, not computational, intermediates as

$$\overline{S\mathcal{H}}^{[n]}_{\{0\}} = \sum_{pqrs} h^p_q \, \hat{c}_p \hat{S}^{[n]} \hat{a}^q + \sum_{pqrs} v^{pq}_{rs} \, \hat{c}_p \hat{c}_q \hat{S}^{[n]} \hat{a}^s \hat{a}^r \tag{3.65}$$

$$\overline{S\mathcal{H}}^{[n]}_{\{1\}} = \sum_{pqrs} (h_{pq} - h^p_q) \, \hat{c}_p \hat{S}^{[n]} \hat{a}^q + \sum_{pqrs} (2v^p_{qrs} - 2v^{pq}_{rs}) \, \hat{c}_p \hat{c}_q \hat{S}^{[n]} \hat{a}^s \hat{a}^r \tag{3.66}$$

$$\overline{S\mathcal{H}}^{[n]}_{\{2\}} = \sum_{pqrs} (v_{pqrs} + v^{pq}_{rs} - 2v^p_{qrs}) \, \hat{c}_p \hat{c}_q \hat{S}^{[n]} \hat{a}^s \hat{a}^r, \tag{3.67}$$

with

$$h_{pq} = \langle \phi_p | \hat{h} | \phi_q \rangle \tag{3.68}$$

$$v^p_{qrs} = \frac{1}{4} \langle \phi^p \phi_q | \hat{v} | \phi_r \phi_s \rangle \tag{3.69}$$

$$v_{pqrs} = \frac{1}{4} \langle \phi_p \phi_q | \hat{v} | \phi_r \phi_s \rangle, \tag{3.70}$$

yields the operator $\hat{S}H$ through different expansion orders as

$$\hat{S}^{[0]}\hat{\mathcal{H}} = \overline{S\mathcal{H}}^{[0]}_{\{0\}} \tag{3.71}$$
$$\hat{S}^{[1]}\hat{\mathcal{H}} = \overline{S\mathcal{H}}^{[1]}_{\{0\}} + \overline{S\mathcal{H}}^{[0]}_{\{1\}} \tag{3.72}$$
$$\hat{S}^{[2]}\hat{\mathcal{H}} = \overline{S\mathcal{H}}^{[2]}_{\{0\}} + \overline{S\mathcal{H}}^{[1]}_{\{1\}} + \overline{S\mathcal{H}}^{[0]}_{\{2\}} \tag{3.73}$$
$$\hat{S}^{[3]}\hat{\mathcal{H}} = \overline{S\mathcal{H}}^{[3]}_{\{0\}} + \overline{S\mathcal{H}}^{[2]}_{\{1\}} + \overline{S\mathcal{H}}^{[1]}_{\{2\}}. \tag{3.74}$$

Summing up the terms within a distinct order in $\hat{S}$, yields

$$\overline{S\mathcal{H}}^{[n]}_{\{m\}} + \overline{S\mathcal{H}}^{[n]}_{\{m+1\}} + \overline{S\mathcal{H}}^{[n]}_{\{m+2\}} = \sum_{pq} h_{pq}\hat{c}_p\hat{S}^{[n]}\hat{a}^q + \sum_{pqrs} v_{pqrs}\hat{c}_p\hat{c}_q\hat{S}^{[n]}\hat{a}^s\hat{a}^r, \tag{3.75}$$

which is hermitian. Hence, for every expansion term $\overline{S\mathcal{H}}^{[n]}_{\{m\}}$, the $m+1$-th term corrects for the biorthogonal one-particle term of the Hamiltonian, by orthogonalizing the subspace it operates in, while the two-particle term is partially corrected for in the same way in $m+1$-th order and fully corrected in $m+2$-th order. This is not term by term hermitian, but two additional expansion orders in $\hat{S}H$ fully hermitianize these terms. The newly introduced non-hermitian terms then yield working equations with densities of higher particle order, yielding smaller contributions to the final energy and thus converging in an approximately hermitian manner. It shall be noted here, that a term by term hermitian expansion can also be build by using the relation

$$c_p S = S c^p, \tag{3.76}$$

along with

$$\hat{\mathcal{H}} = \sum_{pqrs} h_{pq}\hat{c}^p\hat{a}^q + \sum_{pqrs} v_{pqrs}\hat{c}^p\hat{c}^q\hat{a}^s\hat{a}^r, \tag{3.77}$$

which yields

$$\hat{S}\hat{\mathcal{H}} = \sum_{pqrs} h_{pq}\,\hat{c}_p\hat{S}\hat{a}^q + \sum_{pqrs} v_{pqrs}\,\hat{c}_p\hat{c}_q\hat{S}\hat{a}^s\hat{a}^r. \tag{3.78}$$

However, this expansion, which only uses fully symmetric one- and two-particle integrals, has much worse convergence properties, because the biorthogonal integrals in the zeroth order ansatz already account for most of the interaction, whereas the other ansatz treats the orbital bases of the fragments as if they were orthogonal. Therefore, the absolute contributions to the final energy are very large, much larger than the total correlation energy, even at high orders of the expansion, while the ansatz using biorthogonal integrals uses a zeroth order, which already contains most of the correlation, if the states of the fragments are chosen appropriately. Therefore, the ansatz of Eqs. (3.65), (3.66) and (3.67) is used throughout this thesis. Working equations can then be derived as

$$\begin{aligned}\hat{S}^{[0]}\hat{\mathcal{H}} = {} & (1 - P_{12})h^{p_1}_{q_2}\rho_{p_1}\rho^{q_2} + 2(1 + P_{12})v^{p_1 q_1}_{s_2 r_1}\rho^{r_1}_{p_1 q_1}\rho^{s_2} + 2(1 + P_{12})v^{p_1 s_2}_{r_1 q_1}\rho^{q_1 r_1}_{p_1}\rho_{s_2} + 4v^{p_1 r_2}_{q_1 s_2}\rho^{q_1}_{p_1}\rho^{s_2}_{r_2} \\ & + (1 + P_{12})v^{p_1 q_1}_{s_2 r_2}\rho_{p_1 q_1}\rho^{r_2 s_2}\end{aligned} \tag{3.79}$$

$$\begin{aligned}\hat{S}^{[1]}\hat{\mathcal{H}} = {} & -(1 + P_{12})\sum_{p_2 q_1 r_1 s_2}\sigma_{p_2 q_1}h^{s_2}_{r_1}\rho^{q_1}_{r_1}\rho^{s_2}_{p_2} + (-1)^{n_2}(1 - P_{12})\sum_{p_1 q_1 r_1 s_2}\sigma_{r_1 s_2}h^{q_1}_{p_1}\rho^{q_1}_{r_1 p_1}\rho^{s_2} \\ & + (-1)^{n_2}(1 - P_{12})\sum_{p_1 q_1 r_2 s_1}\sigma_{r_2 s_1}h^{q_1}_{p_1}\rho^{s_1 q_1}_{p_1}\rho_{r_2} + (1 + P_{12})\sum_{p_1 q_2 r_1 s_2}\sigma_{p_1 q_2}h^{s_2}_{r_1}\rho_{r_1 p_1}\rho^{q_2 s_2} \\ & + 2(1 + P_{12})\sum_{t_2 u_1 p_1 q_1 r_1 s_2}\sigma_{t_2 u_1}v^{s_2 r_1}_{p_1 q_1}\rho^{u_1 r_1}_{p_1 q_1}\rho^{s_2}_{t_2} + 2(1 + P_{12})\sum_{t_1 u_2 p_1 q_1 r_1 s_2}\sigma_{t_1 u_2}v^{r_1 q_1}_{p_1 s_2}\rho^{r_1 q_1}_{p_1 t_1}\rho^{u_2}_{s_2} \\ & + 4(-1)^{n_2}(1 - P_{12})\sum\sigma_{t_1 u_2}v^{q_1 s_2}_{p_1 r_2}\rho^{q_1}_{p_1 t_1}\rho^{u_2 s_2}_{r_2} + (-1)^{n_2}(1 - P_{12})\sum_{t_2 u_1 p_1 q_1 r_2 s_2}\sigma_{t_2 u_1}v^{s_2 r_2}_{p_1 q_1}\rho^{u_1}_{q_1 p_1}\rho^{r_2 s_2}_{t_2} \\ & + (-1)^{n_2}(1 - P_{12})\sum_{t_1 u_2 p_1 q_1 r_1 s_1}\sigma_{t_1 u_2}v^{r_1 s_1}_{p_1 q_1}\rho^{s_1 r_1}_{p_1 q_1 t_1}\rho^{u_2} + (-1)^{n_2}(1 - P_{12})\sum_{t_2 u_1 p_1 q_1 r_1 s_1}\sigma_{t_2 u_1}v^{r_1 s_1}_{p_1 q_1}\rho^{u_1 r_1 s_1}_{p_1 q_1}\rho_{t_2} \\ & + 2(1 + P_{12})\sum_{t_1 u_2 p_1 q_1 r_1 s_2}\sigma_{t_1 u_2}v^{s_2 r_1}_{p_1 q_1}\rho^{r_1}_{q_1 p_1 t_1}\rho^{u_2 s_2} + 2(1 + P_{12})\sum_{t_2 u_1 p_1 q_1 r_1 s_2}\sigma_{t_2 u_1}v^{r_1 q_1}_{p_1 s_2}\rho^{u_1 q_1 r_1}_{p_1}\rho_{s_2 t_2} \\ & + (-1)^{n_2}(1 - P_{12})\sum_{t_1 u_2 p_1 q_1 r_2 s_2}\sigma_{t_1 u_2}v^{s_2 r_2}_{p_1 q_1}\rho_{p_1 q_1 t_1}\rho^{u_2 r_2 s_2}.\end{aligned} \tag{3.80}$$

As already noted for the overlap matrix, the maximum length of an operator string, from which densities are build, increases by one for each additional order in $\hat{S}$. This yields a cheap and precise approximation for the overlap, since in zeroth order no densities are required, however, for $\hat{S}H$ the zeroth order already requires the neutral two-particle density, so already in first order three particle densities with a length of the operator string of five are required. Nevertheless, truncating the overlap and the Hamiltonian expansion at first order recovers almost 90 % of the error of basic XR around the minimum of the Be_2 dissoziation curve, as shown in Figure 3.8.

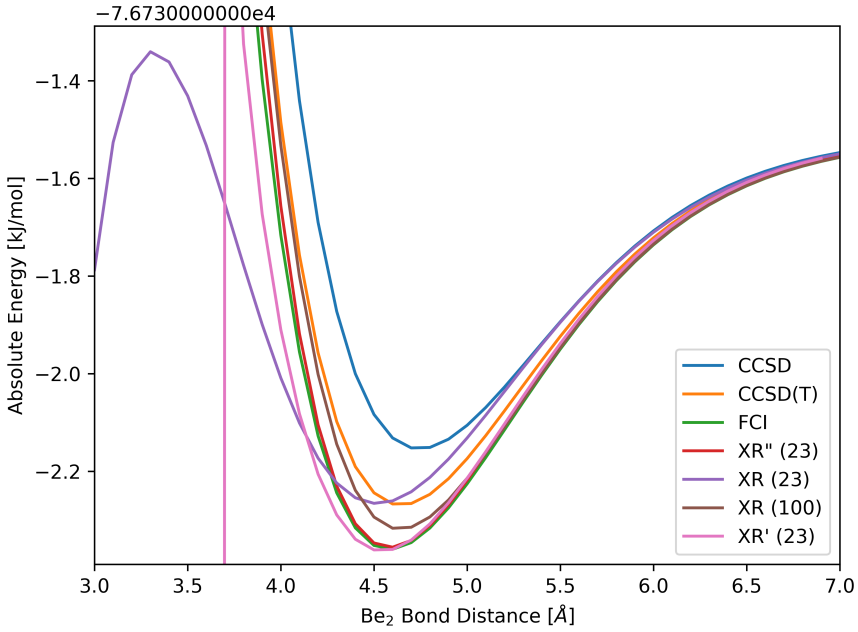

Figure 3.8.: Comparison of XR' against other XR variants as well as established methods for the dissociation curve of the Beryllium dimer.

This approach will further be referred to as XR'. As can be seen in Figure 3.8, XR' yields in principle FCI accuracy at the minimum and for larger bond distances, while slightly deviating for shorter bond distances. Note, that at shorter bond distances, than the minimum, the deviation of XR' is still smaller than that of CCSD(T). This is still true when the Be dimer is compressed above the dissoziation energy limit, until it finally breaks down at an energy well above the dissoziation energy. Note, that XR' requires a five dimensional tensor for all state combinations of the monomer states, but since these are restricted they do not contribute to the memory scaling, which is therefore limited at N^5. Now given the fact, that XR' provides much better accuracy than CCSD(T), while formally scaling as N^5 in CPU time and memory, where e.g. CCSDT already scales as N^8 in CPU time and N^6 in memory, makes XR' a very promising approach for high accuracy in large systems. Furthermore, all XR approaches can make use of all methods with orthogonal state spaces. Hence, for the application of a metal complex the central metal atom can be calculated at the level of a multireference method, while challenging ligands can be computed at a high level of theory and all remaining simple fragments can be evaluated at a low level of theory. The XR' method and higher expansions in $\hat{S}$ are then able to compute the interaction at FCI level for massively truncated fragment state spaces. However, even though great results are obtained for the challenging Be_2 system, three problems need to be addressed. The first is, that the method is still expensive,

even though the scaling is comparably small, because the currently used procedure to obtain the optimized states is very involved. The second problem is, that it is not clear whether the interaction between fragments is similarly precise with less accurate densities, e.g. from CC or ADC. The third problem is, that it is also not clear when higher expansions in $\hat{S}$ as well as higher fragment interactions become relevant. The second problem is obviously the most severe limitation and therefore should be addressed first. The first problem also leads to a large obstacle, since it requires, that the pseudo-density of monomer states for two monomers is solved for all states. The third problem is probably a minor issue, if the first two problems are solved, because higher expansions in both series will then probably not increase the overall scaling of the method, but rather introduce a larger pre-factor.

3.2.3. ADC densities

In order to lower the computational requirements of the post-HF method of each fragment, it shall be investigated whether ADC densities at a low order of perturbation theory are sufficient to recover most of the interaction. Therefore, all required densities need to be evaluated.

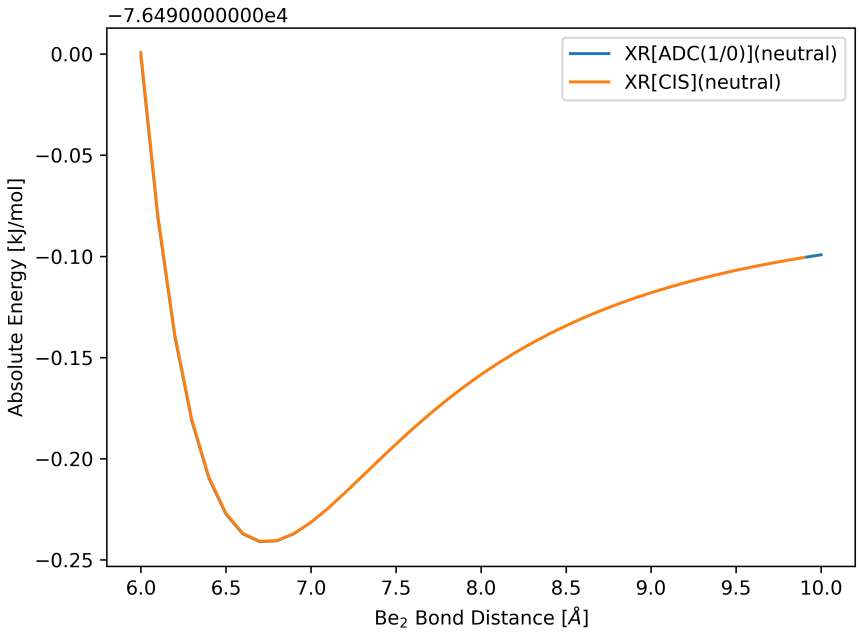

Figure 3.9.: Comparison of XR for all neutral singly excited monomer states evaluated at the level of CIS, XR[CIS](neutral), and ADC(1/0), XR[ADC(1/0)](neutral), for the dissociation curve of the Beryllium dimer.

Taking higher orders of $\hat{S}$ into account this becomes a very tedious task and requires amplitudes of high dimensionality. However, such amplitudes can be computed efficiently using low dimensional objects through a Laplace transformation[68, 69], while using ADC in its ISR formulation, all densities can be obtained from Eq. (2.37), which only requires evaluating Wicks theorem. This task was automized using the "physics.secondquant" module as implemented in the sympy programm package[70], which can be used to evaluate Wicks theorem into strings of Kronecker deltas, which can then be contracted with tensors. This derivation and implementation can be tested for all neutral state to neutral state one and two particle transition densities, since CIS densities can be generated from the FCI code, which must be equal to ADC(1/0) densities. Note, that ADC(n/m) refers to evaluating n-th order ADC states using m-th order ADC densities. The comparison is visualized in Figure 3.9 for the same Be_2 system, as used throughout the previous part of this thesis.

Note, that both methods show excellent overlap with each other, but also significantly differ from XR[FCI](23) not only in absolute energy, but also in position and depth of the minimum. The position of the minimum is overestimated by more than two Angstroms and the depth is underestimated by a factor of more than four. This shows, that the derivation and implementation of the required terms is correct, while also the system under consideration has a large contribution to the correlation in the doubly excited state space, as expected for Beryllium. The result with first order densities, where also charged states are taken into account, i.e. XR[ADC(1/1)](full), is shown in Figure 3.10.

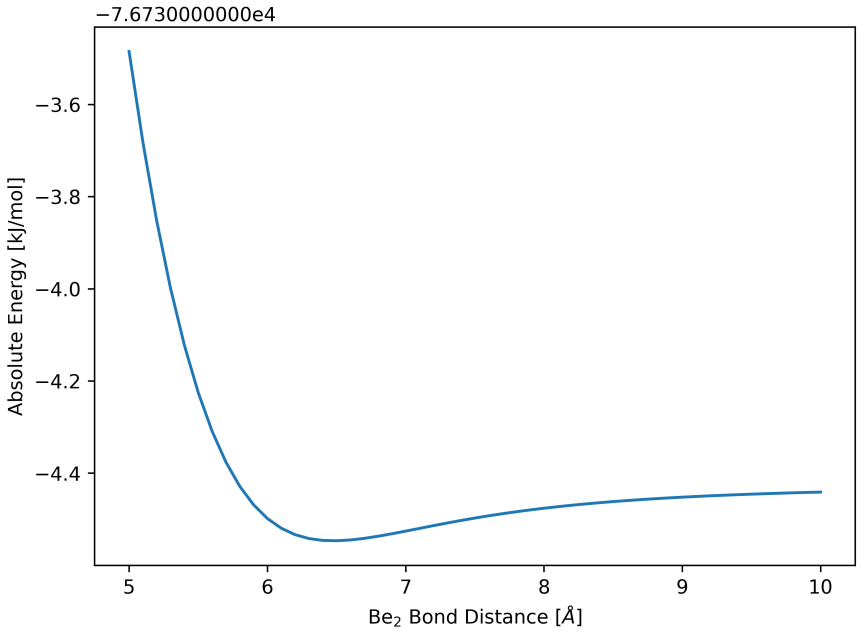

Figure 3.10.: Dissociation curve of the Beryllium dimer at the XR[ADC(1/1)](full) level of theory.

Note, that even though the binding energy did not change significantly, the position of the minimum was shifted towards the correct bond distance by roughly 0.5 Å, while the scale of the absolute energy is now off by only 2 kJ/mol as well. This is a strong hint, that XR quickly converges with increasing perturbation order of the ADC states and densities. The fact, that the depth and location of the minimum are still quite off, can be expected to originate from the significant multi-reference character of the Beryllium atom and will therefore most probably be fixed, as soon as doubly excited contributions are taken into account. The working equations for the ADC densities up to first order of perturbation theory required for XR are provided in section A.1.

3.2.4. Cumulant Ansatz for Densities

Due to the large memory requirement as well as highly increased CPU time, which comes with exceeding the two particle densities, many approaches were applied with the goal of lowering the memory requirement, while staying within the accuracy of XR'. All of the following approaches have been tested using FCI states and densities. One of these approaches is the so-called density matrix reconstruction, which builds higher than two particle densities from tensor products of up to two particle densities. This approach is well developed, because it has a direct application to solving the Schroedinger equation, which can be rewritten using densities instead of states. The easiest derivation can be carried out by probing the doubly excited state space, which probes the full space of the two particle reduced Hamiltonian K[71]. This leaves one with the Schroedinger equation in the following form

$$\sum_{pqrstuvw} K^{rs}_{vw} R^{pqrs}_{tuvw} = 4E^2 D^{tu}_{pq}, \tag{3.81}$$

with $R = \left\langle \tilde{\psi} \right| a_p^\dagger a_q^\dagger a_u a_t a_r^\dagger a_s^\dagger a_w a_v \left| \psi \right\rangle$. Bringing R in normal ordered form yields the so-called 2,4 contracted Schroedinger equation for transition matrices. However, this formulation is not practical, because it requires calculating explicit four particle densities. In theory this can be circumvented though, as proven by Rosina's theorem, which shows, that all information for a two particle Hamiltonian is already contained in the reduced two particle density matrix and hence, all higher particle reduced density matrices can be obtained from the two particle reduced density matrix. Note, that this theorem proofs this relation only for reduced density matrices, i.e. bra and ket state need to be equal. Nevertheless, transition matrices have been shown to numerically converge faster than the reduced density matrices for various density matrix reconstruction schemes. Here the cumulant approach will be applied, which, to the best of my knowledge, shows the best

results published in literature, while also being extendable to higher accuracy by taking further expansion terms into account[71, 72]. This approach is based on the fact, that the cumulant of a sum of independent statistical variables is equal to the the sum of cumulants of each individual variable. Hence, independent statistical variables can be separated from the total cumulant without approximation. This means, that for instance the cumulant, corresponding to a three particle density, is only missing contributions, where all three particles interact with each other. This is the maximum information, which can be recovered without explicitly calculating the three particle density. The required cumulants can then be found by finding a function, whose moments are the targeted densities. This can be achieved by choosing the generating function F as

$$F(J) = \left\langle \psi_i \right| \left[e^{\sum_k J_k a_k^\dagger + J_k^* a_k} \right]_N \left| \psi_j \right\rangle , \tag{3.82}$$

where the subscript N refers to normal ordering, which means, that only normal ordered expansions in the exponential function are allowed. The variable J can be interpreted as Schwinger probes, but remain a mathematical construct, since they only appear in the generating function, as will be seen later. Partial differentiation with respect to the required Schwinger probes and then taking the limit for the Schwinger probes against zero, to get rid of the exponential, then yields the moments, which are the densities

$$\lim_{J\to 0} \frac{\partial F(J)}{\partial J_p \partial J_q \partial J_r^* \partial J_s^*} = \left\langle \psi_i \right| a_p^\dagger a_q^\dagger a_r a_s \left| \psi_j \right\rangle . \tag{3.83}$$

Note, that the densities are normalized. The corresponding cumulants, κ, are then obtained as the moments of $ln(F(J))$. It shall be noted here, that due to the derivative and the limit for $J \longrightarrow 0$, this can only be applied if $\left\langle \psi_i \middle| \psi_j \right\rangle \neq 0$. This can easily circumvented by not building the densities as moments, but the density operator, i.e. the new generating functional is given as $[exp(\sum_k J_k a_k^\dagger + J_k^* a_k)]_N$. This lifts the requirement of choosing non-orthogonal states. The moments of $F(J)$, i.e. the densities or density operators, can then be recursively obtained from the cumulants as

$$D_1 = \kappa_1 \tag{3.84}$$

$$D_2 = D_1^2 + \kappa_2 \tag{3.85}$$

$$D_3 = D_1^3 + 3D_1\kappa_2 + \kappa_3 \tag{3.86}$$

$$D_4 = D_1^4 + 6\kappa_2 D_1^2 + 3\kappa_2 + 4\kappa_3 D_1 + \kappa_4. \tag{3.87}$$

However, due to normalization it can be found, that $D_3 = \kappa_3 + 3D_2D_1$, which is a rather trivial result. One can also estimate κ_3, by tracing out one particle of the four particle density. The relevant part of D_4 can be shown to be $D_1^4 + 3\kappa_2 + 6\kappa_2 D_1^2 = D_1^4 + 3D_2^2$, which is the first non-trivial contribution, since it is a linear combination. Nevertheless, benchmarking against a few small single-reference systems yields errors for the total densities on the order of 10^{-4} for reduced and transition three particle density matrices[71, 72]. As a short numerical example to estimate the order of magnitude of the error, which the density is allowed to include without changing the accuracy of the XR' result, a relative statistical error is introduced into the density of the type ccaaa from the neutral ground state to the cationic ground state and then XR' evaluated for the same Be_2 system as used throughout the previous part of this thesis. It was shown, that this statistical error is allowed to have a magnitude of less than 10^{-2}. This yields an error norm, which is the Frobenius norm of the difference between the exact tensor and the approximate one, of roughly 10^{-2}. This is the upper bound for the error, and given the error in the literature of around 10^{-4} this approach is worth investigating. In order to do so, the scheme needs to be extended to also account for uneven numbers of annihilation and creation operators. Using the ansatz producing density operators as moments this is straightforward but tedious, since the products between densities and/or cumulants is actually a wedge product from the Grassman algebra, which ensures the antisymmetry of the final density by explicit antisymmetrization. Furthermore, in principle all combinations of field operators need to be taken into account. Therefore, as a first naive example, the same expansion shall be used as for densities sandwiched by equally charged states, and exciting/accepting one electron into/from the continuum

$$\left\langle \psi \right| a_p^\dagger a_q^\dagger a_r^\dagger a_s a_t a_u \left| \psi \right\rangle = (1 - P_{pq} + P_{pr}) \left\langle \psi_p \right| a_q^\dagger a_r^\dagger a_s a_t a_u \left| \psi \right\rangle . \tag{3.88}$$

Utilizing the cumulant approach for D_3 yields

$$\begin{aligned}(1 - P_{pq} + P_{pr}) \left\langle \psi_p \right| a_q^\dagger a_r^\dagger a_s a_t a_u \left| \psi \right\rangle = (1 - P_{pq} + P_{pr}) \frac{1}{2} \Bigg(& \left\langle \psi \right| a_q^\dagger a_r^\dagger a_t a_u \left| \psi \right\rangle \wedge \left\langle \psi_p \right| a_s \left| \psi \right\rangle \\ & + \left\langle \psi_p \right| a_r^\dagger a_s a_t \left| \psi \right\rangle \wedge \left\langle \psi \right| a_q^\dagger a_u \left| \psi \right\rangle \Bigg).\end{aligned} \tag{3.89}$$

If p is now restricted to a single value, e.g. such that the cationic bra state is the cationic ground state, the permutations would yield additional terms, which run over all states, while using even lower particle densities. Hence, as a naive approximation the permutations shall be expected to be separable, leaving one with the ansatz

$$\begin{aligned}\left\langle \psi_p \right| a_q^\dagger a_r^\dagger a_s a_t a_u \left| \psi \right\rangle = \frac{1}{2}\Bigg(& \left\langle \psi \right| a_q^\dagger a_r^\dagger a_t a_u \left| \psi \right\rangle \wedge \left\langle \psi_p \right| a_s \left| \psi \right\rangle \\ & + \left\langle \psi_p \right| a_r^\dagger a_s a_t \left| \psi \right\rangle \wedge \left\langle \psi \right| a_q^\dagger a_u \left| \psi \right\rangle \Bigg).\end{aligned} \tag{3.90}$$

Using this ansatz one obtains an error norm of 1.3, which two orders of magnitude larger, than the upper bound determined before. The error norm is 23 % of the total norm of the correct density, which means, that around 77 % of the density are recovered. Not using the linear combination, but only the single terms, reproduce the tensor with a similar accuracy. The same is true for the same operator string but sandwiching it between the anionic and the neutral ground state, where an error norm of 1.2 is achieved, recovering 85 % of the correct density. These results are orders of magnitude worse, than the errors published in literature as well as the required upper boundary. However, given the fact, that most of the density is still recovered, the approach can at least be expected to be a rough approximation to the density. The large deviation from the results published in the literature then is probably due to two reasons. The first one is, that the higher the dimension of the target density, the more precise the approximation becomes. Taking this into account, one can expect a lower accuracy for the three particle IP/EA densities, than for the neutral three particle densities. The second reason for lower accuracy than the published results, which probably has the biggest impact, is the fact, that the system of interest provides significant multi-reference character, whereas the systems investigated in literature are strictly single reference. Due to the high multi-reference character the valence electrons are strongly correlated, which significantly increases the fully correlated contribution of all particles under consideration, which is not accounted for by the cumulant approach. Hence, due to the initially estimated accuracy, which is more than two orders of magnitude larger than the estimated upper boundary, this approach will not be further investigated. It shall be noted here, that this approach might offer sufficient accuracy for single reference systems though, but this is also possible using e.g. ADC densities with similar computational cost for low orders of perturbation theory.

3.2.5. Adapted Integrals

An other approach to lower the computational effort is to cheaply approximate the correction of higher orders in $\hat{S}$. In analogy to Hartree-Fock an ansatz has been chosen, which approximates the two particle integrals by their one-particle mean-field. This approximation can be formulated as

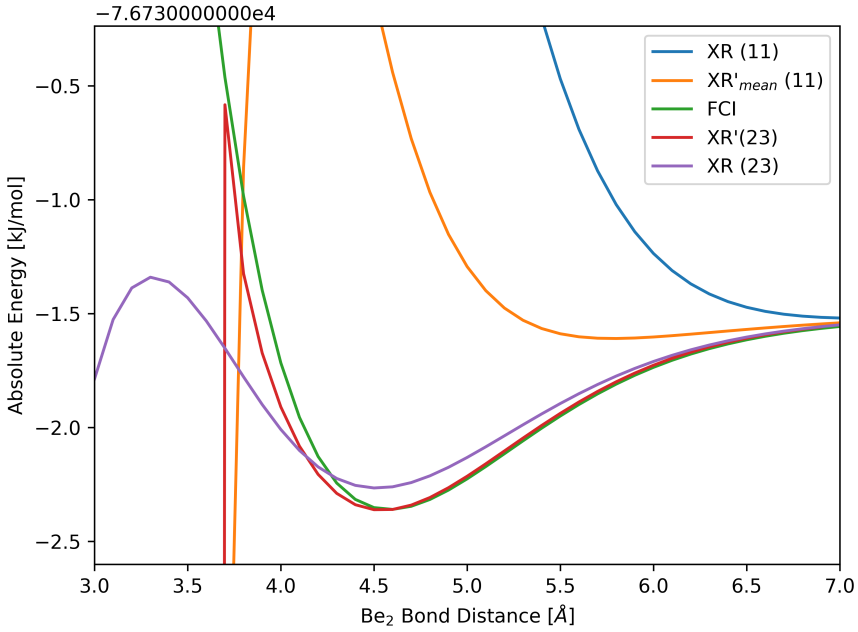

Figure 3.11.: Comparison of XR and XR'$_{mean}$ for the 11 best neutral states against the same methods for the full optimized state space and FCI for the dissociation curve of the Beryllium dimer.

shown in section 2.1, however, since post-HF one particle densities are already calculated, one can increase the precision by building the two-particle mean-field, $\tilde{v}$, as

$$\tilde{v}^{r_0}_{p_0} = 2\rho^{q_0}_{s_0} v^{r_0 s_0}_{p_0 q_0} + 2\rho^{q_1}_{s_1} v^{r_0 s_1}_{p_0 q_1} \tag{3.91}$$

$$\tilde{v}^{r_1}_{p_0} = 2\rho^{q_0}_{s_0} v^{r_1 s_0}_{p_0 q_0} + 2\rho^{q_1}_{s_1} v^{r_1 s_1}_{p_0 q_1} \tag{3.92}$$

$$\tilde{v}^{r_0}_{p_1} = 2\rho^{q_0}_{s_0} v^{r_0 s_0}_{p_1 q_0} + 2\rho^{q_1}_{s_1} v^{r_0 s_1}_{p_1 q_1} \tag{3.93}$$

$$\tilde{v}^{r_1}_{p_1} = 2\rho^{q_0}_{s_0} v^{r_1 s_0}_{p_1 q_0} + 2\rho^{q_1}_{s_1} v^{r_1 s_1}_{p_1 q_1}. \tag{3.94}$$

Applying this approach for purely neutral states corrects the error from XR from roughly 8 kJ/mol to 2 kJ/mol at equilibrium distance of the Be_2 used before. The overall performance along the bond distance is also significantly improved, as shown in Figure 3.11.

This result with the mean field correction was obtained by applying the mean field correction only for the ERI term in $\overline{S\mathcal{H}}^{[1]}_{\{0\}}$, while for the ERI terms in $\overline{S\mathcal{H}}^{[0]}_{\{1\}}$ the actual ERIs were used, since they do not contain $\hat{S}^{[1]}$, even though they contribute to $\hat{S}^{[1]}\hat{H}$. However, using this ansatz for ionized states yields overcorrection of several orders of magnitude. Applying the mean field approach to approximate all ERI terms of $\hat{S}^{[1]}\hat{H}$, results in an overcorrection of the same order of magnitude,

as for the first approach. Note, that approximating zeroth order contributions, in order to achieve consistent treatment of all ERI terms, is not useful, because the zeroth order ansatz, XR, already accounts for most of the correlation, as can be seen in Figure 3.8. Only approximating $v_{p_0 q_0}^{r_0 s_0}$ and $v_{p_1 q_1}^{r_1 s_1}$, i.e. the terms containing five dimensional density tensors, roughly lowers the overcorrection by a factor of one half. Note, that the only relevant term from $\hat{S}^{[1]}\hat{H}$, which cannot be approximated by this mean field ansatz, namely $(-1)^{n_2}(1 - P_{12}) \sum_{t_2 u_1 p_1 q_1 r_2 s_2} \sigma_{t_2 u_1} v_{p_1 q_1}^{s_2 r_2} \rho_{q_1 p_1}^{u_1} \rho_{t_2}^{r_2 s_2}$, provides a very small contribution to the ground state energy on the order of 10^{-2} kJ/mol. Hence, the terms, dominating the overcorrection can be identified as the terms contributing to $\tilde{v}_{p_0}^{r_0}$ and $\tilde{v}_{p_1}^{r_1}$. Pointing out the exact reason, why these terms are so poorly approximated is very hard, because several reasons possible. For instance, the expansion in $\hat{S}$ with XR as the zeroth order ansatz yields large numbers with very delicate cancellations. Hence, small errors in the densities or the integrals, as seen for the cumulant approach, yield large errors in the final ground state energies. Furthermore, $\tilde{v}_{p_0}^{r_0}$ and $\tilde{v}_{p_1}^{r_1}$ provide much larger contributions, than $\tilde{v}_{p_0}^{r_1}$ and $\tilde{v}_{p_1}^{r_0}$, which suffice to approximate $\hat{S}^{[1]}\hat{H}$ for neutral states. By further analyzing this approach, one also notices, that this approach is in fact related to the cumulant approach. For the example of the term containing the three particle EA density from $\hat{S}^{[1]}\hat{H}$ this yields

$$\begin{aligned}
\sum_{t_1 u_2 p_1 q_1 r_1 s_1} \sigma_{t_1 u_2} v_{p_1 q_1}^{r_1 s_1} \rho_{p_1 q_1 t_1}^{s_1 r_1} \rho^{u_2} &= \sum_{t_1 u_2 p_1 q_1 r_1 s_1} \sigma_{t_1 u_2} v_{r_1 s_1}^{p_1 q_1} \rho_{p_1 q_1 t_1}^{s_1 r_1} \rho^{u_2} \\
&\approx \sum_{t_1 u_2 p_1 q_1 r_1 s_1} \sigma_{t_1 u_2} v_{r_1 s_1}^{p_1 q_1} \rho_{p_1 t_1}^{r_1} \rho_{q_1}^{s_1} \rho^{u_2} \\
&= \sum_{t_1 u_2 p_1 r_1} \sigma_{t_1 u_2} \tilde{v}_{r_1}^{p_1} \rho_{p_1 t_1}^{r_1} \rho^{u_2},
\end{aligned} \tag{3.95}$$

where the last term is equal to the corresponding term from $\hat{S}^{[1]}\hat{H}$ with $\tilde{v}_{r_1}^{p_1}$ substituted by $h_{r_1}^{p_1}$, while the approximation $\rho_{p_1 q_1 t_1}^{s_1 r_1} \approx \rho_{p_1 t_1}^{r_1} \rho_{q_1}^{s_1}$ was applied in the second line. This approximation is at the core of the cumulant approach, which was shown to yield insufficient accuracy for the corresponding term containing the three particle IP density. Hence, the approach of approximating higher particle densities, by building a single antisymmetrized tensor product of two lower particle densities can be expected to yield insufficient accuracy for the five dimensional density tensors, and more generally speaking also for the terms containing a two particle EA and a two particle IP density tensor. This also explains, why the results published for the cumulant ansatz are significantly better than for the numerical experiment performed earlier in this chapter, since the published results only include neutral states. At this point it shall be noted, that one can most probably increase the performance not only of this and therefore also the cumulant ansatz, but also of XR and its

expansions in $\hat{S}$ in general by choosing a different set of orbitals. Especially localized orbitals are a seemingly good choice, due to the minimized interaction between fragments. Common choices are the Edminston-Ruedenberg orbitals, which minimize the self interaction by minimizing the following functional

$$f_{ER}(\{\phi\}) = \sum_i v_{iiii}, \tag{3.96}$$

the Boys orbitals, which minimize the sum of variance

$$f_B(\{\phi\}) = \sum_i \left\langle \phi_i \right| \left(r - \langle \phi_i | \, r \, | \phi_i \rangle\right)^2 \left| \phi_i \right\rangle, \tag{3.97}$$

and the Pipek-Mezey orbitals, which are obtained by minimizing

$$f_{PM}(\{\phi\}) = \sum_i \sum_N \left\langle \phi_i \right| \frac{1}{2} \sum_{\mu \in N, \nu} (1 + P_{\mu\nu}) \left| \chi_\mu \right\rangle (S_{\mu\nu})^{-1} \langle \chi_\nu | \left| \phi_i \right\rangle, \tag{3.98}$$

where $|\chi\rangle$ denotes a basis function and N runs over all atoms. Many post-HF methods exist, which can utilize such sets of orbitals, e.g. local ADC[69, 73]. The only difference to standard ADC is, that the Fock matrix is not diagonal anymore, which yield non-diagonal zeroth order terms, as well as first order amplitudes, which need be iterated. Hence, densities can still be build within the same ISR basis, with adapted orbitals and amplitudes, yielding the same working equations as already derived in section 3.2.3. Regarding the presented mean-field approach and therefore also the cumulant ansatz, the Edminston-Ruedenberg set of orbitals seem like a good choice, since they minimize the diagonal of the two-electron integrals, which can be expected to lower the overall norm of the ERIs, and therefore also the impact of the five dimensional density tensors. However, one could also think of spatially localizing orbitals with the Boys orbitals or the Pipek-Mezey orbitals, given atomic orbital basis functions.

3.2.6. Numerical Decomposition Techniques

Finally, one can also utilize methods from computer science, in order to lower the computational effort. However, since the major problems of cheap access to densities and quickly optimizing the monomer states are not solved yet, the only approaches employed are those with the goal of lowering the effective rank of the high dimensional tensors. This has been attempted using Tucker- and singular value decompositions, e.g. the canonical polyadic decomposition, as implemented in the tensorly programm package[74]. These tensor decompositions can be applied very well to the XR

ansatz, because the working equations have to be evaluated at all states of fragment one for all states of fragment two for dimer interactions. These nested loops over four state indices are the reason, why small state spaces are required for efficient computations. Since the densities are only evaluated on a single system a significant speed-up can be achieved by decomposing the density tensors on top of caching intermediates. One can also think of decomposing the ERIs, but it was shown, that they do not profit from decomposition, while also their rank could not be lowered without introducing significant errors to the XR energy. This might seem surprising at first, considering that the integrals also contain contributions between different fragments, which are already quite far apart at the equilibrium geometry of the Be_2 system in the 6-31G basis. However, it was shown in literature, that the ERIs also contain a significant contribution of the multipole interaction between electrons, which reaches far through space and depends on all positions of the electrons and therefore also on their excitation levels. Nevertheless, using batching techniques or non-rank lowering decompositions, computations on including ERIs can still be performed efficiently[75, 76]. For the density tensors on the other hand the effective rank could be lowered slightly, using Tucker decomposition, which results in a tensor of the same dimensionality as the original density tensor, with a reduced size in each dimension, and the corresponding two dimensional tensors, which are the transformation matrices between the original density tensor and the tensor of lower rank. Note, that there is still a lot of room left for further optimization, but decomposition approaches always require building the full tensor first, which is inefficient. Hence, the future focus will be laid on how the densities can be approximated without building the full tensor, which can besides using e.g. ADC densities also be achieved by algorithms like skeleton approaches[77].

3.2.7. Implementation

The implementation, which has been used to obtain the numerical data for this chapter, was written from scratch and can be accessed through https://github.com/adutoi/QodeApplications. Since this package was written from scratch, the basic workflow shall be briefly examined here. The reference data, symmetric overlap-, one- and two-electron integrals in the AO basis and molecular orbital coefficients are currently obtained from the psi4 programm package[60], while the FCI densities are obtained from a homebrew FCI code and the ADC densities are build from prerequisites obtained from the adcc package[58]. All of these backends can be exchanged with little effort. In the next step the densities are either imported as explicit tensors from the FCI backend, or as lazily evaluated contraction schemes in the case of the ADC densities. Note, that the ADC densities can also be numerically evaluated, before using them in the working equations. Having the ADC densities evaluated in a lazy fashion via a contraction scheme, one can make use of the tensor product like

structure of the ADC densities, which only include up to fourth order tensors in low orders of perturbation theory, which lifts the requirement of handling five dimensional tensors. If however, higher orders of perturbation theory are required to obtain densities of sufficient accuracy, six and higher dimensional tensor can be required, which puts the explicit evaluation in favor. Then the (partially-) biorthogonalized integrals are build from the symmetric integrals in the atomic orbital basis, and the molecular orbital coefficients, where the ordering of the molecular orbitals can be exchanged to be in line with the ordering of the molecular orbitals in the density tensors. The integrals are therefore put into a homebrew dynamic array object, which can be cached, so only the required transformations are made, while also taking arguments defining the ordering of the molecular orbitals as well as the wrapper used for the tensors. It also tracks the fragment indices. The densities, or, if they are lazily evaluated, their preliminaries, are also wrapped in the same way. This wrapper has been chosen as the TensorLy wrapper[74], which has the advantage, that linear algebra backends, e.g. NumPy, PyTorch or TensorFlow, can be switched with a single line of code, as well as whether GPU acceleration is desired or not, if the linear algebra backend provides it. The wrapper also takes care of keeping double precision, since e.g. PyTorch uses single precision as the default precision, which is insufficient when going beyond the zeroth order in $\hat{S}$. At this point tensor decompositions can then be applied. In the next step the supersystem overlap matrix for all dimer interactions is calculated, according to Eq. (3.59) for XR and additionally Eq. (3.60) for XR'. Note, that one can also request higher orders in $\hat{S}$. Accordingly the supersystem Hamiltonian matrix is calculated according to Eqs. (3.79) for XR and additionally (3.80) for XR'. At this point lazily evaluated densities can be utilized to lower the computational effort in terms of CPU time and memory requirements for intermediate objects. In order to optimize this final contraction and keep track of previous expression trees, the tensornet library has been developed from scratch. It is still under heavy development, but already takes care of dispatching, which will later be handled by e.g. the optimized NumPy.einsum dispatching, as well as building expression trees, which are finally evaluated using the TensorLy wrapped tensors, so it is agnostic with respect to the backend. The final supersystem matrices are very large, and therefore also build in a lazy fashion. The final evaluation can then be done by explicitly inverting the supersystem overlap and by fully diagonalizing $\left\langle \bar{\Psi}^{\tilde{I}} \right| H \left| \Psi_{\tilde{J}} \right\rangle = \sum_{\tilde{K}} \bar{S}^{\tilde{I}\tilde{K}} \left\langle \Psi_{\tilde{K}} \right| H \left| \Psi_{\tilde{J}} \right\rangle$, or using the XR-CCSD method, already mentioned in section 2.12, which has a very low formal scaling of N^3 with the system size and N^4 with the number of states per fragment, which is always heavily truncated.

3.3. Crystallization-Induced Reversible Ring Opening in Tetraazahexacene Derivatives

3.3.1. Computational Details

In this chapter all calculations have been conducted using standard DFT methodology, utilizing the B3LYP functional and the 6-311G* basis set as implemented in the QChem 5.2 programm package[78], apart from the optimizations using the explicit crystal environments, where GFN2-XTB was applied, as implemented in the xtb 6.4.1 programm package[21], and the crystal environment was fixed.

3.3.2. Experimental Findings

Experimental findings show[47], that some derivatives of Tetraazahexacene crystallize under opening of a Carbon-Carbon bond, leading to a Pyrazinopyrazine core. It was also found, that solvation of said crystals, as well as grinding the crystals to amorphous structures, reverses the ring opening, as shown in Figure 3.12.

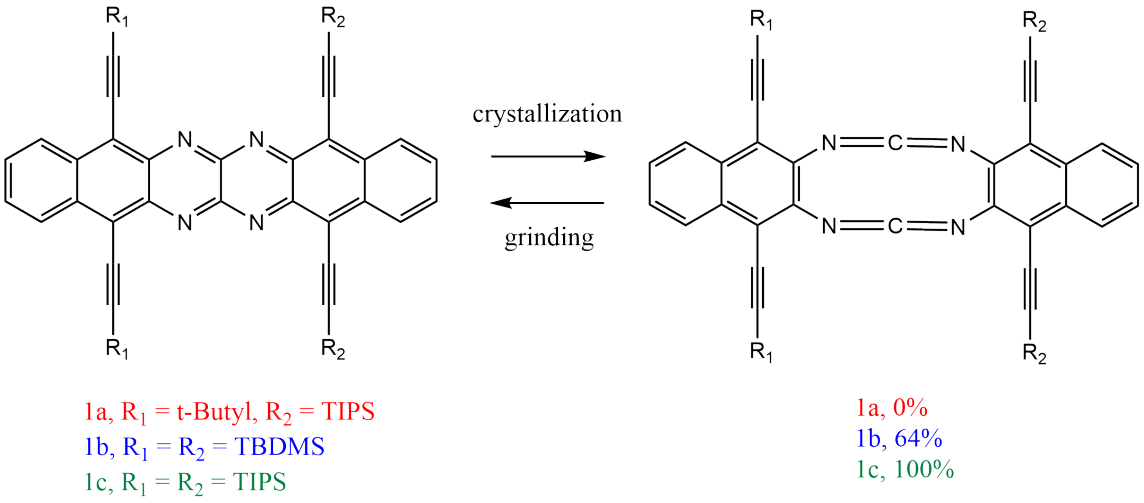

Figure 3.12.: Reversible reaction of three derivatives of Tetraazahexacene to Pyrazinopyrazine under crystallization.

This reaction can be monitored by infrared spectroscopy, since the Pyrazinopyrazine core provides a strong absorption band around 2200 cm^{-1}, which is in line with the simulated spectrum, shown in Figure 3.13. One can also UVVis spectroscopy, where a broad absorption band around 1100 nm shows the existence of a Tetraazahexacene core, which completely vanishes during isomerization

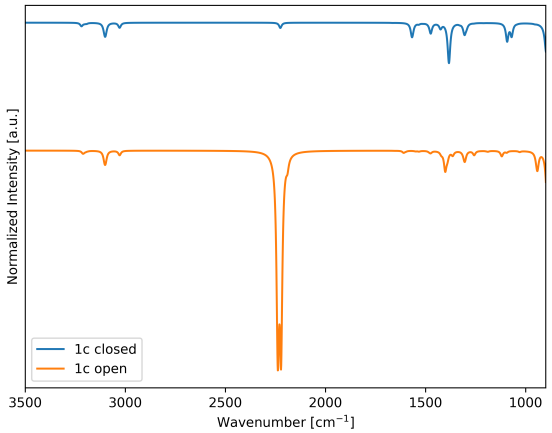

Figure 3.13.: Simulated infrared spectrum of compound **1c** in open and closed form in Dichloromethane with a Lorenzian broadening of 15 cm^{-1} at the half maximum.

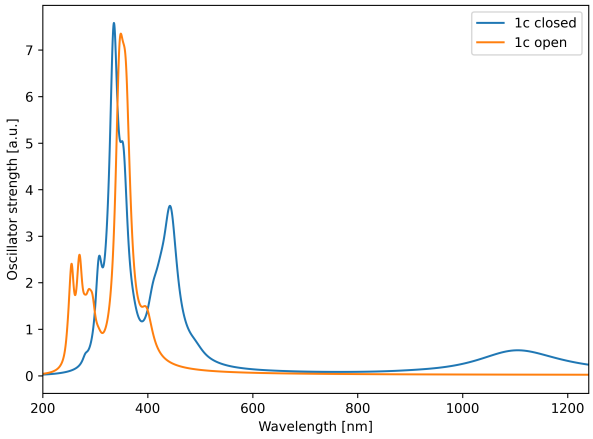

Figure 3.14.: Simulated UVVis spectrum of compound **1c** in open and closed form in Dichloromethane with a Lorenzian broadening of 0.2 eV at the half maximum.

to the Pyrazinopyrazine core. This is also in line with the experiment, and the simulated spectrum is shown in Figure 3.14.

Note, that there are three different classes of possible Pyrazinopyrazine conformers, which can be divided according due to their point group symmetry. The possible symmetries are D2h, C2v and C2, which refer to completely planar, symmetrically distorted out of plane and asymmetrically distorted out of plane, given, that R_1 and R_2 are equal. However, only the asymmetrically distorted conformer will be investigated in the following, since it is the most stable conformer when simulated in Dichloromethane using a polarizable continuum model, while it is also the conformer in the experimentally observed crystal structures of compounds **1b** and **1c**. An additional experimental finding is, that the compound corresponding to compound **1c** with a diazahexacene core crystallizes without breaking a bond, as shown in Figure 3.15.

3.3.3. Computational Investigation

This behaviour upon crystallization shall be investigated in the following for all four compounds. However, since the crystal environment needs to be modelled explicitly, which requires calculations for up to 3000 atoms, sophisticated methods to find reaction paths, like the meta-dynamics reaction path finder, nudged elastic band or growing string methods cannot be applied here. Hence, the reaction path needs to be approximated. For computational simplicity the reaction coordinate is chosen as the distance of the Carbon atoms, whose chemical bond is broken during the crystalliza-

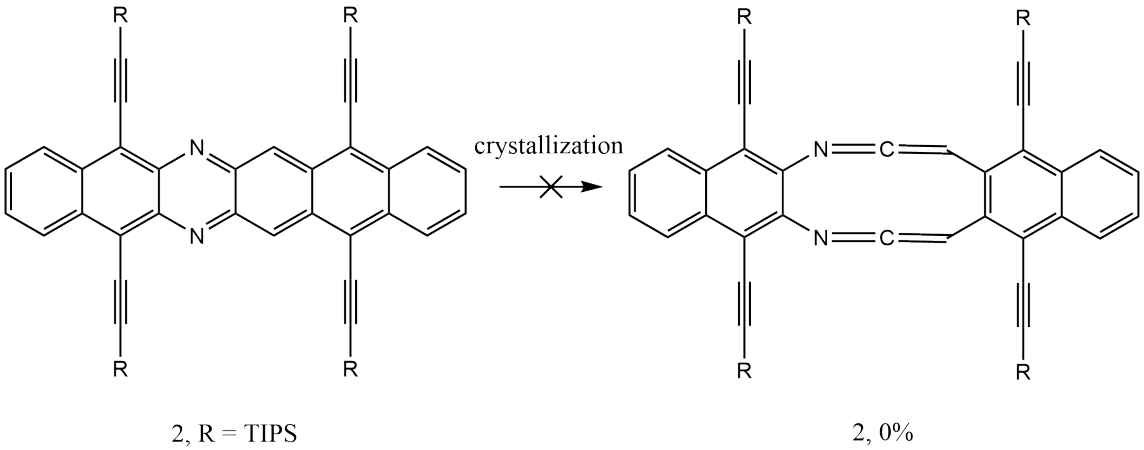

Figure 3.15.: Crystallization of compound **2**, which has the same functionalization as compound **1c**, does not yield an ten membered ring structure upon crystallization.

tion process, while relaxing the remaining degrees of freedom in the constraint of the chemical environment, which is either Dichloromethane modelled with a polarizable continuum model or the crystal environment obtained from the crystal structure. Optimizing the structure in the solvent environment can then be handled by DFT, but an optimization in the explicit crystal environment requires tremendous computational effort on this level of theory, even though the crystal environment is not optimized. Using polarizable embedding also requires high computational effort, because the embedding function needs to be fitted to the compounds, which is rather slow, if the number of atoms in the single molecules surpasses 100. Optimizing by modelling the crystal environment with effective charges at the atom centers, like Mulliken charges, is expected to underestimate the repulsion and therefore yield wrong structures. Hence, the optimization in the crystal environment needs to be performed at a lower level of theory. Note, that one could also use other embedding techniques, like QM/MM, but as already discussed in section 2.9.3, the GFN2-XTB method can easily handle structures with 3000 atoms, while yielding very good results for geometries. The reduced crystal structures were then chosen as such, that the central molecule is surrounded by a shell of the thickness of one molecule. This could be further reduced to a two dimensional shell with the same thickness for compounds **1a** and **1c**, since along the third dimension the two dimensional layers show a significant distance, leading to approximately decoupled layers. This yields a total of 5, 7, 27 and 18 molecules for compounds **1c**, **1a**, **1b** and **2**, respectively. These reduced crystal structures are visualized in Figure 3.17 and the single molecules are shown in Figure 3.16.

Note, that compounds **1a** and **2** crystallize in a brick wall motif, while compound **1c** provides a modified triple block motif. The packing motif for compound **1b** cannot be determined precisely, due to the mixture of Pyrazinopyrazine and Tetraazahexacene cores of roughly 2:1 respectively, which

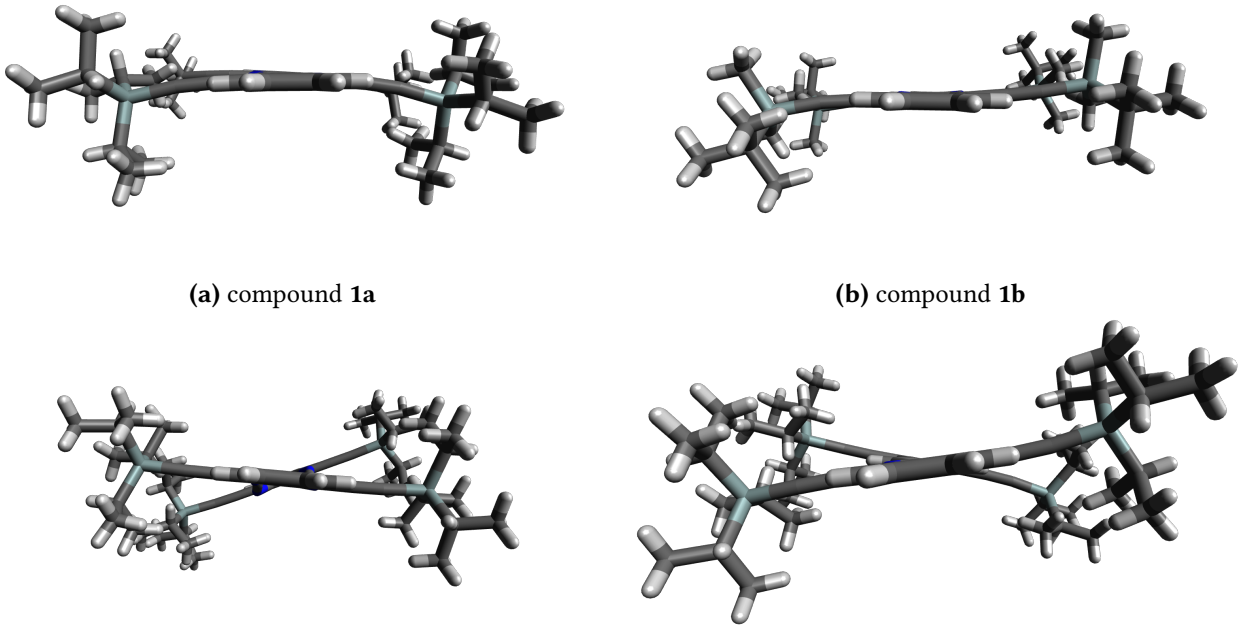

(a) compound **1a**

(b) compound **1b**

(c) compound **1c**

(d) compound **2**

Figure 3.16.: Molecular geometries obtained from single-crystal X-ray spectroscopy.

also leads to minor deviations between orientations of the side chains, which cannot be resolved by the spectrometer. With the geometries from the relaxed scans along the Carbon-Carbon distance of interest in the crystal environment at hand, one can now further refine the result obtained for the relative energies. This is necessary, since GFN2-XTB, and related XTB methods, do not yield reliable relative energies. This is especially true for the systems under investigation, because for instance optimizing the geometry of compound **1c** in gas phase or solvent environment yields the closed, i.e. the Tetraazahexacene, form, even when the Pyrazinopyrazine structure is provided as the initial guess, where e.g. DFT with the B3LYP functional shows a deep local minimum. However, as already discussed, polarizable embedding requires large computational effort. Hence, it was decided to model the environment using the Mulliken charges obtained from the previous GFN2-XTB optimization. Since the charge centers still provide a distance to the central molecule above the van-der-Waals distance, this is a good approximation. Utilizing the same level of theory as used for the solvent environment, without the polarizable continuum model, the reaction paths for all four compounds in the crystal environment can be obtained and are compared to the same reaction path in the solvent environment in Figure 3.18.

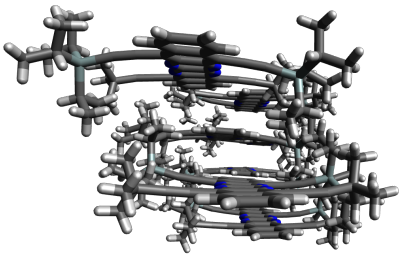

(a) compound **1a**

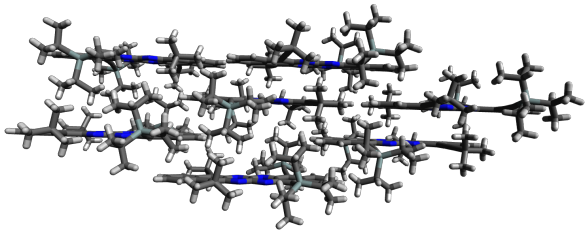

(b) compound **1a**

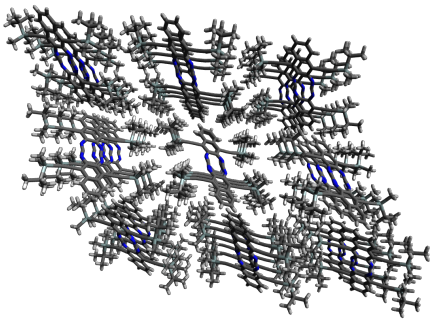

(c) compound **1b**

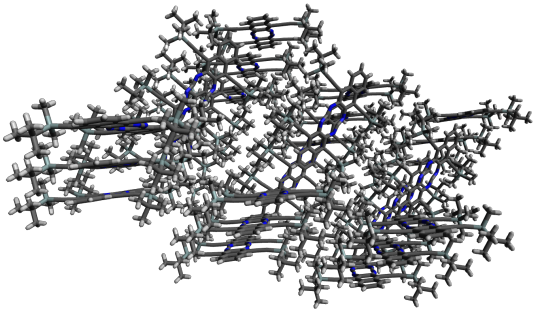

(d) compound **1b**

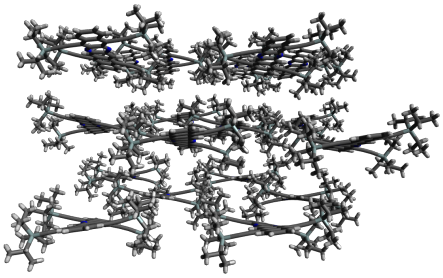

(e) compound **2**

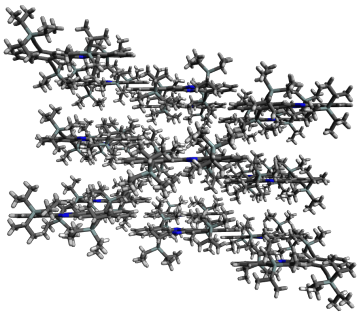

(f) compound **2**

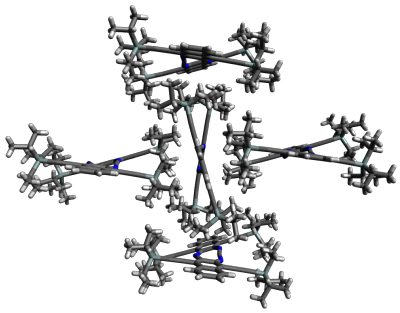

(g) compound **1c**

Figure 3.17.: Effective crystal environments obtained from single-crystal X-ray spectroscopy.

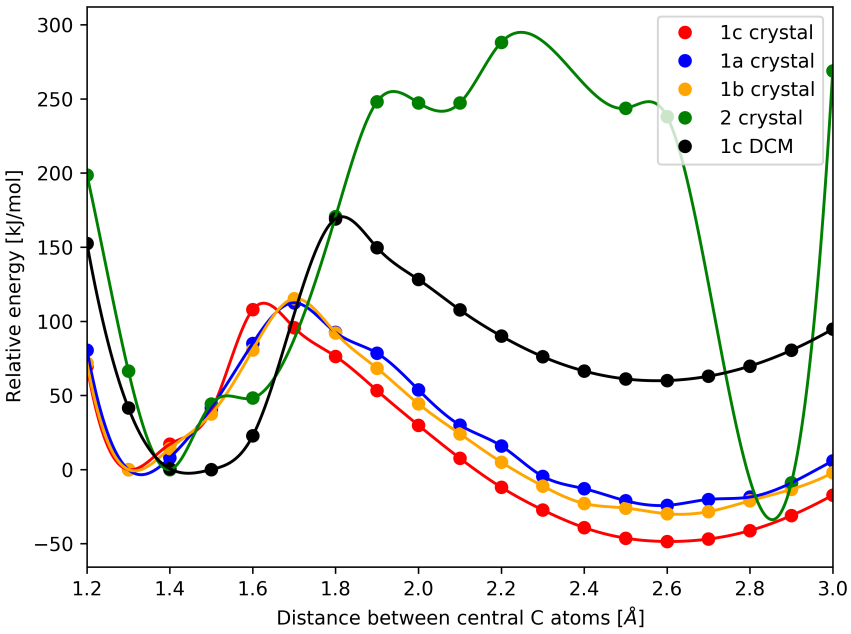

Figure 3.18.: Reaction paths for various compounds obtained from relaxed scans along the central C-C bond in the crystalline and solvated environment. The data points were interpolated using a cubic spline fit, which ensures minimal curvature.

For comparison, using GFN2-XTB for the relative energies yields a single minimum for all compounds in between the Tetraazahexacene and the Pyrazinopyrazine minima obtained from the DFT level of theory. Surprisingly, all compounds show two minima, independent of the environment, and the absolute minimum in energy for all compounds in the crystal environment is the Pyrazinopyrazine form. Only in the solvent environment is the Tetraazahexacene form thermodynamically stable. The calculated reaction barriers from the closed to the open form and $E_{closed} - E_{open}$ are 116 kJ/mol, 115 kJ/mol, 112 kJ/mol, 295 kJ/mol and 173 kJ/mol as well as 21 kJ/mol, 29 kJ/mol, 48 kJ/mol, 34 kJ/mol and -62 kJ/mol for compounds **1a**, **1b**, **1c**, **2** in the crystal and **1c** in the solvent environment, respectively. In order to put these barriers into perspective, activated complex theory is applied here, where the proportionality factor is set to one, and the standard Gibbs free energy is approximated with the energy difference. The latter approximation can be justified by the fact, that the initial and final structures have very similar degrees of freedom, suggesting a very small change in the entropy. Given an energy difference of 105 kJ/mol this yields a half-life time of roughly a day. The energetic differences of the minima can even be compared to experimental findings, when assuming chemical equilibrium. With crystal growth at room temperature, one can then determine the energy difference required to obtain a mixture of 2:1, as observed for the crystal structure of compound **1b**, of roughly 2 kJ/mol from a Boltzmann distribution. Comparison to the

calculated energy difference of 29 kJ/mol shows, that the sign has been determined correctly, but the quantitative error is around 27 kJ/mol. Given this error range, the calculated reaction barriers can range from being large enough to provide kinetic stability of either isomer of compounds **1a**, **1b** and **1c** to small enough to ensure chemical equilibrium at room temperature. Compound **2** is then either kinetically or thermodynamically stable and **1c** in the solvent environment is thermodynamically stable. Furthermore, compound **1a** could also be thermodynamically stable in the Tetraazahexacene form, but compound **1c** still has the global energetic minimum at the Pyrazinopyrazine form. Even though the relative energies cannot be brought to agreement with the experimental data with absolute certainty, it shall be noted, that the barriers and energy differences of the minima show a clear trend, from compound **1a** with highest barrier and smallest energy gap between the minima to compound **1c** with the lowest barrier and the largest gap between the minima with compound **1b** in between. Hence, the remaining question is, given the fact, that compound **1c** can be seen to not be kinetically stable from the experiment, whether compound **1a** is kinetically or thermodynamically stable. This can however be experimentally proven with little effort, by slightly heating the crystal and then performing the single-crystal X-ray crystallography. Now the question arises after the dominant interaction, which forces the break of the innermost Carbon-Carbon bond. This dominant interaction could either be the van-der-Waals repulsion due to small distances between atoms of the central molecule and the crystal environment, or the polarization of the environment, due to the crystal environment. This can be investigated by calculating the optimized open and closed geometries of compound **1c** from the crystal environment in gas phase. This absence of the crystal environment leads to a change in the energy difference between open and closed form of less than 2 kJ/mol compared to the energy difference in the crystal environment. Hence, the polarization due to the crystal environment is negligible, and the geometrical distortion of the molecule is the reason for the isomerization. However, compound **2** is similarly distorted to compound **1c**, as can be seen from Figure 3.16. Hence, one can expect, that only Tetraazahexacene derivatives with very bulky side groups crystallize under opening of the central Carbon-Carbon bond. The mechanism of the ring-opening was found to be of electrocyclic nature. This can be determined from a localized orbital bonding analysis using Pipek-Mezey orbital localization and Lowdin population analysis for compound **1c**, which shows no radicals at the approximate transition state geometry. This result is the same for the crystal and solvent environment, as well as for a restricted orbital ansatz or broken symmetry ansatz, where HOMO and LUMO are mixed 70:30, respectively. Hence, the reaction should obey the Woodward-Hoffman rules, which propose the asymmetrically twisted conformer, which is the one observed from single-crystal X-ray crystallography.

4. Conclusion and Outlook

Excitonic Renormalization

In this thesis crucial steps in the development of a novel fragmentation approach, Excitonic Renormalization, XR, towards practical applicability were presented. The first important achievement was the reformulation of the overlap matrix into a series of orbital rotations, which was shown to converge quickly for the Beryllium dimer. This lifts the necessity of numerically orthogonalizing the full Fock space, build from all fragments. The next achievement was to show, that approximate densities obtained from Møller-Plesset, MP, and Algebraic Diagrammatic Construction Theory, ADC, quickly converge with increasing order of perturbation theory, which strongly indicates, that densities obtained from methods, which do not span the full Fock space, yield sufficient accuracy. However, proving this assumption requires the full second order densities, which will be published in the future. Besides approximating the densities using ADC, method independent approaches of algebraic and numerical nature were presented and tested. For the presented cumulant and adapted integral ansätze a relation has been shown, as well as them managing to approximate densities between neutral states with good accuracy, while densities, which include charged states, were shown to yield insufficient accuracy. The presented numerical decomposition techniques were able to only slightly lower the rank of the density tensors under investigation, while also requiring to build the full high-dimensional tensors first, which is highly inefficient. It was further noted, that the performance of all of these approximations can be improved e.g. by utilizing localized orbitals. Based on these results, one can expect approximate densities, e.g. from ADC, to yield sufficient accuracy for the XR method, where high particle densities need to be approximated on the level of working equations and not with a method independent approximation scheme. Hence, obtaining an XR method of practical relevance requires further evaluation and approximation of method specific densities as well as an efficient scheme to obtain optimized state spaces.

Polaritonic Perturbation Theory

Additionally, an extension to consistently describe polaritons within perturbation theory was presented in this thesis as well. Therefore, two different splittings of the Hamiltonian have been investigated, using either the standard Fock operator, yielding origin invariant methods even for systems with a global charge, or the polaritonic Fock operator, consistently adjusting the orbitals to the vacuum field contribution, as the unperturbed Hamiltonian. Using these splittings of the Hamiltonian, two different ground and excited state methods were developed, which can be interpreted as extensions to MP and ADC, respectively. Numerical results for both splittings were shown to agree well in first order for intermediate coupling strengths. For ground states a similar agreement can be found in second order, while for excited states only the variant based on the polaritonic Fock operator was developed up to second order of perturbation theory. All of these approaches were extensively tested. Furthermore, it was presented how to unitarily transform the ADC variant based on the polaritonic Fock operator into a "quasi-diabatic" representation, which can be used for dynamical simulations of wavepackets in polaritonically coupled states without further adjustments. Comparing three variants of this method within a study on the photodissociation dynamics of Pyrrole in a photonic cavity then showed the importance of including the vacuum field contribution into the Fock operator for strong couplings, which is however not done in most studies published in literature. Considering the negligible computational effort required to build the "quasi-diabatic" representation based on the polaritonic Fock operator, compared to the variant based on the standard Fock operator, it should be used as the default for systems without a global charge, even for small coupling strengths. The developed methodology of polaritonic perturbation theory can also be used to derive consistent polaritonic properties in a straightforward manner, which shall be investigated in the future.

Crystallization-Induced Reversible Ring Opening in Tetraazahexacene Derivatives

Finally, a computational study on the crystallization-induced reversible ring opening of Tetraazahexacene derivatives to Pyrazinopyrazine derivatives was presented. Therefore, the experimental results were presented first and it was shown, that the experimental spectra could be reproduced well. In the following the energy profile along the reversibly opening Carbon-Carbon bond was computed using constraint optimization with and without the explicit crystal environment. The resulting energy profiles show double wells for all derivatives. In solution the closed form was shown to be

kinetically and thermodynamically stable, while the Diazahexacene compound was shown to be only kinetically stable. The remaining compounds show no kinetic stability and thermodynamically favored open forms, which qualitatively agrees only with two of the remaining three compounds. Assuming a Boltzmann distribution an error was then estimated for the energy difference of the open and closed form of one of these compounds, which, applied to the other compounds, yields reasonable agreement with the experimental data. Furthermore, the reaction was found to follow a concerted electrocyclic mechanism and the dominant force, leading to a ring-opening reaction, is the repulsion of the large substituents in the crystal, resulting in a distorted aromatic core. Hence, Pyrazinopyrazine cores are favored over Tetraazahexacene cores, when the substituents force the aromatic system to twist asymmetrically.

Bibliography

[1] *Photosynthesis: From light to biosphere ; proceedings of the Xth International Photosynthesis Congress, Montpellier, France, 20-25 August 1995*, (Ed.: P. Mathis), Kluwer Acad. Publ, Dordrecht, **1995**.

[2] A. G. Lee, *Rhodopsin and G-protein linked receptors*, JAI Press, Greenwich, Conn, **2010**.

[3] G. Verkhivker, *International journal of molecular sciences* **2022**, *23*, DOI 10.3390/ijms23062928.

[4] A. E. Siegman, *Lasers*, University Science Books, Mill Valley, California, **1986**.

[5] A. L. Schawlow, C. H. Townes, *Physical Review* **1958**, *112*, 1940–1949.

[6] H. Häberlin, *Photovoltaics System Design and Practice*, 1. Aufl., Wiley, s.l., **2012**.

[7] J. F. Cox, *Fundamentals of linear electronics: Integrated and discrete*, 2. ed., Delmar Thomson Learning, Albany, NY, **2002**.

[8] R. A. Marques Lameirinhas et al., *Energies* **2022**, *15*, 1823.

[9] D. H. Carr et al., *Lancet (London England)* **1984**, *1*, 484–486.

[10] A. D. Lantada, *Handbook of active materials for medical devices: Advances and applications*, CRC Press, Boca Raton, Fla., **2012**.

[11] I. Rostami et al., *International journal of nanomedicine* **2019**, *14*, 7759–7780.

[12] S. Wen et al., *Nature communications* **2018**, *9*, 2415.

[13] A. Aspuru-Guzik et al., *Science (New York N.Y.)* **2005**, *309*, 1704–1707.

[14] A. Y. Kitaev, Quantum measurements and the Abelian Stabilizer Problem, **1995**.

[15] A. Peruzzo et al., *Nature communications* **2014**, *5*, 4213.

[16] E. Schrödinger, *Annalen der Physik* **1926**, *384*, 361–376.

[17] *Proceedings of the Royal Society of London. Series A Containing Papers of a Mathematical and Physical Character* **1928**, *117*, 610–624.

[18] A. Szabo, N. S. Ostlund, *Modern quantum chemistry: Introduction to advanced electronic structure theory*, 1. publ., unabr., unaltered republ. of the 1. ed., New York 1989, Dover Publications, Mineola, New York, **1996**.

[19] J. Schirmer, *Many-Body Methods for Atoms, Molecules and Clusters*, Springer International Publishing, Cham, **2018**.

[20] F. Jensen, *Introduction to computational chemistry*, Third edition, John Wiley & Sons, Chichester, UK and Hoboken, NJ, **2017**.

[21] C. Bannwarth et al., *WIREs Computational Molecular Science* **2021**, *11*, DOI 10.1002/wcms.1493.

[22] A. Dreuw, M. Head-Gordon, *Journal of the American Chemical Society* **2004**, *126*, 4007–4016.

[23] C. Riplinger, F. Neese, *The Journal of chemical physics* **2013**, *138*, 034106.

[24] B. Jeziorski et al., *Chemical Reviews* **1994**, *94*, 1887–1930.

[25] J. Shen, S. Li, *The Journal of chemical physics* **2009**, *131*, 174101.

[26] S. M. Parker et al., *The Journal of chemical physics* **2013**, *139*, 021108.

[27] K. H. Marti, M. Reiher, *Zeitschrift für Physikalische Chemie* **2010**, *224*, 583–599.

[28] A. D. Dutoi, Y. Liu, *Molecular Physics* **2019**, *117*, 431–445.

[29] Y. Liu, A. D. Dutoi, *Molecular Physics* **2019**, *117*, 446–461.

[30] G. Lerario et al., *Nature Physics* **2017**, *13*, 837–841.

[31] M. A. Sentef et al., *Science advances* **2018**, *4*, eaau6969.

[32] A. Thomas et al., *Science (New York N.Y.)* **2019**, *363*, 615–619.

[33] H. Hiura et al., *Vacuum-Field Catalysis: Accelerated Reactions by Vibrational Ultra Strong Coupling*, **2019**.

[34] R. Chikkaraddy et al., *Nature* **2016**, *535*, 127–130.

[35] O. Vendrell, *Chemical Physics* **2018**, *509*, 55–65.

[36] J. Flick et al., *Proceedings of the National Academy of Sciences of the United States of America* **2017**, *114*, 3026–3034.

[37] M. Kowalewski et al., *The Journal of chemical physics* **2016**, *144*, 054309.

[38] M. Ruggenthaler et al., *Physical Review A* **2014**, *90*, DOI 10.1103/PhysRevA.90.012508.

[39] M. Ruggenthaler, Ground-State Quantum-Electrodynamical Density-Functional Theory.

[40] I. V. Tokatly, *Physical review letters* **2013**, *110*, 233001.

[41] J. Flick et al., *ACS photonics* **2019**, *6*, 2757–2778.

[42] J. Yang et al., *The Journal of chemical physics* **2021**, *155*, 064107.

[43] N. Vu et al., *The journal of physical chemistry. A* **2022**, *126*, 9303–9312.

[44] J. Malave et al., *The Journal of chemical physics* **2022**, *157*, 194106.

[45] T. S. Haugland et al., *Physical Review X* **2020**, *10*, DOI 10.1103/PhysRevX.10.041043.

[46] U. Mordovina et al., *Physical Review Research* **2020**, *2*, DOI 10.1103/PhysRevResearch.2.023262.

[47] W. Zong, PhD thesis, Heidelberg University Library, **2023**.

[48] R. A. Marcus, N. Sutin, *Biochimica et Biophysica Acta (BBA) - Reviews on Bioenergetics* **1985**, *811*, 265–322.

[49] J. Schirmer, *Physical Review A* **1982**, *26*, 2395–2416.

[50] J. Schirmer, A. B. Trofimov, *The Journal of chemical physics* **2004**, *120*, 11449–11464.

[51] R. J. Bartlett, *Annual Review of Physical Chemistry* **1981**, *32*, 359–401.

[52] J. Liu et al., *The Journal of chemical physics* **2018**, *148*, 244110.

[53] H. Laqua et al., *Journal of chemical theory and computation* **2020**, *16*, 1456–1468.

[54] W. Kutzelnigg, *Theoretica Chimica Acta* **1985**, *68*, 445–469.

[55] E. Giner et al., *The Journal of chemical physics* **2020**, *152*, 174104.

[56] J. A. Harrison et al., *Applied Physics Reviews* **2018**, *5*, 031104.

[57] C. Cohen-Tannoudji et al., *Photons and atoms: Introduction to quantum electrodynamics*, Wiley professional paperback ed., Wiley, New York, NY, **1997**.

[58] M. F. Herbst et al., *Wiley Interdisciplinary Reviews: Computational Molecular Science* **2020**, *10*, DOI 10.1002/wcms.1462.

[59] A. E. DePrince III, Hilbert: a space for quantum chemistry plugins to Psi4, https://github.com/edeprince3/hilbert (last accessed October 2022), **2020**.

[60] D. G. A. Smith et al., *The Journal of chemical physics* **2020**, *152*, 184108.

[61] F. Neese et al., *The Journal of chemical physics* **2020**, *152*, 224108.

[62] H.-D. Meyer et al., *Chemical Physics Letters* **1990**, *165*, 73–78.

[63] M. Bauer, A. Dreuw, *The Journal of chemical physics* **2023**, *158*, 124128.

[64] A. E. DePrince, *The Journal of chemical physics* **2021**, *154*, 094112.

[65] J. McTague, J. J. Foley, *The Journal of chemical physics* **2022**, *156*, 154103.

[66] S. Felicetti et al., *The journal of physical chemistry letters* **2020**, *11*, 8810–8818.

[67] V. Vallet et al., *The Journal of chemical physics* **2005**, *123*, 144307.

[68] J. Almlöf, *Chemical Physics Letters* **1991**, *181*, 319–320.

[69] M. A. Ambroise et al., *The Journal of chemical physics* **2023**, *158*, 124121.

[70] A. Meurer et al., *PeerJ Computer Science* **2017**, *3*, e103.

[71] D. A. Mazziotti, *Physical Review A* **1999**, *60*, 3618–3626.

[72] D. A. Mazziotti, *Physical Review A* **1999**, *60*, 4396–4408.

[73] M. Wormit, Frankfurt (Main), Univ., Diss., 2009.

[74] J. Kossaifi et al., *Journal of Machine Learning Research* **2019**, *20*, 1–6.

[75] S. D. Folkestad et al., *The Journal of chemical physics* **2019**, *150*, 194112.

[76] G. Schmitz et al., *The Journal of chemical physics* **2017**, *146*, 134112.

[77] I. Oseledets, E. Tyrtyshnikov, *Linear Algebra and its Applications* **2010**, *432*, 70–88.

[78] Y. Shao et al., *Molecular Physics* **2015**, *113*, 184–215.

[79] A. B. Trofimov, J. Schirmer, *The Journal of chemical physics* **2005**, *123*, 144115.

A. Appendix

A.1. Algebraic Diagrammatic Construction Densities up to First Order of Perturbation Theory Required for Excitonic Renormalization

$$\left\langle \tilde{\Psi}_0 \right| a_p^\dagger a_q^\dagger a_r a_s \left| \tilde{\Psi}_0 \right\rangle$$

oooo :

$$\delta_{p,s}\delta_{q,r} - \delta_{q,s}\delta_{p,r}$$

vvoo :

$$t^{(1)}_{r,s,p,q}$$

oovv :

$$t^{(1)}_{p,q,r,s}$$

$$\sum_{IJ} L_I \left\langle \tilde{\Psi}_I^- \right| a_p^\dagger a_q^\dagger \left| \tilde{\Psi}_J^+ \right\rangle R_J$$

vo :

$$L_p R_q$$

ov :

$$-L_q R_p$$

$$\sum_{IJ} L_I \left\langle \tilde{\Psi}_I^- \right| a_p^\dagger a_q^\dagger a_r a_s \left| \tilde{\Psi}_J^- \right\rangle R_J$$

voov :

$$L_p R_s \delta_{q,r}$$

ovov :

$$-L_q R_s \delta_{p,r}$$

vovo :

$$-L_p R_r \delta_{q,s}$$

ovvo :

$$L_q R_r \delta_{p,s}$$

vvoo :

$$L_q R_b t^{(1)}_{r,s,b,p} - L_p R_b t^{(1)}_{r,s,b,q}$$

oovv :

$$R_s L_a t^{(1)}_{p,q,a,r} - R_r L_a t^{(1)}_{p,q,a,s}$$

$$\sum_{IJ} L_I \left\langle \tilde{\Psi}^-_I \right| a^\dagger_p \left| \tilde{\Psi}_J \right\rangle R_J$$

o :

$$L_a R_{p,a}$$

$$\sum_{IJ} L_I \left\langle \tilde{\Psi}^-_I \right| a^\dagger_p a^\dagger_q a_r \left| \tilde{\Psi}_J \right\rangle R_J$$

vov :

$$L_p R_{q,r}$$

ovv :

$$-L_q R_{p,r}$$

ooo :

$$\delta_{p,r} L_a R_{q,a} - \delta_{q,r} L_a R_{p,a}$$

vvo :

$$L_q R_{i,b} t^{(1)}_{i,r,b,p} - L_p R_{i,b} t^{(1)}_{i,r,b,q} + L_a R_{i,a} t^{(1)}_{i,r,p,q}$$

$$\sum_{IJ} L_I \left\langle \tilde{\Psi}_I^+ \right| a_p^\dagger a_q^\dagger a_r a_s \left| \tilde{\Psi}_J^+ \right\rangle R_J$$

oooo :

$$R_p L_r \delta_{q,s} - R_q L_r \delta_{p,s} - R_p L_s \delta_{q,r} + R_q L_s \delta_{p,r}$$

vvoo :

$$L_s R_j t^{(1)}_{j,r,p,q} - L_r R_j t^{(1)}_{j,s,p,q}$$

oovv :

$$R_q L_i t^{(1)}_{i,p,r,s} - R_p L_i t^{(1)}_{i,q,r,s}$$

$$\sum_{IJ} L_I \left\langle \tilde{\Psi}_I^+ \right| a_p^\dagger \left| \tilde{\Psi}_J \right\rangle R_J$$

v :

$$L_i R_{i,p}$$

$$\sum_{IJ} L_I \left\langle \tilde{\Psi}_I^+ \right| a_p^\dagger a_q^\dagger a_r \left| \tilde{\Psi}_J \right\rangle R_J$$

ovo :

$$L_r R_{p,q} - \delta_{p,r} L_i R_{i,q}$$

oov :

$$-L_q R_{p,r} + \delta_{p,q} L_i R_{i,r}$$

voo :

$$L_q R_{j,a} t^{(1)}_{j,r,a,p} - L_r R_{j,a} t^{(1)}_{j,q,a,p} - L_i R_{i,a} t^{(1)}_{q,r,a,p}$$

$$\sum_{IJ} L_I \left\langle \tilde{\Psi}_I \right| a_p^\dagger a_q^\dagger a_r a_s \left| \tilde{\Psi}_J \right\rangle R_J$$

vovo :

$$L_{s,p} R_{q,r} - L_{i,p} R_{i,r} \delta_{q,s}$$

ovvo :

$$-L_{s,q} R_{p,r} + L_{i,q} R_{i,r} \delta_{p,s}$$

voov :

$$-L_{r,p}R_{q,s} + L_{i,p}R_{i,s}\delta_{q,r}$$

ovov :

$$L_{r,q}R_{p,s} - L_{i,q}R_{i,s}\delta_{p,r}$$

oooo :

$$\delta_{q,s}L_{r,a}R_{p,a} - \delta_{p,s}L_{r,a}R_{q,a} - \delta_{q,r}L_{s,a}R_{p,a} + \delta_{p,r}L_{s,a}R_{q,a}$$

vvoo :

$$\begin{aligned}&- L_{i,p}R_{i,b}t^{(1)}_{r,s,b,q} + L_{i,q}R_{i,b}t^{(1)}_{r,s,b,p} - L_{r,a}R_{j,a}t^{(1)}_{j,s,p,q} + L_{s,a}R_{j,a}t^{(1)}_{j,r,p,q}\\&- L_{r,q}R_{j,b}t^{(1)}_{j,s,b,p} + L_{s,q}R_{j,b}t^{(1)}_{j,r,b,p} + L_{r,p}R_{j,b}t^{(1)}_{j,s,b,q} - L_{s,p}R_{j,b}t^{(1)}_{j,r,b,q}\end{aligned}$$

oovv :

$$\begin{aligned}&- L_{i,a}R_{i,r}t^{(1)}_{p,q,a,s} + L_{i,a}R_{i,s}t^{(1)}_{p,q,a,r} - L_{i,a}R_{p,a}t^{(1)}_{i,q,r,s} + L_{i,a}R_{q,a}t^{(1)}_{i,p,r,s}\\&- R_{q,r}L_{i,a}t^{(1)}_{i,p,a,s} + R_{p,r}L_{i,a}t^{(1)}_{i,q,a,s} + R_{q,s}L_{i,a}t^{(1)}_{i,p,a,r} - R_{p,s}L_{i,a}t^{(1)}_{i,q,a,r}\end{aligned}$$

$$\sum_I L_I \left\langle \tilde{\Psi}^-_I \right| a^\dagger_p \left| \tilde{\Psi}_0 \right\rangle$$

v :

$$L_p$$

$$\sum_I L_I \left\langle \tilde{\Psi}^-_I \right| a^\dagger_p a^\dagger_q a_r \left| \tilde{\Psi}_0 \right\rangle$$

voo :

$$L_p\delta_{q,r}$$

ovo :

$$L_q\delta_{p,r}$$

oov :

$$L_a t^{(1)}_{p,q,a,r}$$

$$\sum_I L_I \left\langle \tilde{\Psi}_I^+ \right| a_p \left| \tilde{\Psi}_0 \right\rangle$$

o :

$$L_p$$

$$\sum_I L_I \left\langle \tilde{\Psi}_I^+ \right| a_p^\dagger a_q a_r \left| \tilde{\Psi}_0 \right\rangle$$

ooo :

$$\delta_{p,q} L_r - \delta_{p,r} L_q$$

ovv :

$$L_i t^{(1)}_{i,p,q,r}$$

$$\sum_I L_I \left\langle \tilde{\Psi}_I \right| a_p^\dagger a_q^\dagger a_r a_s \left| \tilde{\Psi}_0 \right\rangle$$

vooo :

$$\delta_{q,r} L_{s,p} - \delta_{q,s} L_{r,p}$$

ovoo :

$$-\delta_{p,r} L_{s,q} + \delta_{p,s} L_{r,q}$$

oovo :

$$-t^{(1)}_{i,q,a,r} L_{i,a} \delta_{p,s} + t^{(1)}_{i,p,a,r} L_{i,a} \delta_{q,s} + t^{(1)}_{p,q,a,r} L_{s,a}$$

ooov :

$$t^{(1)}_{i,q,a,s} L_{i,a} \delta_{p,r} - t^{(1)}_{i,p,a,s} L_{i,a} \delta_{q,r} - t^{(1)}_{p,q,a,s} L_{r,a}$$

ovvv :

$$-t^{(1)}_{i,p,r,s} L_{i,q}$$

vovv :

$$t^{(1)}_{i,q,r,s} L_{i,p}$$

The remaining densities are either already published elsewhere[50, 79] or can be obtained from hermitian conjugation. Note, that the ISR states are not charged, if not noted otherwise by a minus or plus sign.

Danksagung

Ich will mich an dieser Stelle bei allen bedanken, die zum erfolgreichen gelingen dieser Arbeit beigetragen haben. Dafür gebührt zunächst einmal Prof. Dr. Andreas Dreuw Dank, dass ich in seiner Arbeitsgruppe promovieren durfte. Bedanken möchte ich mich dabei vor allem für alles, was ich bei Ihm außerhalb des fachbezogenen Kontexts gelernt habe und für die Freiheit, die mir beim Arbeiten gelassen wurde.

Ebenso danke ich allen meinen Kollaborateuren für die fruchtbare Zusammenarbeit, wobei ich dabei vor allem Prof. Dr. Anthony Dutoi danken möchte, in dessen Arbeitskreis ich einen tollen Auslandsaufenthalt genießen durfte, und mit dem ich auch darüber hinaus immer gerne zusammengearbeitet habe.

Besonderer Dank gilt ebenfalls Prof. Dr. Oriol Vendrell und Federico Mellini für die angenehme Zusammenarbeit und die Bereitstellung der Dynamik Ergebnisse. Angenehme Zusammenarbeit durfte ich auch mit Stefan Germer genießen.

Außerhalb der wissenschaftlichen Zusammenarbeit möchte ich mich bei der gesamten Arbeitsgruppe für die entspannte Atmosphäre und die zahllosen Doppelkopfrunden bedanken. Dank euch bin ich immer gerne ins Büro gekommen.

Meinen Freunden und meiner Familie möchte ich ebenfalls für die Zeit außerhalb des wissenschaftlichen Kontexts danken.

Zu guter Letzt danke ich vor allem meiner Freundin, die immer für mich da ist, mir unterstützend zur Seite steht und die ich über alles liebe.

Danke!

Eidesstattliche Versicherung gemäß §8 der Promotionsordnung für die Gesamtfakultät für Mathematik, Ingenieur- und Naturwissenschaften der Universität Heidelberg

1. Bei der eingereichten Dissertation zu dem Thema **"Development, Extension and Application of Electronic Structure Methods for Ground and Excited States"** handelt es sich um meine eigenständig erbrachte Leistung.

2. Ich habe nur die angegebenen Quellen und Hilfsmittel benutzt und mich keiner unzulässigen Hilfe Dritter bedient. Insbesondere habe ich wörtlich oder sinngemäß aus anderen Werken übernommene Inhalte als solche kenntlich gemacht.

3. Die Arbeit oder Teile davon habe ich bisher nicht an einer anderen Hochschule des In- oder Auslands als Bestandteil einer Prüfungs- oder Qualifikationsleistung vorgelegt.

4. Die Richtigkeit der vorstehenden Erklärungen bestätige ich.

5. Die Bedeutung der eidesstattlichen Versicherung und die strafrechtlichen Folgen einer unrichtigen oder unvollständigen eidesstattlichen Versicherung sind mir bekannt.

Ich versichere an Eides statt, dass ich nach bestem Wissen die reine Wahrheit erklärt und nichts verschwiegen habe.

Ort, Datum: _____ Unterschrift: _____